Analysis and Design of Broadband Single-Mode Multi-Clad Fibers

by

Liang-Ju Lu

Dissertation submitted to the Faculty of the

Virginia Polytechnic Institute and State University

in partial fulfillment of the requirements for the degree of

Doctor of Philosophy in Electrical Engineering

APPROVED:

Dr. R. O. Claus, Co-Chairman

Dr. A. Safaai-Jazi, Co-Chairman

Dr. I. M. Besieris

Dr. I. Jacobs

Dr. C. L. Prather

August, 1989

Blacksburg, Virginia

Analysis and Design of Broadband Single-Mode Multi-Clad Fibers

by

Liang-Ju Lu

Dr. R. O. Claus, Co-Chairman

Dr. A. Safaai-Jazi, Co-Chairman

(ABSTRACT)

In the last several years, considerable attention has been paid to the study of dispersion-flattened single-mode fibers which offer a high transmission capacity with low losses through a wide range of wavelengths. However, the existing designs are sensitive to bending and manufacturing tolerances, and are not truly single-mode at most wavelengths of interest.

To remedy these problems a new series of broadband dispersion-flattened truly single-mode fiber designs are proposed. These fibers have both dispersion-shifted and dispersion-flattened features with low splice and bend losses. Results demonstrating a total dispersion of $\pm$ 0.97 ps/km-nm over the entire spectral range between 1.31 μm to 1.66 μm are presented. Such dispersion-flattening is achieved while simultaneously maintaining a mode-field radius of 3 μm to 5 μm in the dispersion-flattened wavelength range. The most significant achievement is that the proposed multi-clad fiber design is strictly single-mode and splice and bend losses are smaller than those of double-clad, triple-clad, and quadruple-clad fibers with the same value of dispersion.

Ultralow dispersion fibers, whose chromatic dispersion and the first and second-order derivatives of the chromatic dispersion are zero at 1.5 μm or 1.55 μm, are described. This effectively increases the laser emission tolerance. Ultralow dispersion fibers open the way to wavelength multiplexing with currently available

inexpensive multifrequency lasers, either in local or long distance networks. These fibers also have low splice and bend losses compared to double-clad, triple-clad, and quadruple-clad fibers.

An inverse waveguide synthesis program, which can trace multiple objective functions and optimize multiple parameters simultaneously, is developed. An objective function is applied, for the first time, to optimize the dispersion-flattened single-mode fiber index profile with respect to: (1) minimum dispersion, (2) the wavelengths of zero-dispersion, (3) maximum width of dispersion-flattened window, (4) maximum layer index difference less than 0.8%, and (5) layer thickness larger than 3.5 μm.

The accuracy of chromatic dispersion calculations in dispersion-flattened fibers is evaluated. It has been shown that the accuracy of approximate methods is influenced not only by the index differences, but also by their derivatives with respect to wavelength.

The matrix method and direct numerical integration of the wave equation are used to compute the mode propagation constants, cutoff frequencies, field distributions, mode-field radius, and splice loss, and carry out production tolerance analysis for multi-clad step-index fibers and graded-index fibers, respectively. Detailed analysis and optimized fiber data are presented.

Table of Contents

List of Illustrations

List of Tables

Acknowledgements

I would like to express my sincere gratitude to both Dr. R. O. Claus and Dr. A. Safaai-Jazi, my major advisors, under whose supervision this dissertation was completed. Without their guidance, encouragement and support this study could have not been completed.

I would also like to thank Dr. I. M. Beseris for his technical advice, Dr. I. Jacobs and Dr. C. L. Prather for serving on my committee and for their time and effort spent.

I also wish to express my appreciation to my fellow graduate students and friends at Virginia Tech, and to my parents and relatives back home for their support.

Chapter 1. Introduction

1.1. Background Information

The first practical low-loss optical fibers were introduced in 1970 by researchers at Corning Glass Works [1]. These fibers generally displayed losses in the range of 20 dB/km. Since then remarkable progress has been made in reducing transmission losses and now fibers are produced with losses well below 0.5 dB/km. Corning and many other companies are manufacturing single-mode fibers with attenuation factors of 0.22 dB/km. Single-mode fibers with step-index profiles are indispensable to present high performance optical fiber communication systems. System requirements for the future will be more demanding and may require new types of single-mode fibers. System designers want to increase repeater spacing beyond 50 Kilometers and data rates from megabits to gigabits per second [2]. To achieve such high performance, new types of fibers or highly monochromatic light sources are required.

The limiting factors for all optical fiber systems are attenuation and dispersion. Dispersion is the spreading out of pulses as they travel along the fiber. Dispersion will cause interferences that limit the data transmission rate. The primary causes of pulse dispersion in single-mode fibers are:

- material dispersion due to the dependence of the refractive index on wavelength,
- waveguide dispersion, because group velocity is dependent on fiber parameters, namely the radial dimensions and indices.

Current fibers are near the theoretical minimum of attenuation. Therefore, transmission improvements may be achieved through changes in dispersion characteristics. Two approaches are possible to reduce dispersion at the attenuation minimum: packing light sources with extremely narrow linewidths [3-6], or designing fibers with zero-dispersion at the wavelength of minimum loss. The former was achieved from laboratory work with a transmission rate of 2 Gbit/sec through a 130 km of repeaterless fiber [7]. However, the single frequency lasers are hard to produce and require precise control during operation, which is difficult to maintain outside the laboratory. From a technological point of view, narrow-linewidth lasers at both 1.3 μm and 1.55 μm appear to be at least a few years from a low-cost commercial reality. Changes in the dispersion characteristics of single-mode fibers derived from new waveguide structures appear more promising in the near future.

Wavelength division muliplexing (WDM) has been shown in recent years to be an important approach to increase system information capacity and system design flexibility. With WDM technology, the cost and weight of the required fiber cable in the system would be greatly reduced. In optical fiber communication systems employing wavelength division multiplexing, it is desirable that all optical channels ex-

hibit nearly the same dispersion. This can be achieved only with dispersion-flattened fibers.

Bandwidth and repeater spacing are the most important considerations in long distance optical fiber communications. The primary optical fiber properties determining these parameters are attenuation and dispersion. For SiO_2-GeO_2 based fibers fabricated by vapor-deposition techniques, the wavelength window of low attenuation occurs near 1.3 μm and also near 1.55 μm. It has been verified both theoretically and experimentally that the ultimate low-loss spectral range of single-mode fibers lies in the 1.55 μm window [8]. To take advantage of such a low-loss spectral region, it is essential to shift the zero-dispersion wavelength to the 1.55 μm window [9-22]. In single-mode fibers the index profile can be tailored so that the dispersion minimum is made to coincide with the attenuation minimum at 1.55 μm. Manipulation of waveguide dispersion can lead to new fiber designs.

Two classes of fibers have been reported to tailor waveguide dispersion characteristics. They are dispersion-shifted single-mode (DSSM) fibers and dispersion-flattened single-mode (DFSM) fibers with the following index profiles:

- Graded profile [23-26] for DSSM fiber;
- Double-clad (DC) [27-29], triple-clad (TC) [30-32], and quadruple-clad (QC) [33-36] geometries for both DFSM and DSSM fibers;
- Graded-core with DC, TC, or QC geometries for both DFSM and DSSM fibers [37-42].

Reduction of chromatic dispersion in the 1.55 μm transmission window can be achieved by dispersion-shifted single-mode fiber, but values as high as 8 ps/km-nm are still apparent at 1.45 μm and 1.65 μm for zero-dispersion at 1.55 μm. The total

dispersion can be reduced to zero only at one wavelength and increases as the wavelength departs from the optimum wavelength for the dispersion-shifted fibers. This restricts the choice of laser sources and limits wavelength multiplexing potential. It is desirable that the total dispersion of a single-mode fiber be reduced to a minimum over an extended spectral range covering the low-loss window. The problem of the dispersion-shifted fibers can be overcome only with dispersion-flattened fibers which produce, for example, less than 1 ps/km-nm in the whole 1.3 μm to 1.7 μm window.

The possibility of low dispersion over an extended wavelength range was first presented by Kawakami and Nishida in 1974 [27]. They proposed a double-clad (DC) fiber with a W-shape step-index profile and examined the effect of the depressed inner cladding on the dispersion characteristic and cutoff of the fundamental LP_{01} mode. Dispersion flattening in DC fibers as well as other multiple-clad fibers is maintained by partial cancellation of waveguide dispersion by material dispersion in a desired spectral range. By properly tailoring the index profile, the total dispersion can be made to vanish at two wavelengths and to assume small values in between.

Analysis, design, and fabrication of dispersion-flattened DC fibers have been addressed by several researchers [27-29]. Apart from providing low chromatic dispersion, practical dispersion-flattened fibers need to meet other requirements, including low scattering, bend, and splice losses as well as being single-mode in the desired spectral range. The parameters which influence the losses mentioned above are index differences, cutoff of the LP_{01} mode, and mode-field radius, respectively. The single-mode nature of the fiber is determined by the cutoff of the second mode which is usually the LP_{11} mode. A major drawback of dispersion-flattened DC fibers is their high sensitivity to bending, because the fundamental mode exhibits a finite cutoff wavelength [43], which is very close to the dispersion-flattened region [33].

Furthermore, the chromatic dispersion is highly sensitive to variations of fiber parameters.

To overcome the bend-sensitivity of DC fibers, Cohen, et al. introduced a raised-index cladding between the inner and the outer claddings, thus developing a new structure with four claddings which was named quadruple-clad (QC) fiber [33]. The proposed QC fiber exhibited much improved bend-sensitivity, low loss, and dispersion below 2 ps/km-nm in the 1.28 μm - 1.65 μm wavelength range. Other researchers have also carried out experimental as well as theoretical work on QC fibers, among them Bhagavatula, et al. [34], Bachmann, et al. [36], and Francois [44]. Triple-clad (TC) fibers also offer low dispersion in a wide spectral range and have been considered as a high capacity transmission medium for long distance optical fiber communications [30-32].

Despite being much less bend-sensitive, TC and QC fibers are, as in the case of DC fibers, sensitive to parameter variations, thus imposing stringent manufacturing tolerances. This problem, however, becomes less important as the fiber fabrication technology improves. A more serious problem with TC and QC fibers is their multimode nature at most wavelengths in the low attenuation window of glass fiber. The possibility of higher-order modes being excited could severely limit the information carrying capacity of these fibers. Truly single-mode QC fibers have been investigated by Francois, et al. [44-46], with the conclusion that the chromatic dispersion of such fibers is low at long wavelengths and over a narrower spectral range and that they are more sensitive to fiber imperfections. It thus appears that QC fibers cannot be single-mode and maintain low dispersion over a wide spectral range simultaneously. More details on DC, TC, and QC fibers are given by Ainslie and Day [47].

Many advanced designs have been reported on dispersion-shifted fibers with triangular, trapezoidal, depressed-cladding triangular, ring triangular, and Gaussian

structures [47]. It is possible to shift the dispersion minimum of step-index single-mode fibers to 1.55 μm by making the core small and by increasing the refractive index difference Δn between the core and cladding [47,48]. Increasing Δn will likely increase the infrared absorption and Rayleigh scattering loss and requires high doping levels [48]. Moreover, large Δn introduces mechanical stress within the fiber, resulting in large optical losses. Decreasing core size is likely to increase microbend and optical losses.

The original concept of the graded-index profile designs for dispersion-shifted single-mode fibers is to reduce the mechanical stress gradient at the interface of the core and cladding, which is generated by increasing the core-cladding index difference. When optical fibers are produced by the modified chemical vapor deposition (MCVD) process they inevitably possess a central dip in their index profile because of evaporation of the dopant during the preform collapsing stage. Triangular profile fibers are sensitive to bending because they have a central dip in their index profile [24]. The depressed-cladding triangular profile design results in a great reduction in the microbend loss, but suffers from higher splice losses [47]. In any case, the triangular-core profile behavior dominates these modified triangular-core fibers. Other major problems for these graded-index fibers are their poor reproducibility and high production costs.

1.2. Scope of Investigation

The goals of this research are:

1. to find a new series of multi-clad fiber designs, which offer both dispersion-shifted and dispersion-flattened properties, and
   a. have a maximum dispersion-flattened window with the lowest possible dispersion;
   b. have a reasonable mode-field radius (3 - 5 μm), and splice and bend losses smaller than DC, TC, and QC fibers;
   c. have a simple step-index structure and reasonable layer thicknesses which could be easily fabricated;
   d. have layer index differences less than 0.8%, i.e., small optical losses;
   e. have transmission properties less sensitive to the manufacturing tolerances.
2. to find novel ultralow dispersion (< 0.01 ps/km-nm) fibers whose first-order and second-order derivatives of total dispersion are zero in the wavelength range of 1.5 μm - 1.55 μm.
3. to assess the accuracy of chromatic dispersion calculations in dispersion-flattened fibers.
4. to develop a optical fiber profile optimization method which can trace multiple objective functions and optimize multiple parameters simultaneously.

Based on the waveguide dispersion behavior, multi-clad fiber can be classified into two major types [35]: one type with a uniform and high waveguide dispersion for the LP_{01} mode, and another type with a steep slope for the waveguide dispersion of the LP_{01} mode. Results from multi-clad fiber designs with uniform waveguide

dispersion can be used in the design of dispersion-shifted fibers. On the other hand, results on steep slope waveguide dispersion are useful in designing dispersion-flattened fibers with two or three zero-dispersion points. The latter case is discussed in this study because in this research we try to design a fiber with both dispersion-shifted and dispersion-flattened properties.

1.3. Approach

Dispersion behavior of single-mode fibers with discontinuous, piecewise continuous, and continuous index profiles in Figs. 1 and 2 are examined by the matrix method [49] and direct numerical integration in conjunction with the shooting method [50,51].

The slope of the waveguide dispersion can be controlled so that the waveguide dispersion cancels the material dispersion at any wavelength of interest, while keeping the total dispersion below a certain limit. We are primarily concerned with the propagation constants of the fundamental mode and the cutoff parameters for the next higher-order mode which defines the single-mode region. In this work we assume the fiber profile indices $n_j \simeq n_{j+1}$, so that vector properties may be built onto the scalar modes which are considered here. The solutions are linearly polarized (LP) modes.

A new class of dispersion-flattened fibers are proposed which are truly single-mode for $\lambda > 1.26\ \mu m$, provide a total dispersion of less than 1 ps/km-nm over 1.31 μm - 1.66 μm wavelength range, and have a fundamental mode cutoff wavelength greater than 1.66 μm, indicating that they suffer low bend losses. Furthermore, these fibers may be designed such that the chromatic dispersion vanishes in the neigh-

borhood of 1.55 μm, which corresponds to minimum attenuation wavelength of glass fibers. Finally, a mode-field radius of 3 μm to 5 μm in the dispersion-flattened wavelength range leads to a reasonably low splice loss. The proposed fibers have a step-index profile and consist of a central core, five inner claddings, and an outer cladding. The structure may be viewed as a modification of the quadruple-clad fiber, incorporating a raised-index ring whose effect is to maintain a large separation between the cutoff wavelengths of the LP_{01} and LP_{11} modes. The index differences are kept below 0.8% to ensure low losses due to Rayleigh and stress-induced scatterings. Using an objective function and parameter constraints, the index profile is optimized with respect to (1) desired minimum dispersion, (2) wavelengths of zero-dispersion, (3) maximum width of dispersion-flattened window, (4) maximum layer index difference less than 0.8%, and (5) layer thickness larger than 3.5 μm.

In this study, we also propose novel ultralow dispersion fibers. Ultralow dispersion fibers are those whose dispersion is $< 10^{-2}$ ps/km-nm throughout a 1 μm wavelength range centered at 1.5 μm or 1.55 μm, and their first-order and second-order dispersion are zero at 1.5 μm or 1.55 μm wavelength. Although it is noted that in this range of dispersion values, polarization dispersion may dominate, such dispersion effects are not considered in this study.

Chapter 2. Field and Dispersion Equations of Multi-Clad Fibers

Dispersion behavior of single-mode fibers with discontinuous, piecewise continuous, and continuous index profiles will be examined. Two methods will be used in this study. One is a matrix method [49] for the analysis of step-index profiles and the other is a direct numerical integration method in conjunction with the shooting method [50,51]. The former method is efficient for the analysis of discontinuous step-index profiles while the latter method is more suitable for treating continuous or piecewise continuous index profiles as shown in Fig. 2. Both methods require solving transcendental equations.

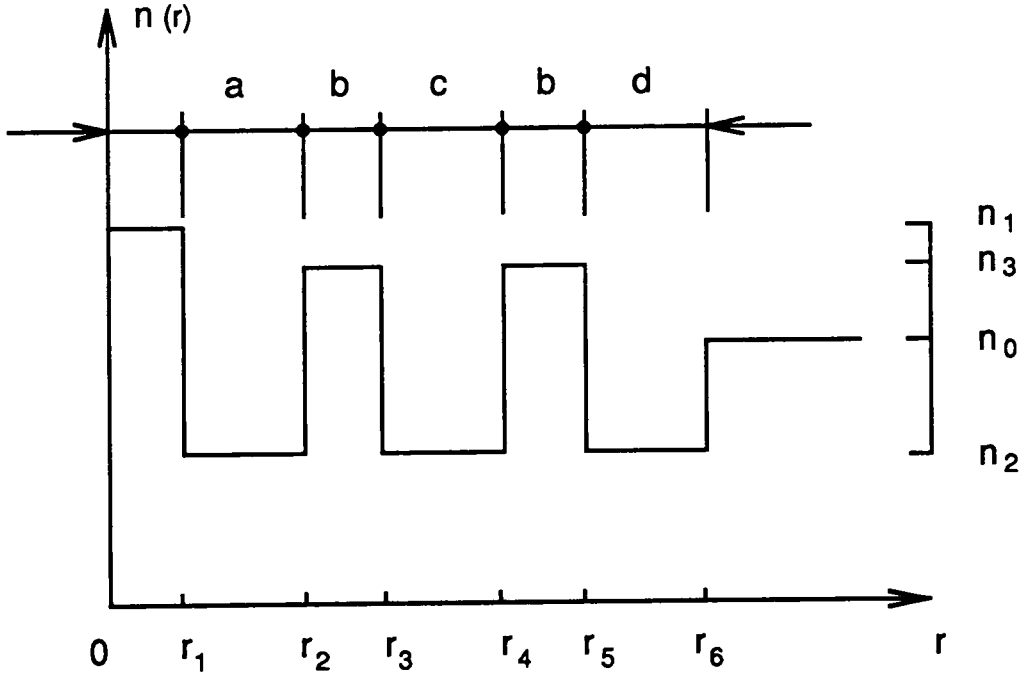

Figure 1. Multi-clad fiber index profile.

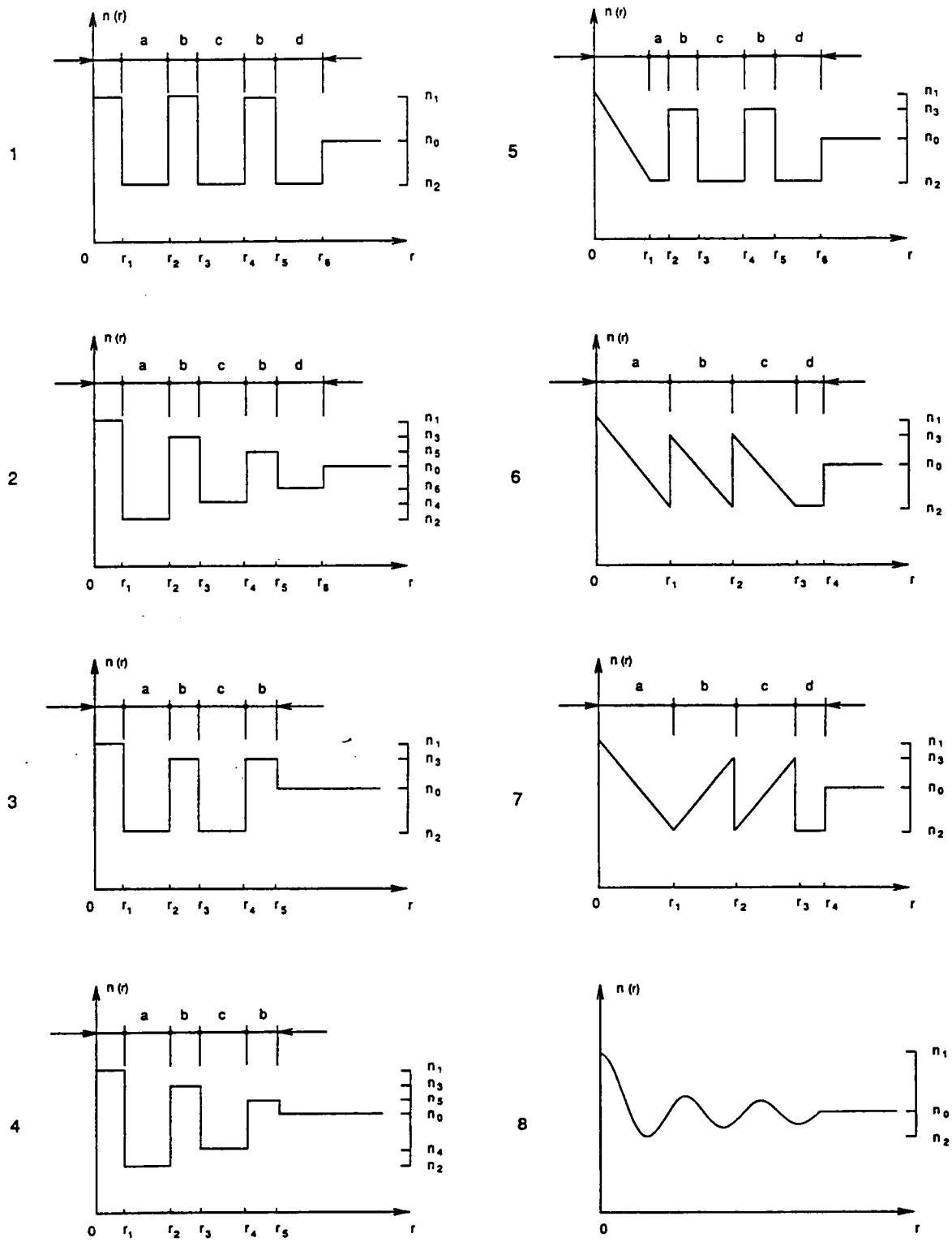

Figure 2. Representative multi-clad fiber index profiles.

2.1. Matrix Method for Derivation of Field Distributions and Dispersion Equation

The proposed multi-clad fibers consist of a central core, five inner claddings, and an outer cladding. Figure 1 illustrates a typical index profile for such fibers. The jth layer is characterized by a refractive index n_j and has inner and outer radii r_{j-1} and r_j, respectively. The outermost cladding is assumed to extend to infinity. Since the index differences are very small, the fiber is weakly guiding and scalar-wave solutions can be employed (Appendix A). The time and z dependences of fields take the usual form $\exp[j(\omega t - \beta z)]$, where β is the axial propagation constant and ω is the angular frequency. This term is dropped from the field solutions. The solutions of the scalar wave equation for the guided modes of multi-clad structure of Fig. 1 are the Bessel and modified Bessel functions of integral order n. The requirements that the field be finite at $r = 0$ and decay exponentially for large r eliminate the Y_n or K_n Bessel functions for $r < r_1$, and the I_n modified Bessel function in the outer cladding. For convenience functions Z_{nj} and $\bar{Z}_{nj}$ [52], which are summarized in Table 1, are introduced. Choosing a cylindrical coordinate system (r, ϕ, z), the scalar fields in the central core, in an inner cladding, and in the outer cladding are summarized as

$$\Psi_1(r, \phi) = A_1 Z_{n1}\left(\frac{u_1 r}{a}\right) Q(\phi), \qquad r \le r_1 \quad (2.1a)$$

$$\Psi_j(r, \phi) = \left[A_j Z_{nj}\left(\frac{u_j r}{a}\right) + B_j \bar{Z}_{nj}\left(\frac{u_j r}{a}\right)\right] Q(\phi), \qquad r_{j-1} < r \le r_j \quad (2.1b)$$

$$\Psi_k(r, \phi) = B_k K_n\left(\frac{u_k r}{a}\right) Q(\phi), \qquad r_k < r \quad (2.1c)$$

Table 1. Definition of functions Z_{nj} and $\bar{Z}_{nj}$

Z_{n1}		Z_{nj}		$\bar{Z}_{nj}$	
$\bar{\beta} < n_1$	$\bar{\beta} > n_1$	$\bar{\beta}_j < n_j$	$\bar{\beta} > n_j$	$\bar{\beta} < n_j$	$\bar{\beta} > n_j$
J_n	I_n	J_n	I_n	Y_n	K_n

- The subscript n is the order of Bessel and modified Bessel functions

where Ψ_j is a transverse electric or magnetic field component, A_j and B_j are constant coefficients, $Q(\phi) = \cos(n\phi)$ or $\sin(n\phi)$, where n is an integer; and u_j is a parameter that is related to the normalized propagation constant of a guided mode $\bar{\beta}$ by

$$u_j = k_0 a \left| (n_j^2 - \bar{\beta}^2) \right|^{1/2}, \tag{2.2a}$$

with $\bar{\beta} = \beta / k_0$. In Eq. (2.2a), a ($= r_6$) is the overall core radius, n_j , j = 1, 2, 3, ... k, is the refractive index of the jth layer, and $k_0 = 2\pi/\lambda$ is the free-space wave number. The parameters u_1 and u_k are combined to provide a third parameter V, defined as

$$V = (u_1^2 + u_k^2)^{1/2} = k_0 a (n_1^2 - n_k^2)^{1/2}, \tag{2.2b}$$

which can be regarded as a normalized frequency. With continuity of field components Ψ_j and its derivative $d\Psi_j/dr$ at the interface between the jth and $(j+1)$th layers, the field coefficients can be expressed as a set of linear equations in terms of transfer matrices as follows [49]:

$$\begin{bmatrix} A_{j+1} \\ B_{j+1} \end{bmatrix} = T_j \begin{bmatrix} A_j \\ B_j \end{bmatrix}, \tag{2.3a}$$

$$B_k \begin{bmatrix} 1 \\ C_k \end{bmatrix} = T_{k-1} \begin{bmatrix} A_{k-1} \\ B_{k-1} \end{bmatrix}, \tag{2.3b}$$

where $C_k = u_k/u_{k-1}$. The column vector denotes the field coefficients. From Eqs. (2.3a,b), one can obtain field coefficients A_j and B_j by the recurrence method. The transfer matrices for the first, an intermediate, and the outermost layers are

$$T_1 = \begin{bmatrix} \bar{Z}'_{n2} Z_{n1} - C_2 \bar{Z}_{n2} Z'_{n1} & 0 \\ -\bar{Z}'_{n2} Z_{n1} + C_2 Z_{n2} Z'_{n1} & 0 \end{bmatrix}, \tag{2.4a}$$

$$T_j = \begin{bmatrix} \bar{Z}'_{n(j+1)} Z_{nj} - C_j \bar{Z}_{n(j+1)} Z'_{nj} & \bar{Z}'_{n(j+1)} \bar{Z}_{nj} - C_j \bar{Z}_{n(j+1)} \bar{Z}'_{nj} \\ -Z'_{n(j+1)} Z_{nj} + C_j Z_{n(j+1)} Z'_{nj} & -Z'_{n(j+1)} \bar{Z}_{nj} + C_j Z_{n(j+1)} \bar{Z}'_{nj} \end{bmatrix}, \tag{2.4b}$$

$$T_k = \begin{bmatrix} Z_{n(k-1)}/Z_{nk} & \bar{Z}_{n(k-1)}/Z_{nk} \\ Z'_{n(k-1)}/Z'_{nk} & \bar{Z}'_{n(k-1)}/Z'_{nk} \end{bmatrix}, \tag{2.4c}$$

where $C_j = u_j/u_{j-1}$, and Z'_{nj} denotes differentiation with respect to the argument. Applying Eqs. (2.3a,b) to a fiber structure with k layers results in

$$\begin{bmatrix} T_{11} & T_{21} \\ T_{21} & T_{22} \end{bmatrix} \begin{bmatrix} A_1 \\ 0 \end{bmatrix} = B_k \begin{bmatrix} 1 \\ C_k \end{bmatrix}, \tag{2.5a}$$

where the 2×2 matrix in terms of transfer matrices $[T_j]$ is expressed as

$$\begin{bmatrix} T_{11} & T_{21} \\ T_{21} & T_{22} \end{bmatrix} = \prod_{j=1}^{k-1} [T_j]. \tag{2.5b}$$

In Eq. (2.5a), the field amplitude A_1 is normalized to unity at $r = 0$. Substituting the value of C_k in Eq. (2.5a), the dispersion equation is found to be

$$u_k T_{11} - u_{k-1} T_{21} = 0 . \tag{2.6}$$

2.2. Direct Numerical Integration Method for Field Distributions and Dispersion Equation

Mode analysis of optical fiber with an arbitrary refractive index profile may be necessary for generating ultralow dispersion fibers. The normalized propagation constant, group velocity, total dispersion, and field distribution of lower-order modes are calculated by means of a combination of direct numerical integration of two first-

order differential equations and numerical solution of a transcendental equation derived from the boundary condition at the outmost cladding.

The scalar wave equation derived from Maxwell's equations is

$$\frac{d^2\Psi}{dr^2} + \frac{1}{r}\frac{d\Psi}{dr} + \left[u^2 - v^2 f(r) - \frac{n^2}{r^2}\right]\Psi = 0\,, \tag{2.7a}$$

where u and v are normalized parameters and for the jth layer are defined as

$$u_j = k_0 a\left[n_j^2(r) - \overline{\beta}^2\right]^{1/2}; \qquad j = 1, 2, \ldots k\,, \tag{2.7b}$$

$$v = k_0 a\left[n_1^2(0) - n_k^2\right]^{1/2}\,, \tag{2.7c}$$

where $f(r)$ is an index profile function. $\overline{\beta}$ is the normalized propagation constant, k_0 is the free-space wave number, and n is the azimuthal mode number. Assuming that $n_1(0)$ is the largest index in the vicinity of $r = 0$, the scalar wave function $\Psi(r)$ is approximated as

$$\Psi(r) = A_1 J_n\left(\frac{u_1 r}{a}\right), \tag{2.8a}$$

while for $r > r_k$ $\Psi(r)$ is expressed as

$$\Psi(r) = B_k K_n\left(\frac{u_k r}{a}\right). \tag{2.8b}$$

The IMSL subroutine DIVPRK [53] is used to solve (2.7a). However, this subroutine solves only the first-order differential equations. Thus, Eq. (2.7a) is expressed in terms of two first-order differential equations

$$\frac{d\Psi_1}{dr} = \Psi_2, \tag{2.9a}$$

$$\frac{d\Psi_2}{dr} = -\frac{1}{r}\Psi_2 - \left[u^2 - v^2 f(r) - \frac{n^2}{r^2}\right]\Psi_1, \tag{2.9b}$$

subject to boundary conditions

$$\Psi_1|_{r=0} = 1\,, \tag{2.10a}$$

$$\Psi_2|_{r=0} = 0\,. \tag{2.10b}$$

This is a boundary-value problem. IMSL routine DIVPRK, which uses the Runge-Kutta-Verner fifth-order and sixth-order method, is used to solve Eqs. (2.9-2.10) by shooting the characteristic equation Eq. (2.11), which is derived from the boundary conditions at the outermost cladding.

$$\Psi - \Psi' \frac{a}{u_k} \frac{K_n(u_k)}{K'_n(u_k)} = 0. \tag{2.11}$$

The propagation constant of an arbitrary refractive index profile fiber is determined by the field functions which satisfy scalar wave equations (2.9a,b) and boundary condition Eq. (2.11) simultaneously. First, let the normalized propagation constant $\overline{\beta}$ be given a value somewhat smaller than $n_1(0)$. The normalized frequency V is chosen as a fixed value. Then the scalar wave equation is solved by DIVPRK under the boundary conditions of Eqs. (2.10a,b). Next, whether the value of the left side of Eq. (2.11) is close enough to zero or not must be determined. If the value is not close

to zero, the initial value of $\bar{\beta}$ at the first step is revised and the preceding steps are repeated until the value from the left side of Eq. (2.11) converges to zero. When this value converges to zero the normalized propagation constant $\bar{\beta}$ is obtained. The results for normalized propagation constant $\bar{\beta}$ calculated based on the integration method agree with the results calculated by the matrix method and yielded results accurate up to 10^{-16}.

Field distribution is obtained from the DIVPRK output when the propagation constant is input. Discontinuities of the profile are treated by DIVPRK, one can write an index profile function routine by using a logical IF statement.

The power density in the core and in the claddings can be expressed as

$$Intensity = |\Psi_j|^2 , \tag{2.12a}$$

$$P_j = \int_{s_j} |\Psi_j|^2 ds = \int_0^{2\pi} \int_{r_{j-1}}^{r_j} |\Psi_j|^2 r dr d\varphi , \qquad j = 1, 2, \ldots k , \tag{2.12b}$$

and the total power is

$$P_{\text{total}} = \sum_{j=1}^{k} P_j . \tag{2.12c}$$

2.3. Dispersion Effects

Dispersion in single-mode fibers occurs because spectral components radiating from a light source travel with different group velocities and therefore arrive at different times at the output end. The total dispersion is the sum of two effects, material

dispersion and waveguide dispersion. Material dispersion is a bulk property which occurs because the group velocity of a plane wave is a nonlinear function of frequency due to the dependence of the refractive index of the material on wavelength. On the other hand, waveguide dispersion occurs because the group velocity of a waveguide mode is also a nonlinear function of frequency through its dependence on the geometry of the waveguide; that is, the radial dimensions and the shape of the refractive index profile.

2.3.1. Waveguide Dispersion

Equation (2.6) is solved numerically to determine the normalized propagation constant $\overline{\beta}$ as a function of normalized frequency V. The first and second derivatives are also calculated simultaneously to evaluate the group velocity and waveguide dispersion of the LP_{01} mode. The group velocity can be expressed as

$$V_g = \left[\frac{d\beta}{d\omega} \right]^{-1} = c\left[\overline{\beta} + V\frac{d\overline{\beta}}{dV} \right]^{-1}, \tag{2.13a}$$

where c is the velocity of light in vacuum. The group velocity can also be expressed as a function of normalized propagation constant $\overline{\beta}$ and the free-space wavelength λ,

$$V_g = c\left[\overline{\beta} - \lambda\frac{d\overline{\beta}}{d\lambda} \right]^{-1}. \tag{2.13b}$$

Waveguide dispersion may be expressed in terms of the normalized propagation constant $\overline{\beta}$ and the normalized frequency V as

$$D_{wg} = \frac{V}{c\lambda}\left[2\frac{d\overline{\beta}}{dV} + V\frac{d^2\overline{\beta}}{dV^2}\right]. \tag{2.14a}$$

Waveguide dispersion may also be expressed in terms of the normalized propagation constant $\overline{\beta}$ and the free-space wavelength λ as

$$D_{wg} = \frac{1}{2\pi c}\left[2\lambda\frac{d\overline{\beta}}{d\lambda} + \lambda^2\frac{d^2\overline{\beta}}{d\lambda^2}\right]. \tag{2.14b}$$

At cutoff, the propagation constant $\beta = k_0 n_k$, and $u_k = 0$. Close to cutoff, the term u_k approaches zero. The cutoff condition can be obtained by calculating the limit of the dispersion equation when $u_k \to 0$. Here we find the near cutoff normalized frequency by setting $\overline{\beta}$ very close to n_K.

2.3.2. *Material Dispersion*

Delay time τ of a light pulse propagating along a fiber of length L with a normalized propagation constant $\overline{\beta}$ at λ is [48]

$$\tau = -L\frac{\lambda^2}{2\pi c}\frac{d\overline{\beta}}{d\lambda}. \tag{2.15}$$

The pulse broadening of the light emitted by a source having a spectral width $\Delta\lambda$ centered around λ is given by

$$\Delta\lambda\frac{d\tau}{d\lambda} = -\frac{L}{2\pi c}\Delta\lambda\left[2\lambda\frac{d\overline{\beta}}{d\lambda} + \lambda^2\frac{d^2\overline{\beta}}{d\lambda^2}\right], \tag{2.16}$$

where $\overline{\beta} = f(n_j, V)$ and $V = k_0 a\sqrt{n_1^2 - n_K^2}$. The normalized propagation constant $\overline{\beta}$ depends on the wavelength λ since the refractive index n of the silica varies with the wavelength, i.e., material dispersion, and also because the normalized frequency V depends upon the value of a/λ which is the waveguide dispersion. Strictly speaking, the material and waveguide dispersion are not independant. Material dispersion can be obtained by neglecting the waveguide effects in Eq. (2.16) and assuming that the fields can be considered as plane wave with the propagation constant $\beta = 2\pi n/\lambda$. The effect of material on the delay time τ is

$$\tau_m = \frac{L}{c}\left(n - \lambda \frac{dn}{d\lambda}\right). \tag{2.17}$$

Therefore, the material dispersion is

$$D_{mat}(\lambda) = -\frac{\lambda}{c}\frac{d^2 n}{d\lambda^2}. \tag{2.18}$$

The variation curve of the pure silica refractive index versus the wavelength presents an inflection point around 1.27 μm, corresponding to a minimum delay time and to a zero material dispersion. The addition of GeO_2 doping to a pure silica core increases the zero material dispersion wavelength, while fluorine doping decreases zero material dispersion wavelength. The Sellmeier parameters for fused silica, F doped silica, GeO_2 doped silica, P_2O_5 doped silica, B_2O_3 doped silica, and silica doped with GeO_2 and B_2O_3 [49] are used to calculate the material dispersion. The material dispersion in jth layer, $(D_{mat})_j$, is given [49] as

$$(D_{mat})_j = \frac{\lambda}{cn_j}\left[\frac{m_j(n_j - m_j)}{\lambda^2} + \lambda^2 4\sum_{i=1}^{3}\frac{A_{ji}\lambda_{ji}^2}{(\lambda^2 - \lambda_{ji}^2)^3}\right], \tag{2.19a}$$

where refractive index in the jth layer, n_j, is obtained from the Sellmeier equation

$$n_j = \sqrt{\sum_{i=1}^{3} \frac{A_i \lambda^2}{(\lambda^2 - \lambda_i^2)} + 1}\,, \tag{2.19b}$$

and the group index in the jth layer, m_j, is

$$m_j = n_j + \frac{\lambda^2}{n_j} \sum_{i=1}^{3} \frac{A_{ji} \lambda_{ji}^2}{(\lambda^2 - \lambda_{ji}^2)^2}\,, \tag{2.19c}$$

where A_i are constants related to material oscillator strengths, and λ_{ji} are oscillator wavelengths for the material of the jth layer. The parameters of the fitted three-term Sellmeier relationship are listed in reference [49]. Clearly, the total dispersion is a function of wavelength λ and the fiber index profile, i.e.,

$$D_{\text{total}} = f(\lambda,\ \bar{\beta},\ n_j,\ r_{j-1};\quad j = 1,\ 2,\ \ldots k)\,, \tag{2.20}$$

where r_{j-1} is the jth layer inner radius. In Fig. 1, the multi-clad fiber is characterized by nine parameters: four layer thickness aspect ratios $\eta_1 = a/r_1$, $\eta_2 = d/r_1$, $\alpha = b/r_1$, $\gamma = c/r_1$, four indices n_1, n_2, n_3, and n_4 and total core radius r_6. The interplay of these parameters influences the propagation properties of the fiber.

Chapter 3. Design Considerations and Transmission Properties of Broadband Multi-Clad Fiber

The purpose of this study is to address the following points: Designing a single-mode fiber which has (1) the lowest dispersion over a maximum transmission window, (2) a profile structure which lends itself to simple preform manufacturing processes and a structure which has the broadest tolerance to variation of fiber parameters, (3) small index differences between adjacent layers in order to maintain low optical losses, and (4) low splice and bend losses. The fibers are optimized for operation in the 1.3 μm to 1.7 μm wavelength range and have a cutoff wavelength of $\lambda_{c11} < 1.27$. Various fiber structures as shown in Figs. 1 and 2 are analyzed.

3.1. Design Considerations

First, we address the choice of the index profile which would meet the design criteria. The refractive index profile of the proposed multi-clad fiber shown in Fig. 1 is used as a basis for designing broadband fibers. The multi-clad fiber consists of three substructures; one basic structure is a DC structure, the other two are tubular structures. The reason for selecting this structure is that wide bandwidth and the confinement of energy to the core can be simultaneously achieved by a DC structure, and in a tubular structure the modes with on-axis intensity are affected most by the region of the depressed-index. At higher frequencies the energy is more tightly confined to regions of higher index; i.e., the ring portions [54]. Thus, adding raised-index rings to the DC fiber would increase the mode-field radius. It has been shown both theoretically and experimentally that TC and QC fibers may exhibit mulitmode nature. By weakening the intermediate raised-index ring, higher-order modes can be removed and the TC and QC fibers degenerate to DC fibers [45,46] which have been shown to be sensitive to bending [44]. To keep the advantages of the TC and QC fibers and avoid higher-order modes in the low dispersion window, one raised-index ring and one depressed-index ring are added to the QC structure. With this modification, the light leaking from the inner QC waveguide can be retrapped within the waveguide formed by additional layers, resulting in a greater prevention of higher-order modes. In addition, the outermost depressed-index ring is made thicker than the inner layers to further suppress higher-order modes. Thus, higher-order modes can be suppressed sufficiently so that their influence becomes negligible, while the LP_{01} mode continues to propagate with a relatively low loss.

Fiber structures with depressed inner claddings, shown in Fig. 1 have many interesting features which have been emphasized both theoretically and experimentally: (1) compared with single-clad structures, they allow a lower GeO_2 concentration in the core, and thus smaller intrinsic losses for given overall index differences [55,56]. (2) they have a larger mode-field radius than the conventional single-clad structures thus reducing the problem of splicing, and (3) they have a very low chromatic dispersion over a wide spectral range [27-29].

On the other hand, our investigation indicates that index profile with raised-index outer rings, as shown in Figs. 2.3 and 2.4, result in a smaller dispersion-flattened wavelength range and are more sensitive to bending than the profiles with depressed-index outer rings. It has been shown experimentally that the dispersion characteristics of 4-layer fiber are less sensitive to macrobending than those of 6-layer fiber [57].

The depressed-index outer ring increases the single-mode operation wavelength range, while keeping higher-order modes away from the dispersion-flattened wavelength range and making the designed fiber strictly single-mode. Hence, in DFSM fiber design, a profile with depressed-index outer ring is preferred. The design with a raised-index outer ring is not generally a single-mode fiber. In addition, its dispersion-flattened curve is more sensitive to manufacturing tolerances.

3.2. Modal Properties

The requirement that the designed fiber be single-mode is the most important aspect in this design. Care must be taken to ensure that the multi-clad fiber has a sufficiently high normalized LP_{11} mode cutoff frequency, noting that the LP_{01} mode al-

ways propagates. That is, we wish to find a bandwidth as wide as possible over which the fiber remains single-mode. The upper limit of the mode cutoff wavelength at 2.05 μm is chosen to be close to the operating window with an adequate safety margin. The lower limit of 1.20 μm ensures a reasonably wide tolerance while also permitting sufficient guiding at 1.55 μm . The choice of a mode-field radius between 3 μm and 5 μm is made as a compromise (for low splice loss) between wavelengths of 1.3 μm and 1.55 μm. Equation (2.2b) is used to estimate the normalized cutoff wavelengths of the LP_{01} , LP_{02}, and LP_{11} modes with known normalized cutoff frequencies, core radius, and the maximum core index and outermost cladding index. Large LP_{11} mode cutoff frequency implies a large fiber core diameter; this will increase layer thicknesses so that the dimensional sensitivity of the multi-clad fiber will be reduced.

Table 2 summarizes the parameters for six fibers which have been optimized for the desired transmission properties. In this Table, $\Delta n_j = |n_0^2 - n_j^2|/2n_j^2$ for j = 1, 2, 3, $\eta_1 = a/r_1$, $\eta_2 = d/r_1$, $\alpha = b/r_1$, and $\gamma = c/r_1$. The index differences have been calculated at a wavelength λ = 1.3 μm, and the index of the reference layer n_0 = 1.446918 for fibers no. 2, 5, and 6; n_0 = 1.444817 for fibers no. 3 and 5; and n_0 = 1.450875 for fiber no. 1. From Tables 2 and 3, we can observe that: (1) when the average layer thickness increases the cutoff frequencies of the LP_{01} and LP_{11} modes also increase so that the range of single-mode operation of the multi-clad fiber can be extended toward a longer wavelength by an appropriate choice of the fiber layer thickness ratios, (2) when the total core radius, r_6, increases, the mode-field radius increases, and (3) smaller layer index differences produce a larger mode-field radius, and a larger mode-field radius results in a smaller dispersion-flattened window.

Cladding materials for 7-layer fibers are presented in Table 4. The material compositions are shown in Appendix B.

Table 2. Index profile parameters for 7-layer fibers

Fiber	Δn_1	Δn_2	Δn_3	η_1	α	γ	η_2	r_6
1	0.338%	0.158%	0.433%	1.055	1.400	2.400	2.500	35.0
2	0.323%	0.153%	0.322%	1.290	1.450	2.000	2.500	35.0
3	0.418%	0.183%	0.201%	1.630	1.200	4.000	3.990	39.0
4	0.418%	0.145%	0.201%	1.344	1.400	3.515	3.550	38.0
5	0.379%	0.153%	0.322%	1.350	1.411	2.000	2.640	32.25
6	0.273%	0.153%	0.322%	0.874	1.144	2.500	2.500	39.25

Table 3. 7-layer fiber performance data

Fiber	λ_{c01}	λ_{c11}	$\omega_{1.3}$	$\omega_{1.55}$	DF (< 1 ps/km-nm)
1	1.66	1.24	3.19	4.03	1.32 - 1.67
2	1.71	1.30	3.44	4.28	1.33 - 1.66
3	1.86	1.21	3.25	4.20	1.33 - 1.67
4	2.01	1.22	3.12	4.14	1.33 - 1.68
5	1.71	1.19	3.31	3.97	1.33 - 1.72
6	1.85	1.26	3.24	4.93	1.31 - 1.66

- the units for cutoff wavelength λ_c are μm.
- the units for mode-field radius ω are μm. The definition of mode-field radius is in Section 3.2.3.

Table 4. Cladding materials for 7-layer fibers

Fiber	*layer 1*	*layer 2*	*layer 3*	*layer 4*	*layer 5*	*layer 6*	*layer 7*
1	M8	M9	M2	M9	M2	M9	M3
2	M6	M12	M10	M12	M10	M12	M1
3	M3	M11	M4	M11	M4	M11	M5
4	M3	M11	M1	M11	M1	M11	M5
5	M7	M12	M10	M12	M10	M12	M1
6	M3	M12	M10	M12	M10	M12	M1

3.2.1. Propagation Constant $\bar{\beta}$ and Cutoff Frequencies

To obtain the normalized propagation coefficient $\bar{\beta}$ as a function of frequency, the dispersion equation (2.6) is solved numerically using the root search technique.

For the 7-layer fibers in Table 3, the normalized cutoff frequency for the LP_{01} mode is in the range 14 to 17.5, and the LP_{11} mode is in the range of 21 to 27. Figure 3 represents the V_c value of the normalized frequency V at cutoff as a function of $\Delta n_2/\Delta n_1$ for fiber no. 4 in Table 2. We notice that the fundamental mode LP_{01} has a nonzero cutoff value, and as the ratio $\Delta n_2/\Delta n_1$ decreases, the LP_{01} mode cutoff separates from the LP_{11} mode cutoff, while the separation of the LP_{02} mode cutoff and the LP_{11} mode cutoff remains almost constant. It is also verified that increasing Δn_3 and decreasing Δn_1 and Δn_2 simultaneously causes V_{c01} and V_{c11} to increase.

The depressed refractive index layer thickness must be large enough ($\gamma > 1$, $\eta_2 > 1$, or $\Delta n_1 > \Delta n_2$) for the dispersion characteristic to be modified as shown in Ta-

bles 2 and 3. When α is reduced and γ and η_2 are increased, λ_{c11} moves toward shorter wavelengths and the λ_{c01} moves toward longer wavelengths, resulting in an increase in the span of the single-mode operating window. The migration of λ_{c11} is much more rapid than that of λ_{c01} . Increasing Δn_3 moves λ_{c01} and λ_{c11} toward lower wavelengths. Thus, by increasing or decreasing Δn_3, the center of the dispersion-flattened window can be adjusted.

3.2.2. *Dispersion Curves*

Dispersion spectra and $\overline{\beta} - V$ curves for the fibers listed in Tables 2 and 3 are presented in Figs. 4 and 5. Dispersion curves are obtained by the optimization method in Chapter 6. Here six design examples are presented. Figure 4 shows six dispersion-flattened spectra (data are listed in Tables 2, and 3). Figure 5 shows the $\overline{\beta} - V$ curves for the corresponding dispersion curves in Fig. 4. From Fig. 5, we notice that in order to fit the dispersion-flattened window into a single-mode operating range, one should choose a difference for the cutoff frequencies of LP_{01} and LP_{11} larger than 10. Designs in Figs. 5.1 and 5.5 demonstrate that the dispersion-flattened window is too close to the LP_{01} mode cutoff. Figure 5.2 shows that a small portion of the dispersion-flattened window is beyond the LP_{11} mode cutoff. Figures 5.3, 5.4, and 5.6 are the best designs among those illustrated.

3.2.3. *Mode-Field Radius*

Mode-field radius can provide a qualitative measure of splice and bend losses, and is thus an important transmission property of a fiber.

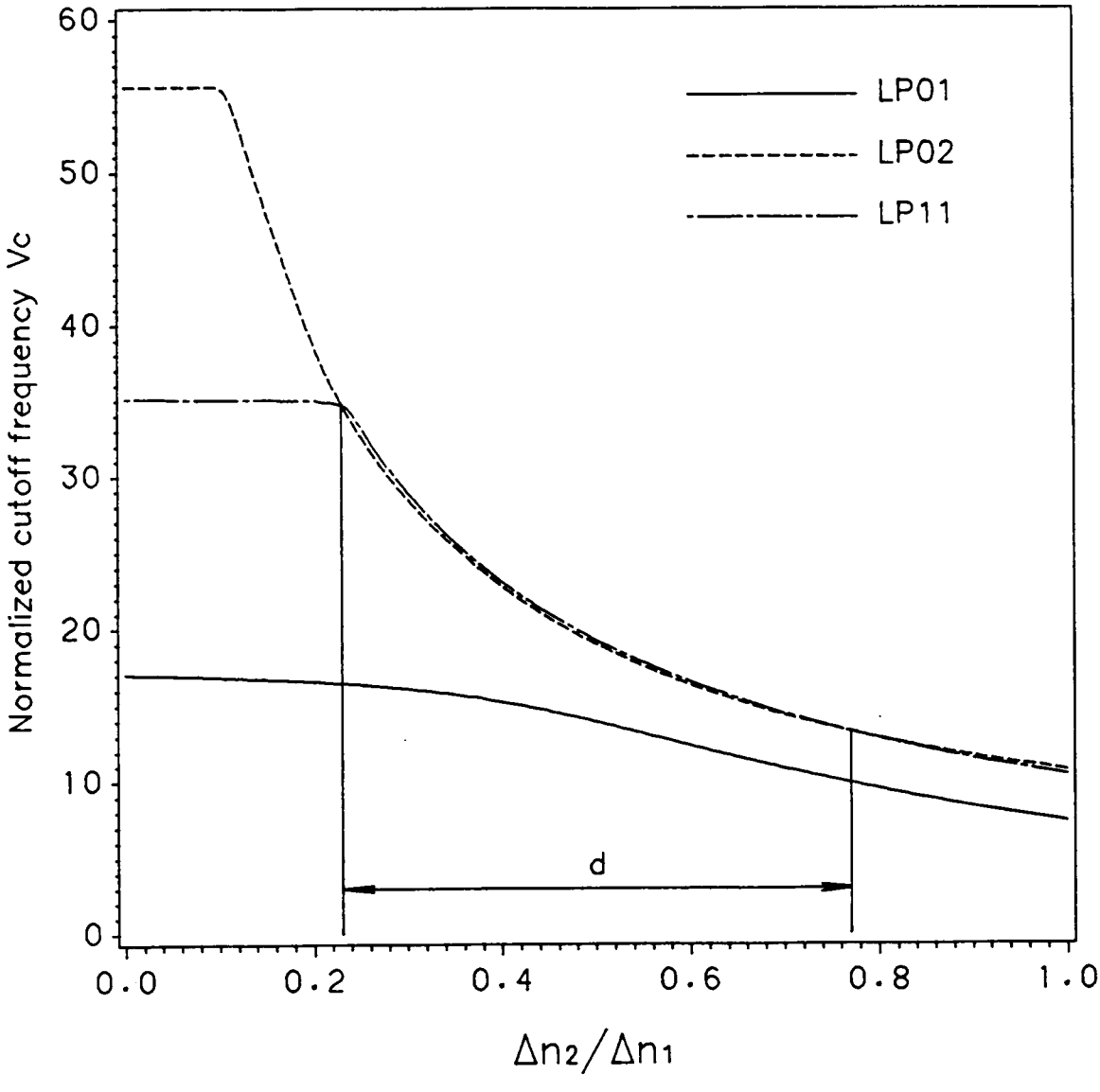

Figure 3. Normalized frequency at cutoff, V_c, versus $\Delta n_2/\Delta n_1$ for optimum fiber no. 4. In the range d the LP_{02} mode is guided, whereas the LP_{11} mode is leaky.

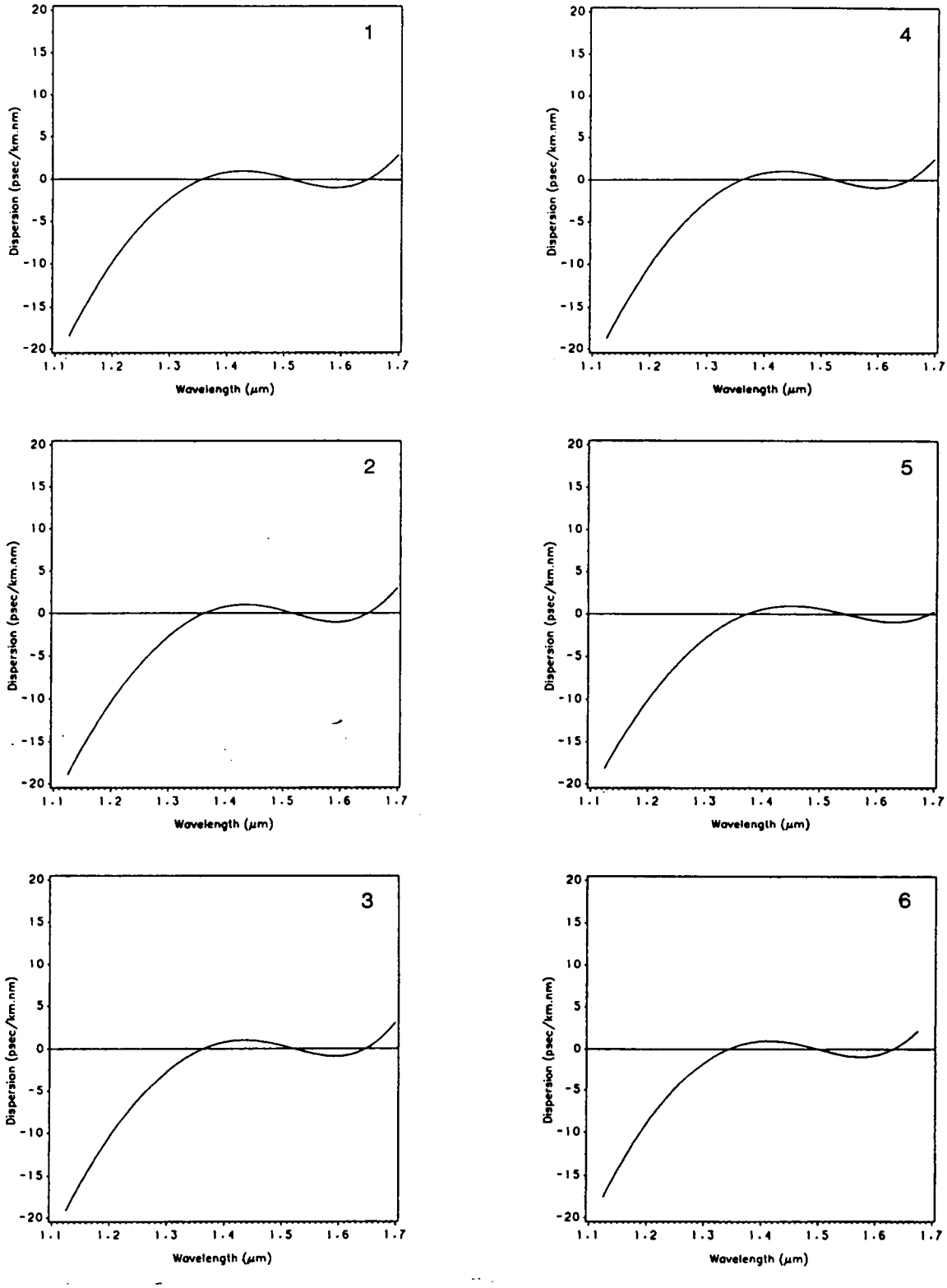

Figure 4. Dispersion curves for the 7-layer fibers in Table 2.

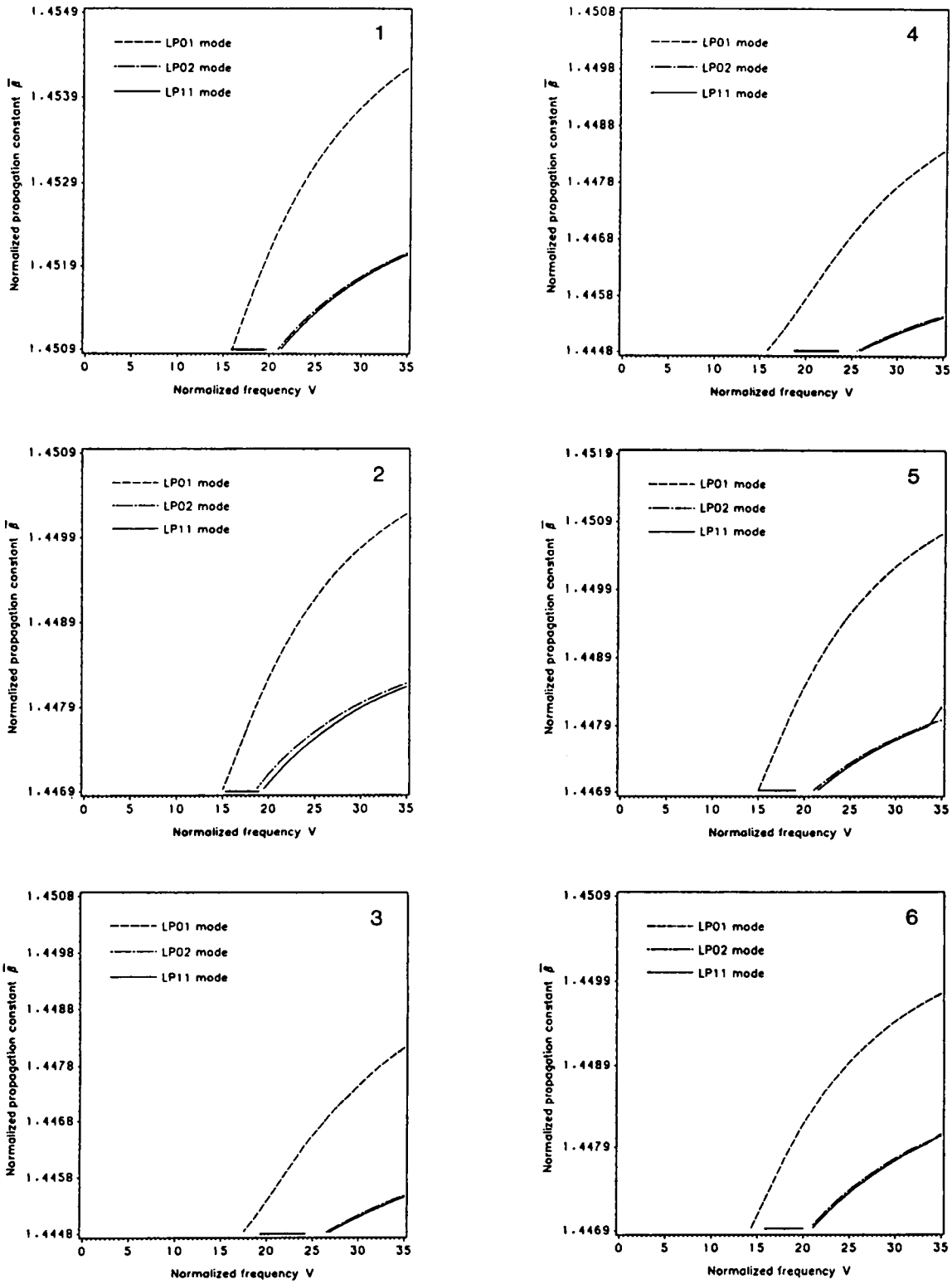

Figure 5. $\bar{\beta} - V$ curves for the 7-layer fibers in Table 2.

When $\bar{\beta}$ is known, plots of the field distribution $\Psi(r, \varphi)$ can be obtained. Equations (2.3a,b) can be solved for field coefficients A_j and B_j (A_1 is determined from the source condition), or we can obtain a field distribution directly from Eqs. (2.9,2.10).

To minimize intrinsic scattering and splice loss, the power should be spread over a large radial region. A large mode-field radius is also beneficial, since power distributed over regions with different indices and dispersions can significantly alter the total waveguide dispersion. However, microbend and macrobend losses are minimized by designs which restrict the mode-field distribution. These physical requirements are in obvious conflict. For the QC fibers, a mode-field radius of 4.3 μm to 4.5 μm has been suggested [34].

To reduce the splice loss, the DFSM fiber must have a reasonable mode-field radius for the fundamental mode. However, when the bend loss effects are considered, the fiber should be designed with a smaller mode-field radius, in the range of 3 μm to 5 μm. The mode-field radius is calculated by the second Petermann definition of mode-field radius [58] which can be used to predict microbend and splice losses.

$$\omega_0^2 = 2\frac{\int_0^\infty \Psi^2(r) r dr}{\int_0^\infty \left(\frac{d\Psi(r)}{dr}\right)^2 r dr}, \tag{3.1}$$

where $\Psi^2(r)$ is the near-field intensity distribution as a function of radial coordinate r. It is the solution of the scalar wave equation under the weakly guiding assumption. One of the key advantages of using Eq. (3.1) to define mode-field radius is that the 7-layer fiber field distribution does not resemble a Gaussian form. Another benefit derives from the fact that this definition is able to accurately predict the splice losses

incurred between single-mode fibers with small lateral offsets. Equation (3.1) is solved by IMSL routine DIVPRK. For $r > r_k$, $\Psi(r)$ is approximated by Eq. (2.8b).

3.2.4. *Splice Loss Calculations*

In addition to intrinsic fiber losses (Rayleigh scattering and absorption losses), two other main loss components in single-mode waveguide systems are splice and microbend losses. Splice loss consists of lateral offset loss, angular offset loss, and longitudinal separation loss. To have a measure of splice loss, here we only consider lateral offset loss.

Lateral offset loss is computed in terms of the power transmission coefficient, which is in turn a ratio of power accepted by the receiving fiber to the power emitted by the transmitting fiber. For single-mode fibers this is equivalent to calculating the overlap integral of the modal fields of the two fibers while giving appropriate consideration to any defects.

$$\rho = \frac{4\int_0^\infty \int_0^\infty \Psi\left(\sqrt{(x-d)^2 + y^2}\right)\Psi\left(\sqrt{(x+d)^2 + y^2}\right)dxdy}{2\pi\int_0^\infty |\Psi(r)|^2 r dr}, \tag{3.2}$$

where d is the lateral offset. The offset loss in dB is

$$Loss_{offset} = -10 \log_{10}\rho . \tag{3.3}$$

Again, Eq. (3.2) is solved by IMSL routine DIVPRK. For $r > r_k$, Ψ is approximated by Eq. (2.8b). Calculations of splice loss are presented in Section 5.4.

Chapter 4. Tolerance Effects of Seven-Layer Fiber

Much research has been dedicated to the minimization of chromatic dispersion by designing fibers with propagation characteristics such that the material dispersion is compensated by the waveguide dispersion. If these two effects are to exactly cancel each other only small tolerances can be permitted in the manufacturing process [59].

In designing DFSM fibers, dispersion is one property that imposes strict limits on production tolerances. The dispersion characteristics of DC, TC, and QC fibers are quite sensitive to dimensional tolerances, and cause serious manufacturing problems. In this study, this sensitivity is reduced by increasing the cladding thickness ratios η_1, α, γ , η_2 and total core radius r_6. The reason for this is that the influence of fields on the outer layer is greatly reduced when the thicknesses of the inner layers are increased. By increasing the ratios η_1, α, γ , η_2 and total core radius r_6, the waveguide cutoff frequency is increased as was discussed in Section 3.2.

First we will discuss the relationship between dispersion properties for 7-layer fiber around the nominal zero-dispersion wavelength λ_0 and the relative standard deviations σ_a/a and σ_Δ/Δ on the two scale parameters of the index profile which are

total core radius, a ($= r_6$), and maximum index difference Δ. Then actual dispersion versus radius tolerances and total core radius will be presented.

4.1. Dispersion-Determined Limits on Design Tolerances of DFSM Fibers

In single-mode fibers the chromatic dispersion D_{total} consists of two components: the material dispersion D_{mat} and the waveguide dispersion D_{wg}. D_{mat} closely resembles the material dispersion of fused silica for the lightly doped single-mode fibers. The total dispersion in single-mode fibers may therefore be obtained from

$$D_{\text{total}} = D_{wg} + D_{mat} . \tag{4.1}$$

Using Eq. (4.1) the sensitivity of the dispersion to core and index variations at the zero-dispersion wavelength can be expressed approximately using scalar wave theory as [60]

$$a \frac{dD_{\text{total}}}{da} = D_{mat} + \lambda D'_{mat} - \lambda D'_{\text{total}} , \tag{4.2a}$$

$$\Delta \frac{dD_{\text{total}}}{d\Delta} = \frac{1}{2} (- D_{mat} + \lambda D'_{mat} - \lambda D'_{\text{total}}) , \tag{4.2b}$$

where the prime denotes differentiation with respect to λ. The IMSL routine DDERIV [61] is used to calculate the differentiations. Equations (4.2a,b) mean that the sensitivities do not depend explicitly on the index profile but only on the wavelength slope of the total dispersion $D'_{total}(\lambda_0)$. Since the standard deviations σ_a and σ_Δ are nearly uncorrelated, assuming that total core radius, a, and index difference Δ are the main factors causing dispersion variations, the standard deviation of the dispersion [60] is

$$\sigma_D = \sqrt{\left(\frac{\sigma_a}{a} a \frac{dD_{\text{total}}}{da}\right)^2 + \left(\frac{\sigma_\Delta}{\Delta} \Delta \frac{dD_{\text{total}}}{d\Delta}\right)^2} \ . \tag{4.3}$$

If $D'_{\text{total}}(\lambda_0) \geq 0$ in Eqs. (4.2, 4.3), a maximum value of σ_a/a as a function of σ_Δ/Δ can be found while keeping $\sigma_D \leq D_{\text{max}}$. This means that minimum requirements can be determined for quality control to produce DFSM fiber with a flat dispersion curve around the nominal zero-dispersion wavelength λ_0. Figure 6 indicates maximum allowable production tolerances, σ_a/a and σ_Δ/Δ (for σ_D = 0.96 ps/km-nm), for fiber no. 4 at nominal zero-dispersion wavelengths of 1.35 μm, 1.51 μm, and 1.65 μm. Figure 6 indicates that if σ_a/a = 0, σ_Δ/Δ should be less than 7.5% when λ_0 = 1.65 μm, less than 2.4% when λ_0 = 1.35 μm, and less than 1.6% when λ_0 = 1.51 μm. This relationship shows that (1) it is easier to produce a fiber with local dispersion-flattening around 1.65 μm than to produce one with dispersion-flattening around 1.35 μm , as shown in Figs. 7, 8, 9, and 12. (2) strict control of tolerances is required to produce a fiber with local dispersion-flattening around 1.51 μm. This also has been shown in Figs. 7, 8, 9 and 12. Statement (1) is obvious since, as wavelength increases, the rate of increase for material dispersion is far less than the rate of decrease for the first-order derivative of the material dispersion. Statement (2) indicates that negative $D'_{\text{total}}(\lambda_0)$ will require that production tolerances to be tightly controlled. This also demonstrates the reason for the poor reproducibility of the DC, TC, and QC fibers since these fibers have a large negative $D'_{\text{total}}(\lambda_0)$ in their second zero-dispersion wavelength around 1.55 μm. Therefore, a $D'_{\text{total}}(\lambda_{1.55}) \geq 0$ is recommended for the design of a DFSM fiber. A larger σ_D implies that a larger σ_a/a and a larger σ_Δ/Δ can be allowed.

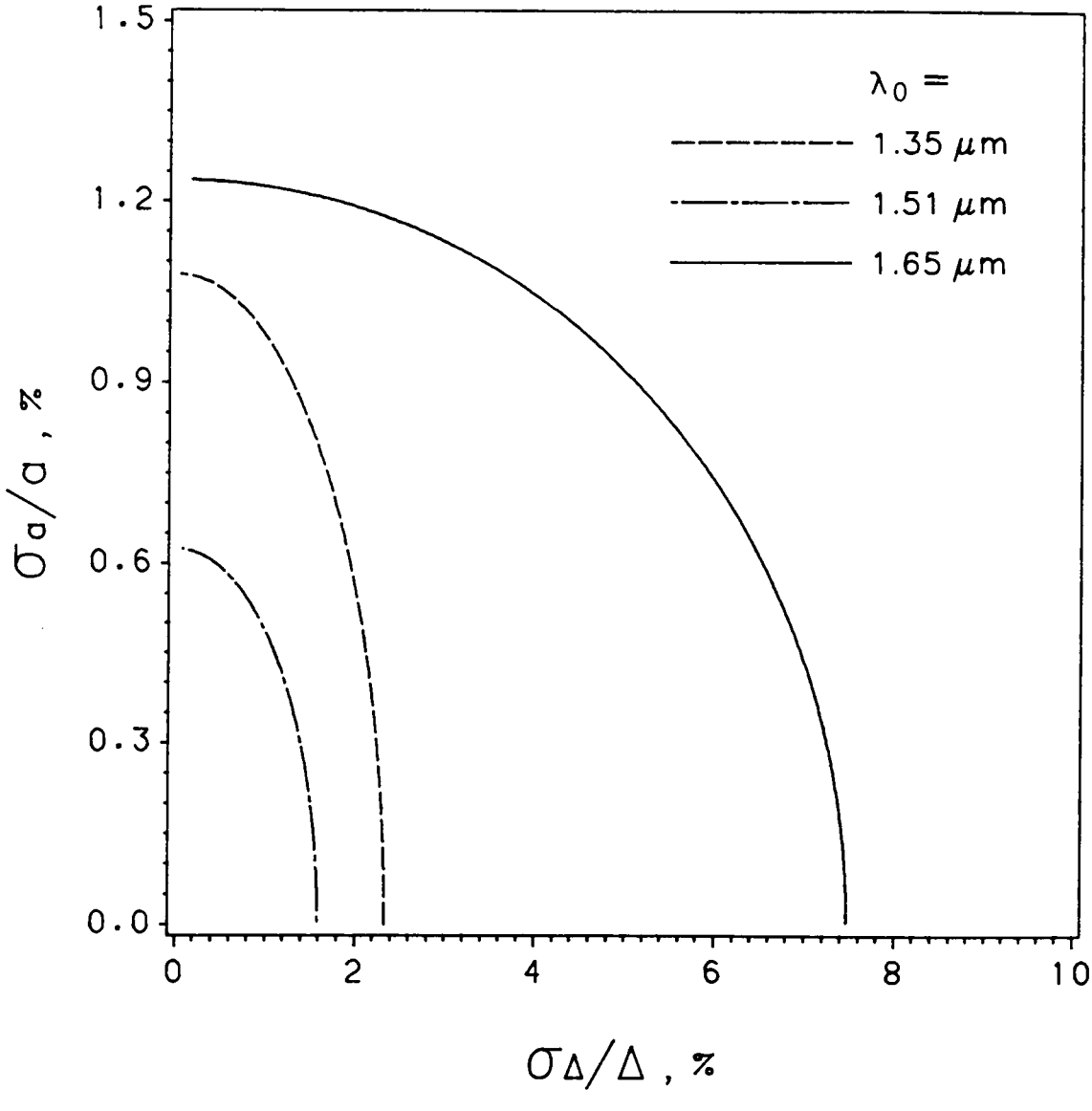

Figure 6. Maximum allowable production tolerances σ_a/a and σ_Δ/Δ for fiber no. 4 dispersion-flattened at $\lambda_0 = 1.35\ \mu m$ (solid line), $\lambda_0 = 1.51\ \mu m$ (broken line), and $\lambda_0 = 1.65\ \mu m$ (broken dot line).

4.2. Sensitivity to Parameter Variations

In this Section dispersion sensitivities to radius tolerances are discussed. The analysis shows the tolerance effect of two layer thicknesses on dispersion characteristics.

When fabricating fibers, the zero-dispersion wavelength of actual fiber responds sharply to tolerance effects, so that the analysis of tolerance effects is of considerable importance. The fiber index profile tolerance, chemical fluctuations, and the mole percentage of dopant concentrations on the substrates must be considered to estimate the degree of control that must be exercised during the production process. The tolerance analysis is based on the wave equation of the fiber for each layer thickness and on core radius variations.

The deviation in dispersion δD is [62]

$$\delta D = \sum_{j=1}^{k} \frac{\partial D}{\partial \Delta_j} \delta \Delta_j + \sum_{j=1}^{k} \frac{\partial D}{\partial S_j} \delta S_j, \tag{4.4}$$

where $\delta \Delta_j$ is the jth layer index error and δS_j is the jth layer thickness error.

For fiber no. 4, when the total dispersion $D_{total}(\lambda, x_i)$ (where x_i represents layer indices, layer radii, and total core radius) is examined as a function of the six layer radii, r_1, r_2, r_3, r_4, r_5, and total core radius r_6 individually, the following is observed:

Keeping all other parameters constant, when r_1 is increased, the third zero-dispersion point moves toward lower wavelengths, as shown in Fig. 7. When r_1 increases further, the first and second zero-dispersion point appear, then the second zero-dispersion point is shifted to longer wavelengths, and finally the second and the third zero-dispersion points disappear. Calculated values of $\partial D/\partial r_1$ show that at the

1.52 μm zero-dispersion point, the magnitude of $\partial D/\partial r_1$ is less than 40 ps/km-nm-μm. The degree of tolerance allowed in the variation of δr_1 can be calculated for a specified dispersion δD . For example, we have a 100 km length fiber and a transmission rate of 1 Gbit/sec. If a laser diode of 5 nm spectral width is used, the chromatic dispersion deviation δD from zero is required to be 2 ps/km-nm. The absolute tolerance value δr_1 is then ± 0.05 μm for the value of $\partial D/\partial r_1 = 40$ ps/km-nm-μm.

Figure 8 shows that when r_2 increases, the third zero-dispersion point nearly remains within the 1.65 - 1.68 μm range. When r_2 increases further, the first and the second zero-dispersion points appear, and finally the second and the third zero-dispersion points disappear and the first zero-dispersion point moves toward lower wavelengths. Calculated values of $\partial D/\partial r_2$ show that at the 1.52 μm zero-dispersion point, the magnitude of $\partial D/\partial r_2$ is less than 15 ps/km-nm-μm. The degree of tolerance allowed in the variation of δr_2 can be calculated for a specified dispersion δD . With the same example, the chromatic dispersion deviation δD from zero is required to be 2 ps/km-nm. The absolute tolerance value δr_2 is then ± 0.13 μm for the value of $\partial D/\partial r_2 = 15$ ps/km-nm-μm.

Figure 9 shows that when r_3 increases, the first zero-dispersion point moves from 1.34 μm to longer wavelengths slowly, and with further increases in r_3, the second and the third zero-dispersion points appear. Finally, the first and second zero-dispersion points disappear and the third zero-dispersion point moves toward longer wavelengths. Calculated values of $\partial D/\partial r_3$ show that at the 1.52 μm zero-dispersion point, the magnitude of $\partial D/\partial r_3$ is less than 10 ps/km-nm-μm. The degree of tolerance allowed in the variation of δr_3 can be calculated for a specified dispersion δD . With the same example, the chromatic dispersion deviation δD from zero is required to be 2 ps/km-nm. The absolute tolerance value δr_3 is then ± 0.20 μm for the value of $\partial D/\partial r_3 = 10$ ps/km-nm-μm.

Figure 10 shows that the values of $\partial D/\partial r_4$ are always small if the tolerance values of δr_4 are positive. By contrast, Fig. 11 shows that the values of $\partial D/\partial r_5$ are always small if the tolerance values of δr_5 are negative.

Figure 12 shows that when a $(=r_6)$ increases, the third zero-dispersion point almost remains within the 1.63 - 1.68 μm range. When a increases further, the first and the second zero-dispersion points appear, and finally, the second and the third zero-dispersion points disappear and the first zero-dispersion point moves toward lower wavelengths. Calculated values of $\partial D/\partial a$ show that at the 1.52 μm zero-dispersion point, the magnitude of $\partial D/\partial a$ is less than 9 ps/km-nm-μm. The degree of tolerance allowed in the variation of δa can be calculated for a specified dispersion δD . With the same example, the chromatic dispersion deviation δD from zero is required to be 2 ps/km-nm. The absolute tolerance value δa is then ± 0.22 μm for the value of $\partial D/\partial a$ = 9 ps/km-nm-μm. For fiber no. 4 the drawing tolerance requirements have been estimated to be $\pm$ 1.2 μm with a diameter of $2a$ in order to maintain satisfactory performance.

In summary, variations in dispersion are most sensitive to changes in r_1 . It is seen that the tolerance effects of r_4 are opposite to those of r_5 . The tolerances of r_4 and r_5 tend to cancel each other when r_4 and r_5 increase or decrease simultaneously. The case of r_1 and r_3 and of r_2 and r_3 are similar. The outside layer thickness tolerances are relaxed (one sided), but the inner layer thickness tolerances are extremely tight. Preparation of a dispersion-flattened single-mode 7-layer fiber with dispersion below 2.8 ps/km-nm and with three zero-dispersion wavelengths in the spectral range between 1.3 μm and 1.7 μm requires control of the drawing tolerance to less than $\pm 2.4\%$, as shown in Fig. 12. These requirements are less stringent than those for the case presented in reference [30]. However, the central core radius should not change more than 1.6% for the dispersion to remain less than 2.5 ps/km-nm, as

shown in Fig. 7. When both errors $\delta\Delta_j$ and δS_j exist, both influences are combined, as shown in Eq. (4.4).

Dispersion spectral regions with a positive dispersion slope, for example, the first or the third zero-dispersion wavelengths, require less rigid production tolerances than spectral regions with a negative dispersion slope, for example, the second zero-dispersion wavelength, where the sensitivity coefficients exceed the 'ideal' coefficients $a\frac{dD}{a} \simeq 125$ ps/km-nm and $\Delta\frac{dD}{d\Delta} \simeq 40$ ps/km-nm [63]. Since the dispersion slope at the first zero-dispersion point is always positive, care must be taken at the second zero-dispersion wavelength. At present only two types of dispersion-flattened spectra, quadratic and sinusoidal, have been found. Considering design tolerance a sinusoidal dispersion curve is preferred, since the dispersion slope at the third zero-dispersion point is always ≥ 0. This would fully capitalize upon the low D'_{mat} at longer wavelengths and reduce dispersion sensitivity coefficients resulting in relatively flexible production tolerances for certain dispersion requirements.

In order to obtain accurate tolerance requirements for the various parameters, Δ_j and S_j should be centered random variables with uniform probability laws. Detailed analysis can be found in reference [62].

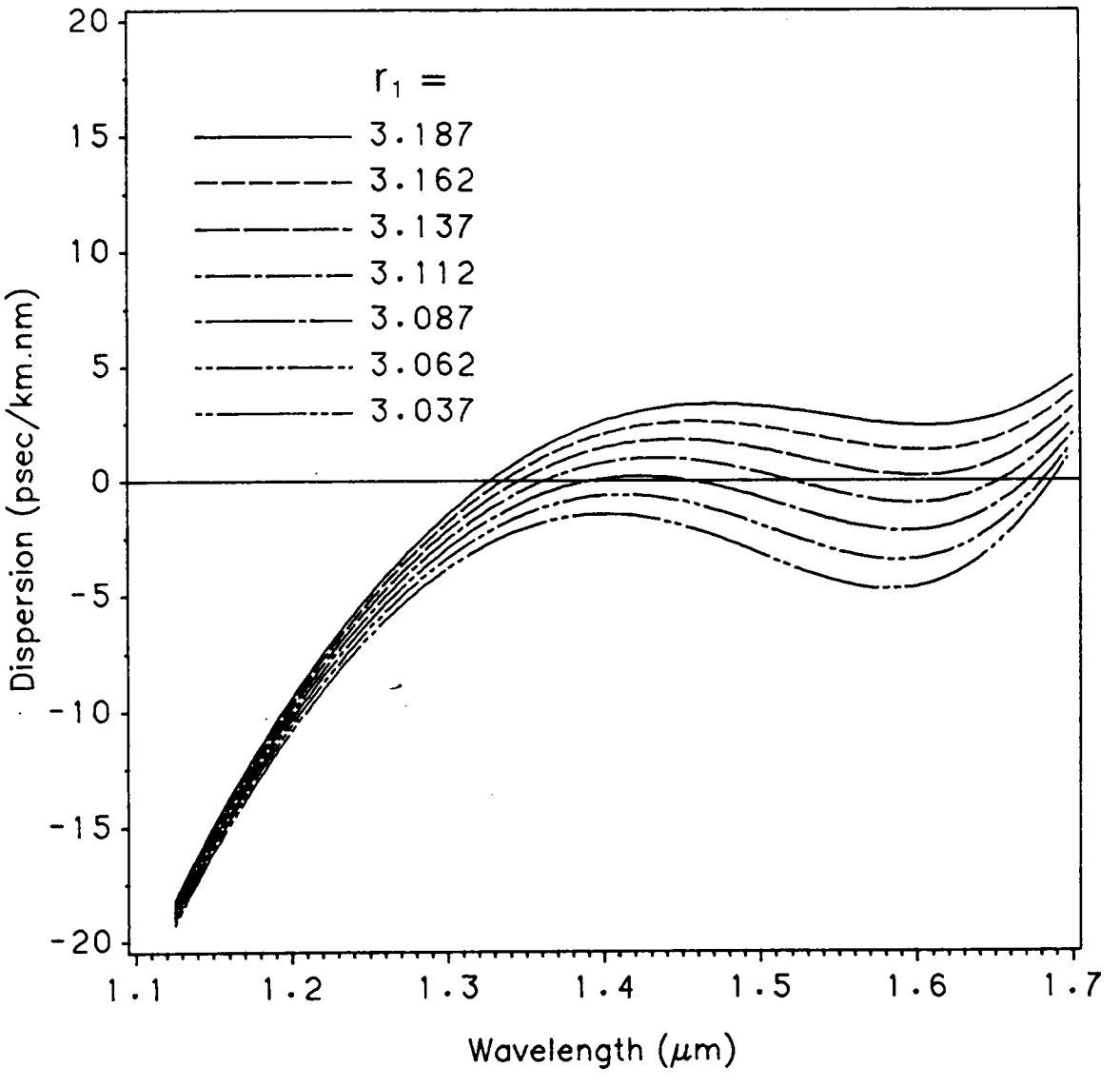

Figure 7. Variations of dispersion for fiber no. 4 as a function of r_1 for constant r_2, r_3, r_4, r_5, and r_6.

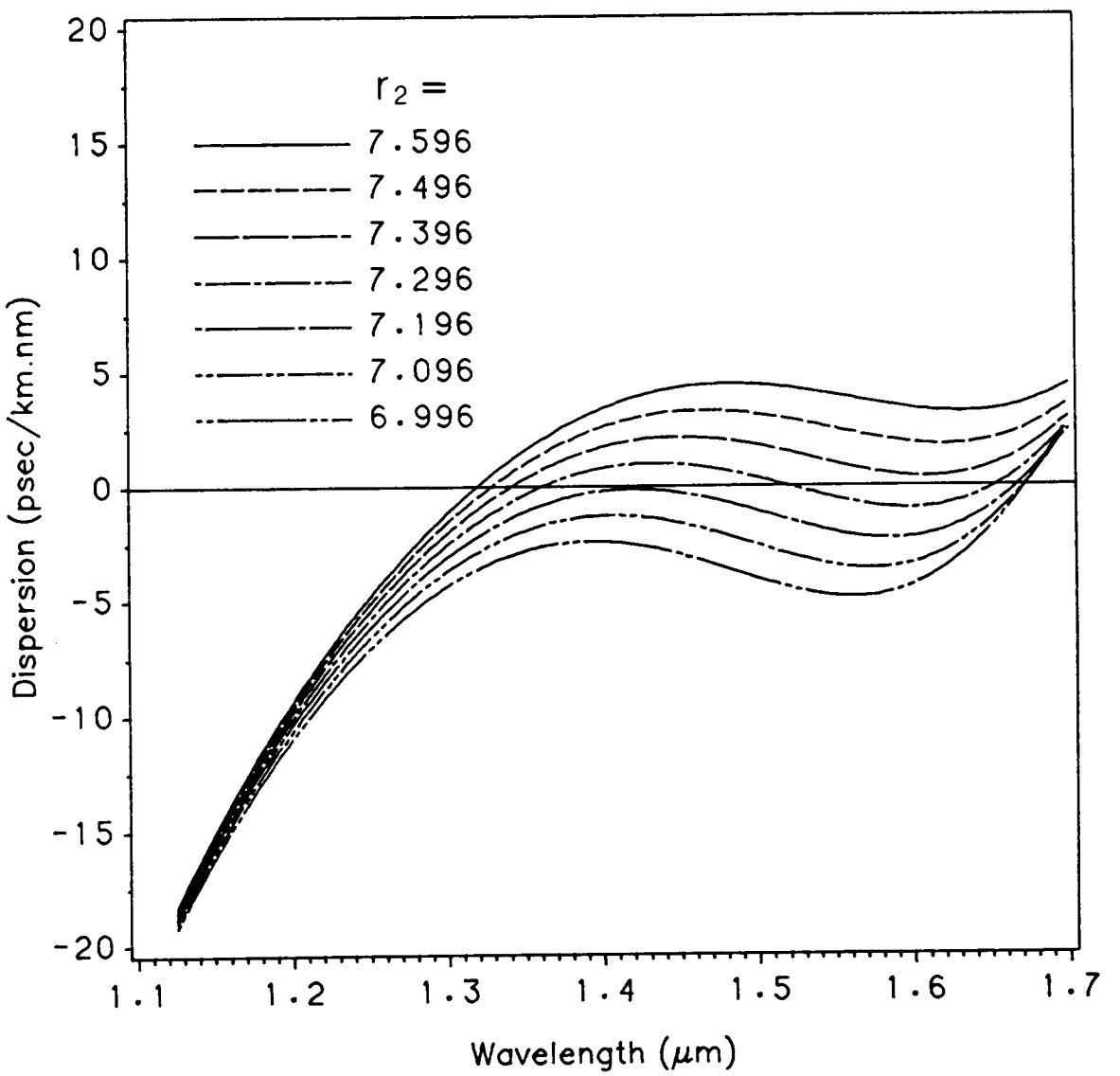

Figure 8. Variations of dispersion for fiber no. 4 as a function of r_2 for constant r_1, r_3, r_4, r_5, and r_6.

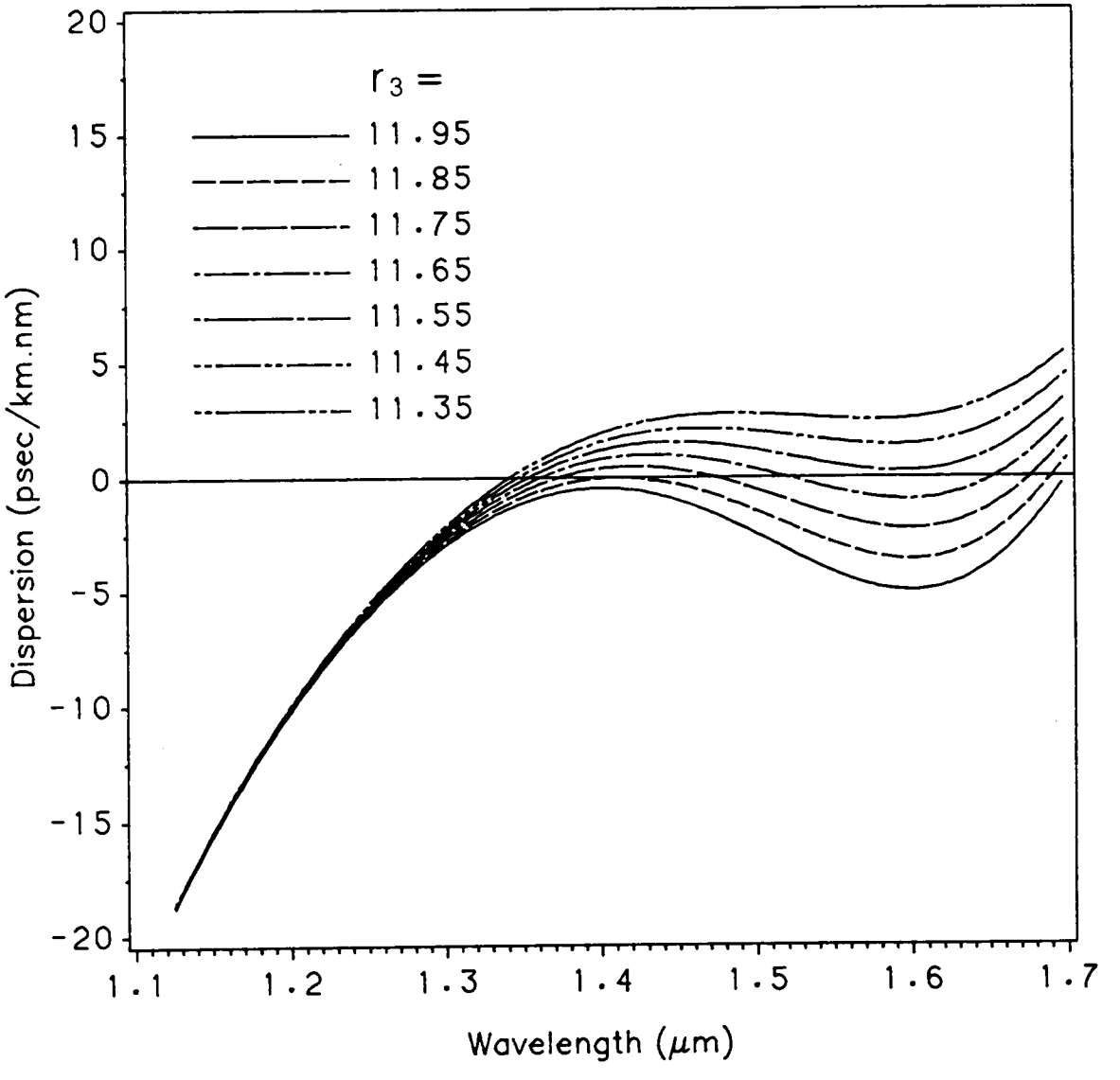

Figure 9. Variations of dispersion for fiber no. 4 as a function of r_3 for constant r_1, r_2, r_4, r_5, and r_6.

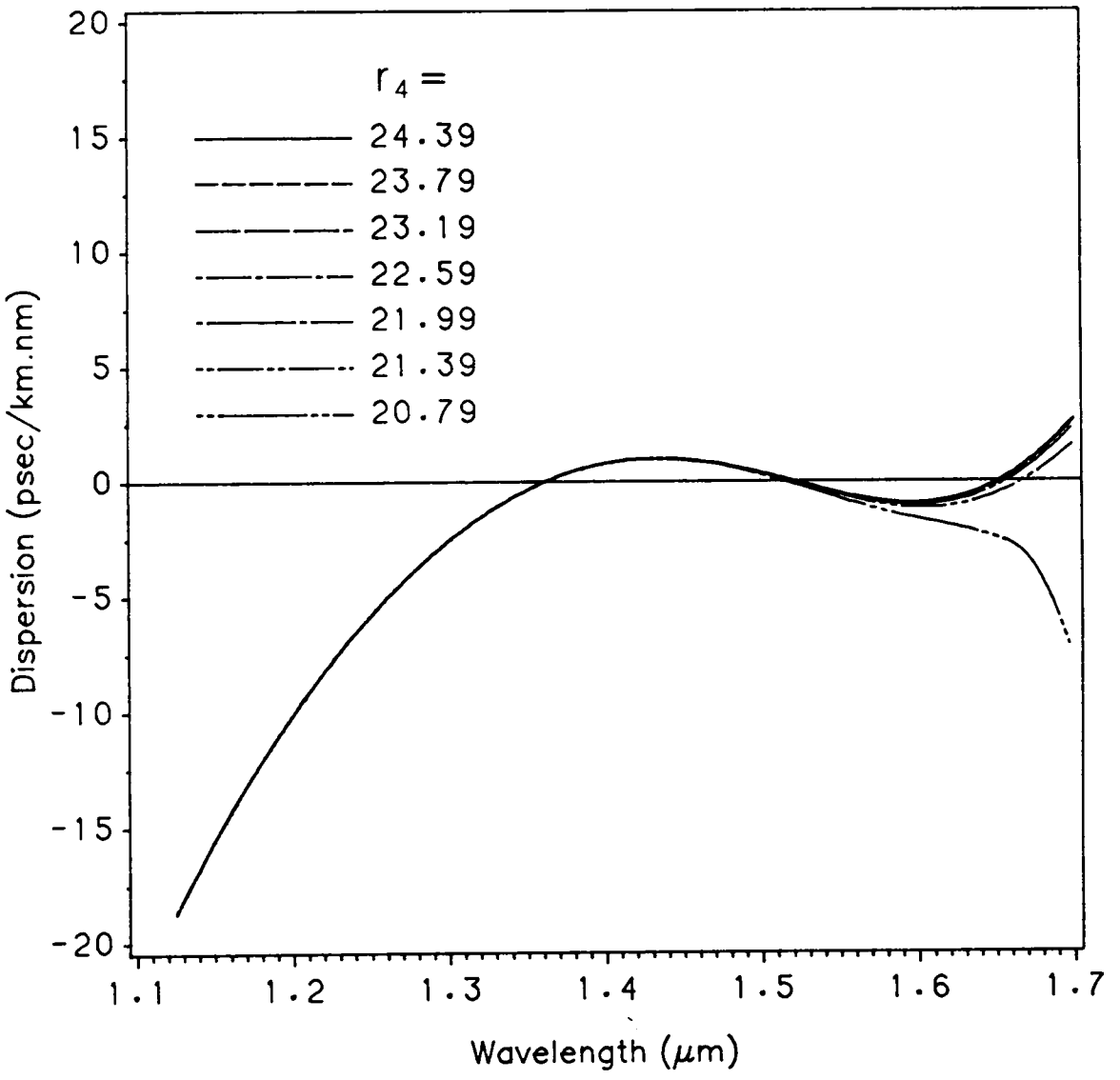

Figure 10. Variations of dispersion for fiber no. 4 as a function of r_4 for constant r_1, r_2, r_3, r_5, and r_6.

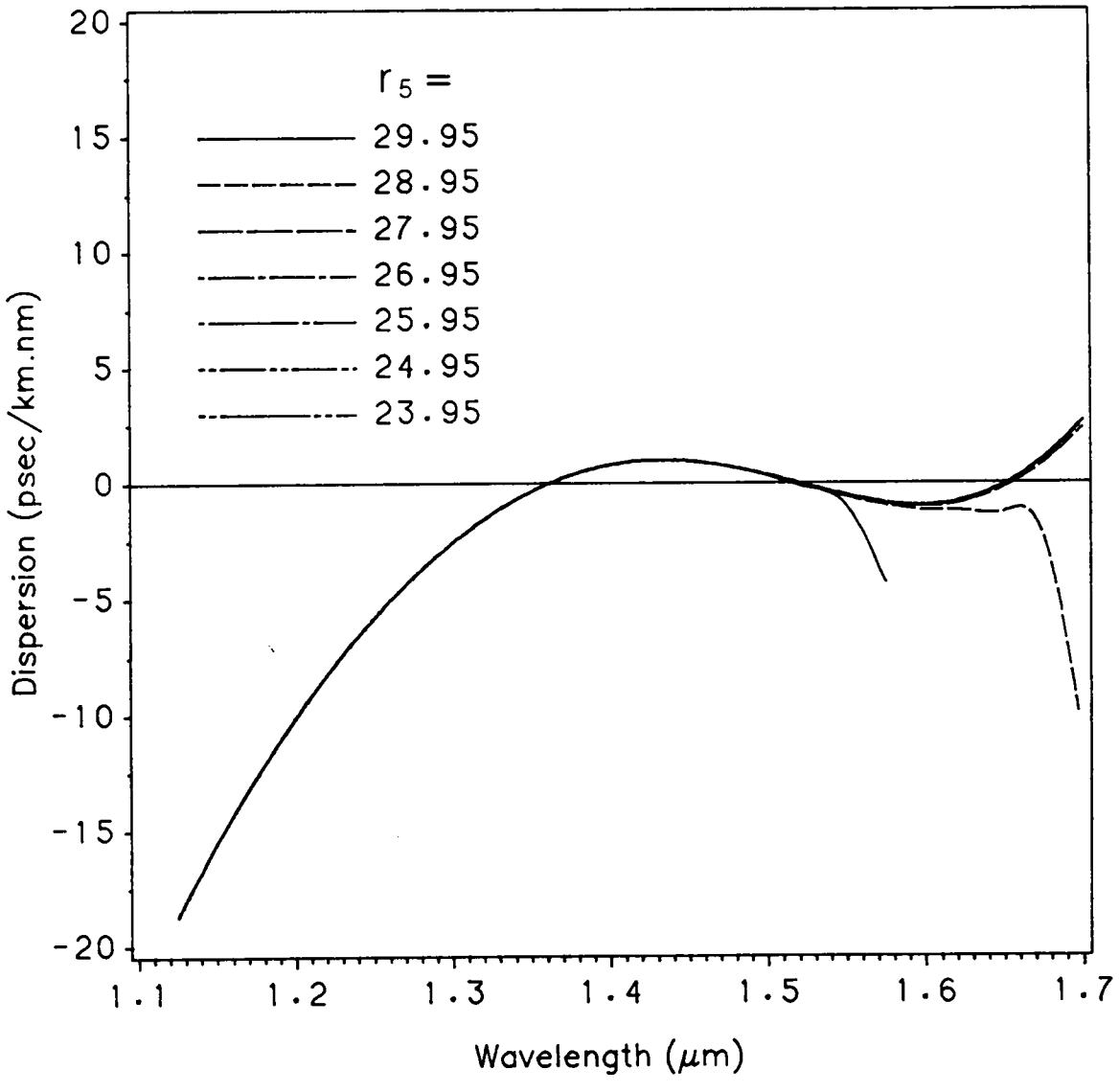

Figure 11. Variations of dispersion for fiber no. 4 as a function of r_5 for constant r_1, r_2, r_3, r_4, and r_6.

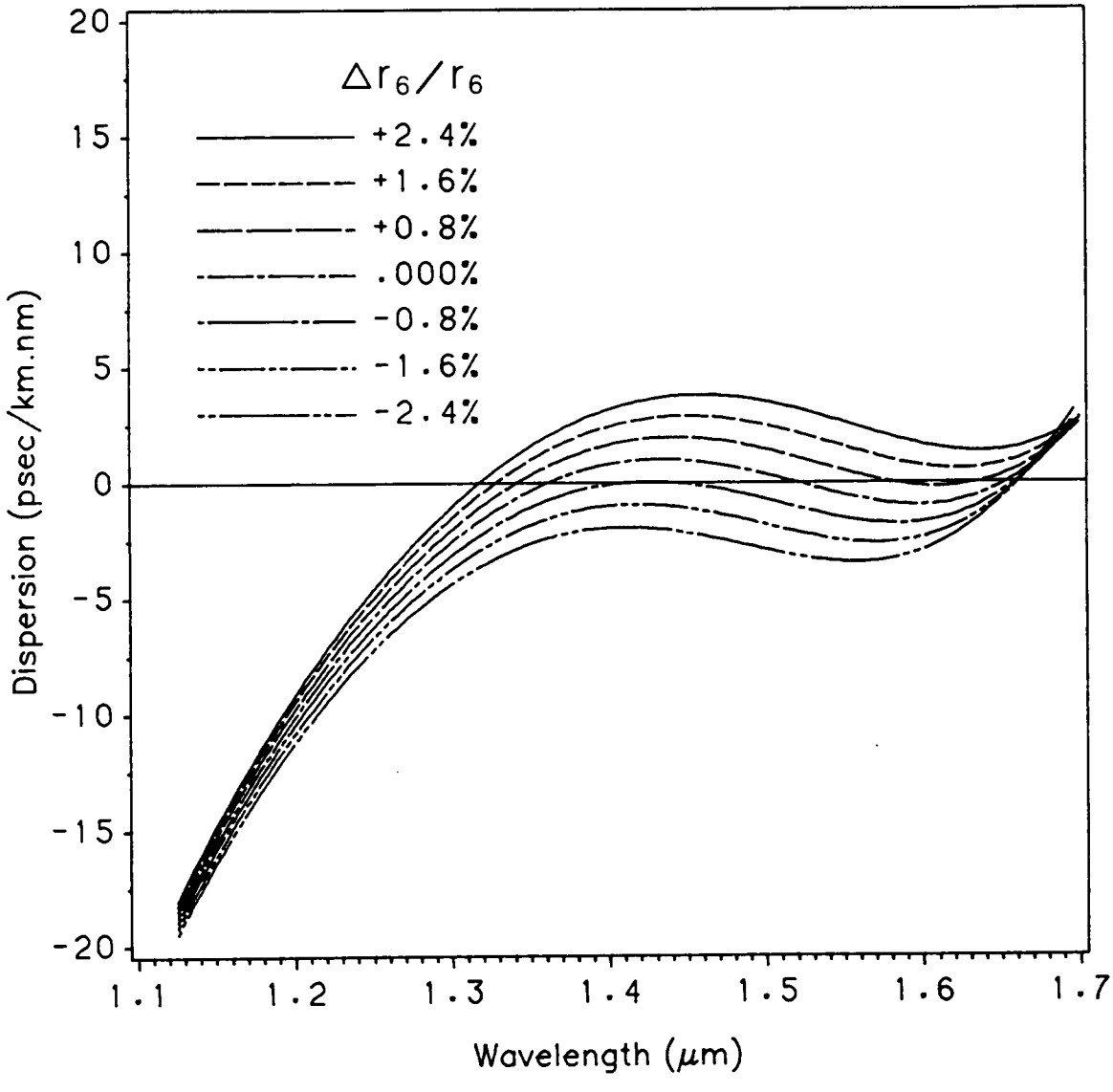

Figure 12. Variations of dispersion for fiber no. 4 as a function of r_6 for constant layer thickness ratios η_1, η_2, α, and γ.

Chapter 5. Comparison of Transmission Properties

In this Chapter, transmission properties of the proposed 7-layer fiber are compared with those of DC, TC, and QC fiber with respect to (1) group velocity, (2) dispersion-flattened span, (3) mode-field radius, and (4) bend-sensitivity. All these fibers are optimized with a dispersion of 0.97 ps/km-nm. To compare the fields of the fundamental mode of DC, TC, QC, and 7-layer fiber, we have computed numerically the modal field by integrating Eqs. (2.9,2.10), and the corresponding plots are show in Fig. 13. The vertical lines in Fig. 13 are the boundaries, r_1, of the innermost layer.

5.1. DC Fiber

A DC fiber consists of three portions: the core, inner cladding, and outer cladding. The core has the largest refractive index of the three layers and the inner cladding has the lowest. The advantage of DC fiber over conventional single-clad fibers is a tighter confinement of energy which minimizes the total dispersion and reduces absorption loss in the cladding. The short horizontal line along the frequency

axis in Fig. 14 corresponds to the dispersion-flattened wavelength range of the DC fiber. It is very close to the cutoff of the LP_{01} mode, implying that the bend losses of a DC structure are very sensitive to wavelength and fiber parameters. DC fiber's chromatic dispersion is very sensitive to index profile geometry and its dispersion-flattened window is small. Furthermore, it has poor reproducibility.

5.2. TC Fiber

Adding one raised-index ring to the outer cladding of a DC fiber results in TC fiber. The short line in Fig. 15 corresponds to the dispersion-flattened wavelength range of the TC fiber. Again from Fig. 15, we notice that the dispersion-flattened wavelength range is very close to the LP_{01} mode cutoff. This implies that sensitivity to bending is not improved by adding an extra layer to DC fibers. Furthermore, the dispersion-flattened range of the TC fiber is smaller than that of the DC fiber, shown in Fig. 16, since λ_{c01} is greatly reduced. Compared to DC fibers, there is more power flow outside of the core, as shown in Fig. 13. It is known that the second cladding makes the LP_{02} mode appear before the usual first higher-order mode LP_{11} [44].

5.3. QC Fiber

Adding one raised-index ring to the DC fiber's depressed-index range forms a QC fiber. This could be the principal cause of the increase in the slope of group velocity toward longer wavelengths, as presented in Fig. 17, and therefore the waveguide dispersion is increased in the long wavelength range implying that the

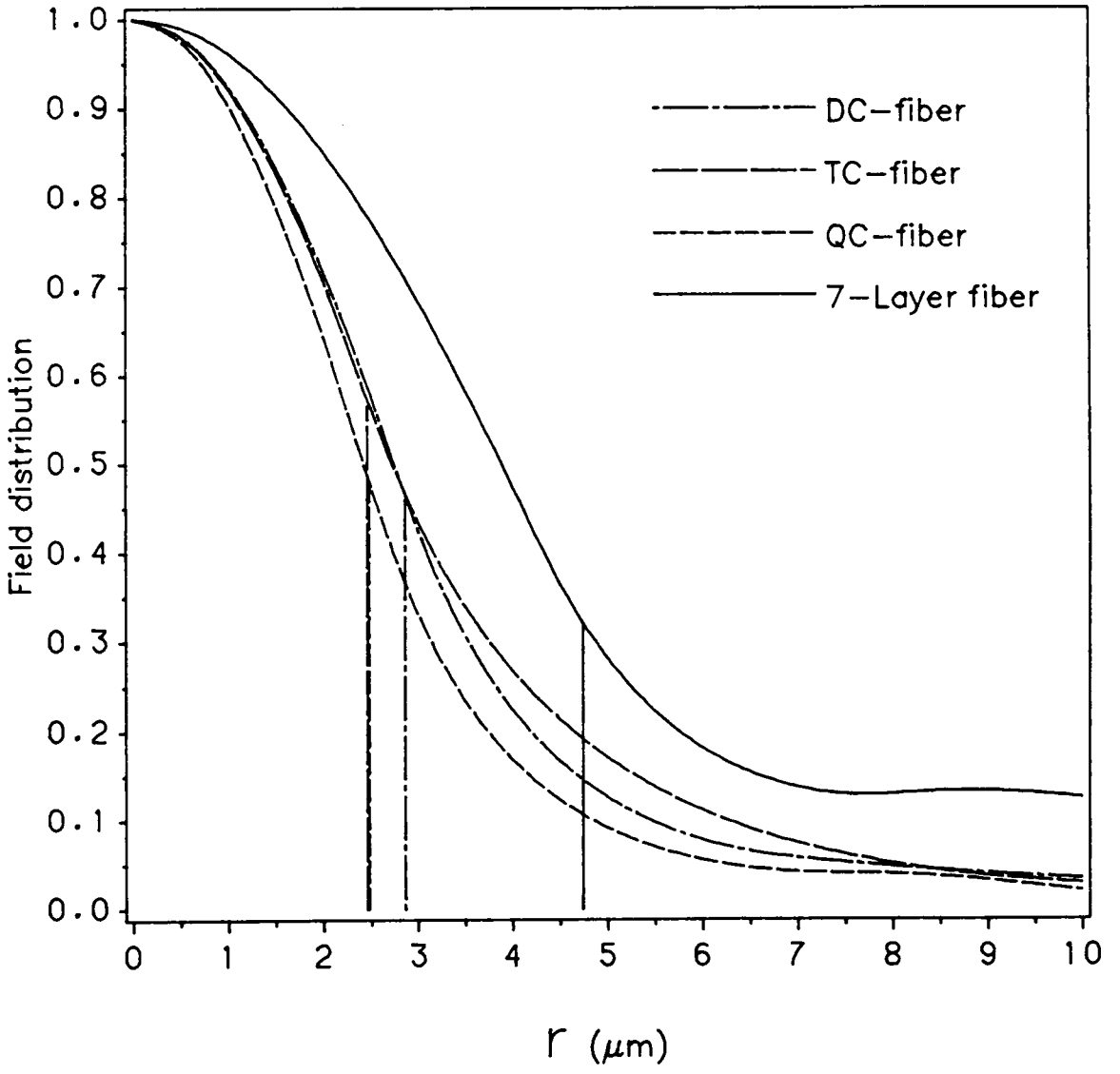

Figure 13. Modal field comparison for DC, TC, QC, and 7-layer fiber for the LP_{01} mode at 1.3 μm.

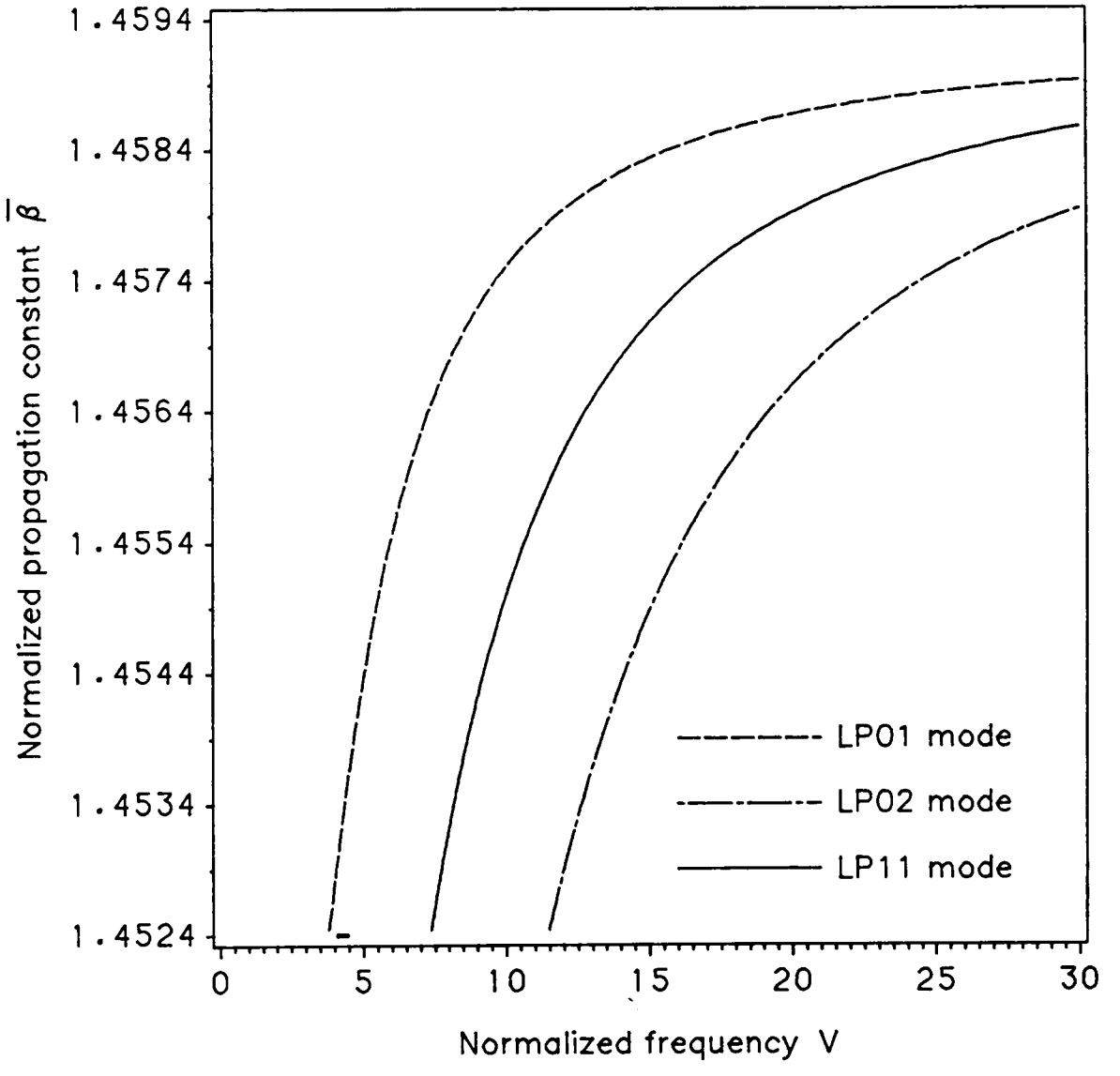

Figure 14. $\overline{\beta} - V$ curves for the LP_{01}, LP_{02}, and LP_{11} modes of DC fiber.

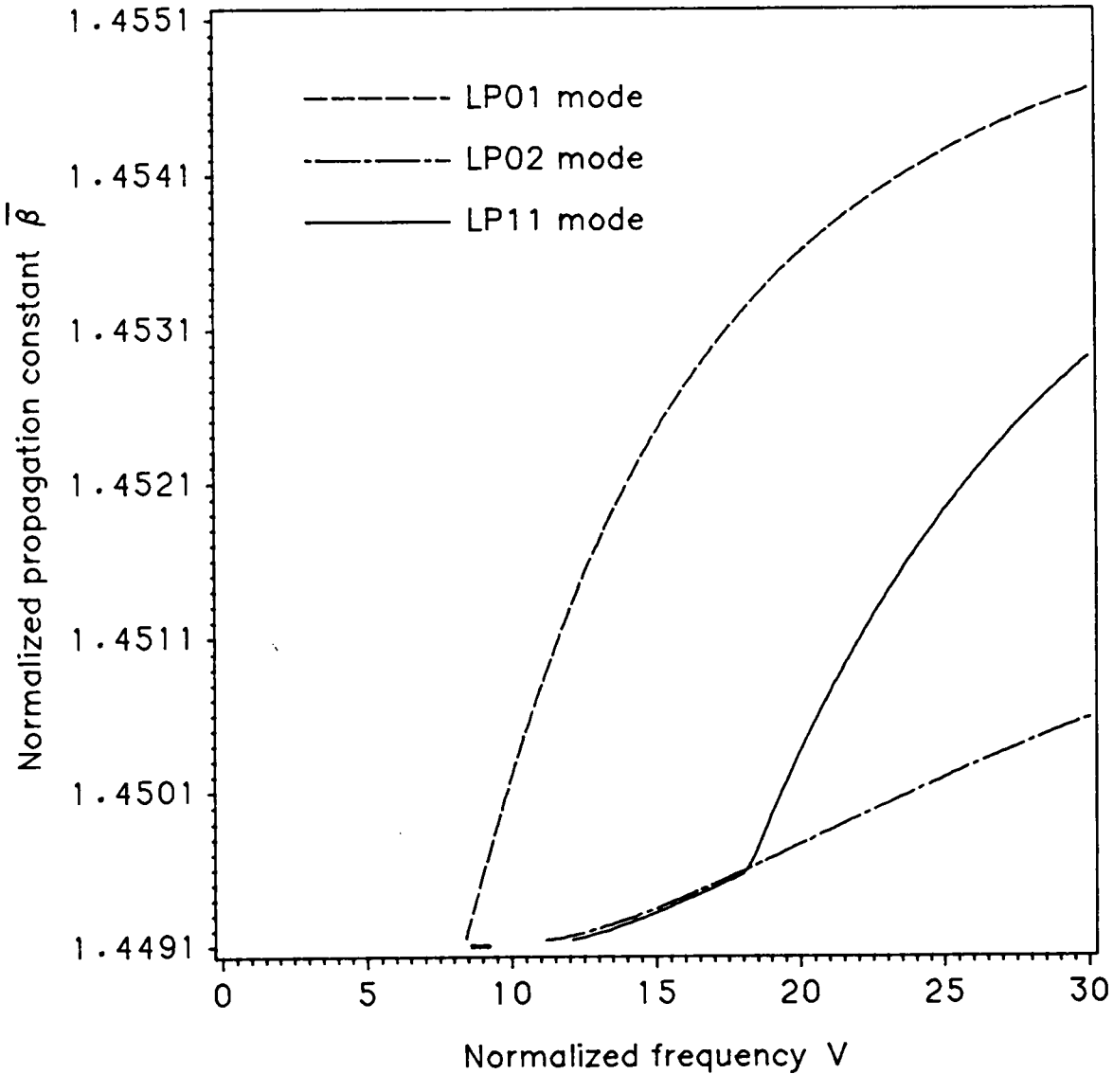

Figure 15. $\overline{\beta} - V$ curves for the LP_{01}, LP_{02}, and LP_{11} modes of TC fiber.

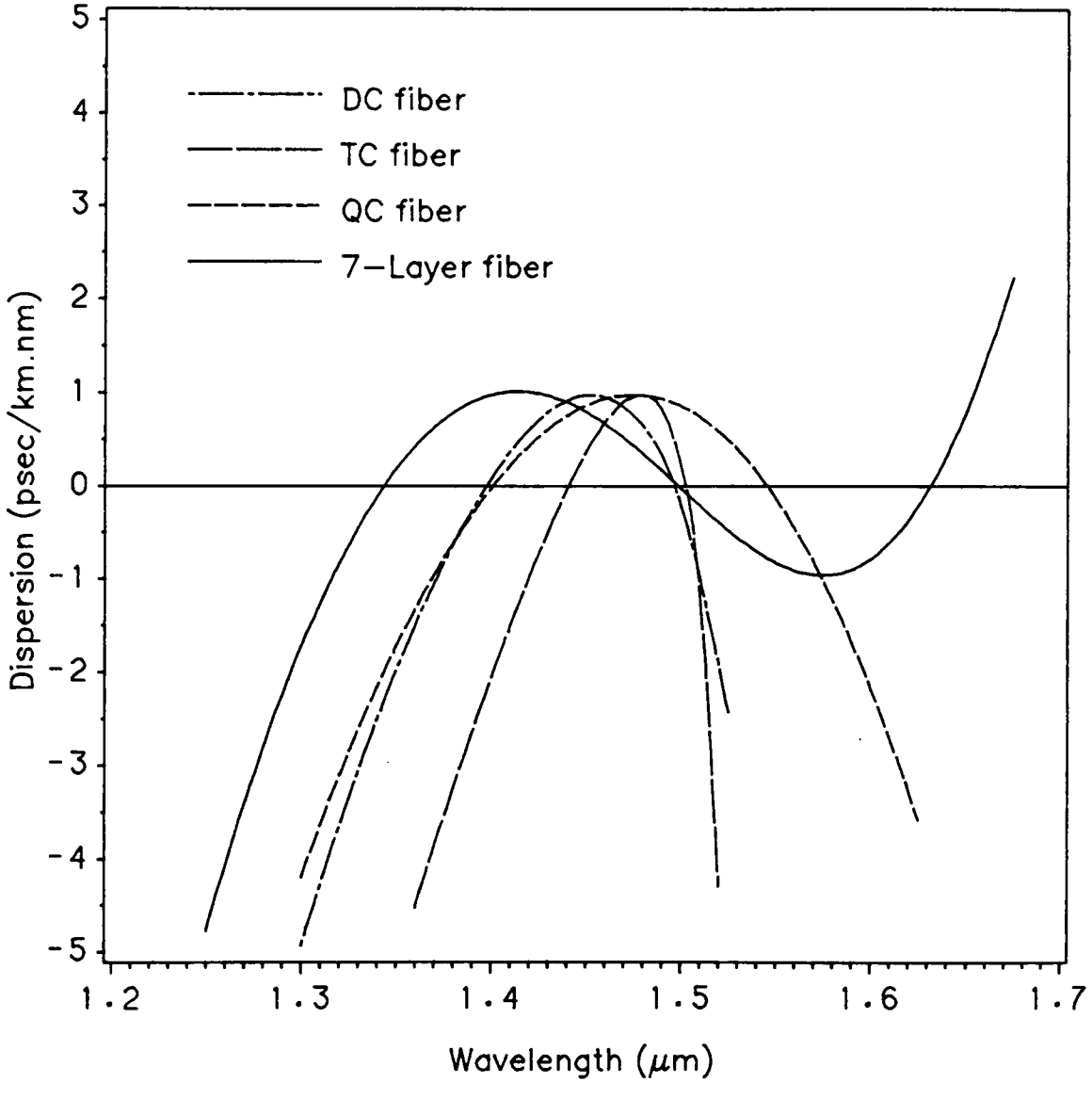

Figure 16. Chromatic dispersion spectra comparison for DC, TC, QC, and 7-layer fiber.

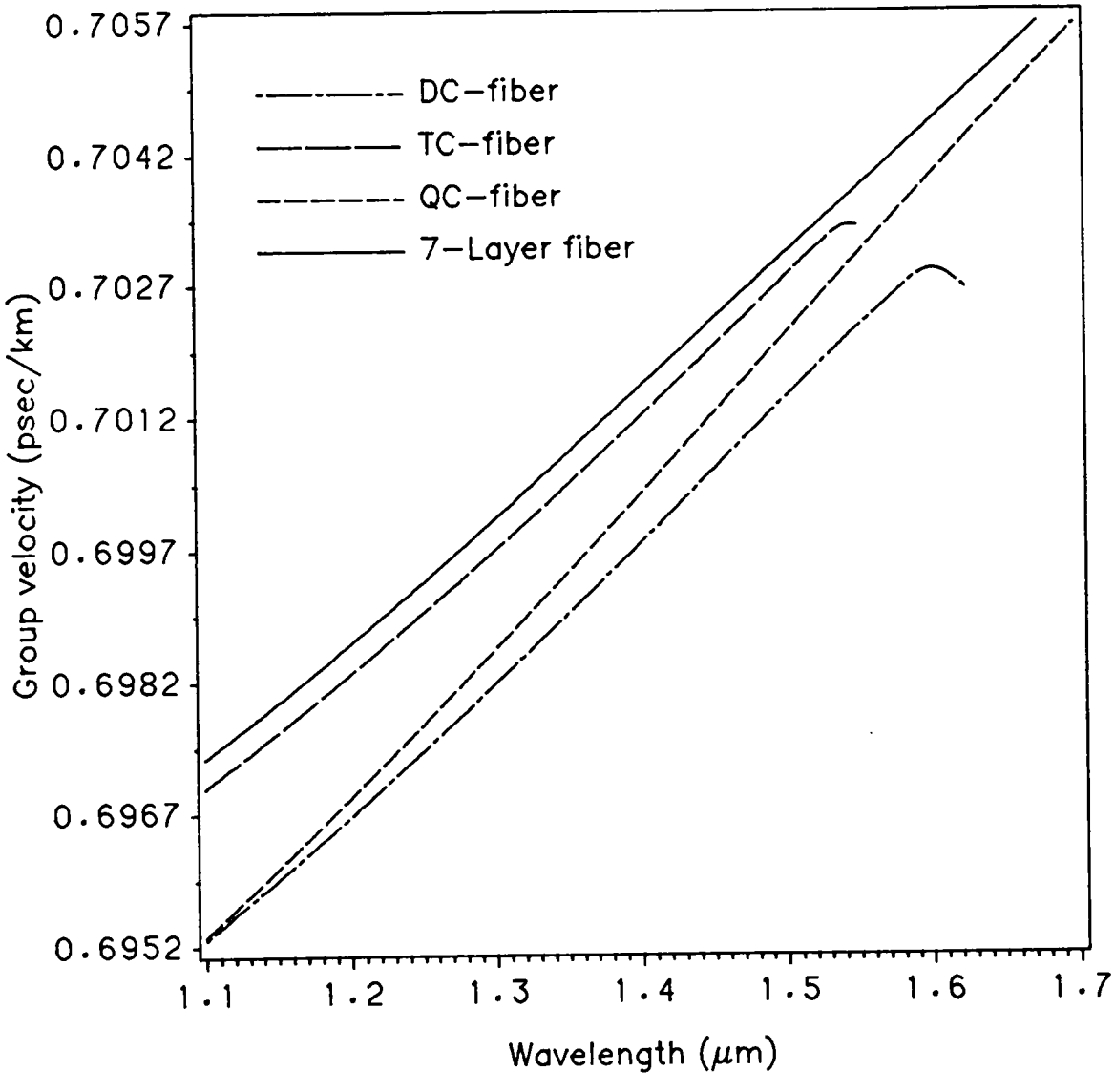

Figure 17. Group velocity comparison for DC, TC, QC, and 7-layer fiber.

QC fiber does not provide a flattened dispersion characteristic below 1.3 μm, as shown in Fig. 16. Consequently, the dispersion-flattened range moves toward the longer wavelength range. The short line in Fig. 18 corresponds to the dispersion-flattened wavelength range of the QC fiber. The bend loss is less than those of DC and TC fiber as shown in Fig. 13.

5.4. 7-Layer Fiber

Adding two layers of cladding to the QC fiber's depressed-index range results in a 7-layer fiber, as shown in Fig. 1. The group velocity of 7-layer fiber is larger than that of QC fiber. The rate of increase of the group velocity in the lower wavelength range is higher than that at the longer wavelength, i.e., the slope of the group velocity is less than that of QC fiber, as shown in Fig. 17. The overall results extend the dispersion-flattened wavelength range.

It is evident from Fig 13. that in the case of the 7-layer fiber, the fraction of the power outside the core r_1 is much less in comparison to the DC, TC, and QC fiber, which implies that microbend losses in the 7-layer fiber will also be small [39]. Furthermore, Table 6 shows that the ω/r_1 ratio for the 7-layer fiber is the smallest, again suggesting that microbend loss for the 7-layer fiber will be the smallest [42]. Also, it may be seen from Fig. 13 that the mode-field radius of a 7-layer fiber is larger than that of the DC, TC, and QC fiber which is better from the splicing point of view [39]. Overall design data and performance data are presented in Tables 5 to 7.

In summary, DC fiber is better for splicing than QC fiber. An example of the lateral offset loss comparison for DC, TC, QC, and 7-layer fiber is given in Fig. 19, where the excess loss for 1.55 μm wavelength is plotted as a function of lateral offset.

Figure 19 shows that the DC fiber is superior to QC fiber and at a lateral offset of 2 μm, 7-layer fiber has 56% lower loss than QC fiber. The 7-layer fiber has the largest dispersion-flattened window among these dispersion-flattened fibers; and also has the largest mode-field radius and the lowest bend-sensitivity.

Figure 15 shows that there is a curvature sign change around $V = 18$ in TC fiber for the LP_{11} mode $\overline{\beta} - V$ curve. Similarly, in Fig. 18, for QC fiber there is a curvature sign change around $V = 26$. This curvature sign change has been repoted for DC fiber [56] but the cause is unknown. In our investigation, if the depressed-index layer thickness ratios η_1, η_2, and γ are less than 1.5, and raised-index layer thickness ratio α is larger than 0.7 for TC fiber, 0.9 for QC fiber, and 1.2 for 7-layer fiber, the LP_{11} mode $\overline{\beta} - V$ curve for DC, TC, QC, and 7-layer fibers will become smooth. This is consistent with reference [56].

The fiber profile data and fiber performance data of Fig. 16 are listed in Table 5 and Table 6. Cladding materials for the fibers are presented in Table 7. The material compositions are shown in Appendix B.

Table 5. Index profile parameters for DC, TC, QC, and 7-layer fiber

Fiber	Δn_1	Δn_2	Δn_3	Δn_4	η_1	α	γ	η_2	r_6
DC	0.462%	0.378%	—	—	1.448	—	—	—	7.00
TC	0.461%	0.283%	0.188%	—	4.592	0.500	—	—	15.0
QC	0.647%	0.381%	0.228%	0.378%	2.000	0.841	4.000	—	19.5
7L	0.273%	0.153%	0.322%	—	0.874	1.144	2.500	2.500	39.25

- where $\Delta n_j = |n_0^2 - n_j^2|/2n_j^2$, $j = 1, 2, \ldots k-1$.

Table 6. Performance data for DC, TC, QC, and 7-layer fiber

Fiber	λ_{c01}	λ_{c11}	$\omega_{1.3}$	$\omega_{1.55}$	DF (< 1 ps/km-nm)	$\omega_{1.55}/r_1$
DC	1.63	0.84	3.00	3.49	1.37 - 1.51	1.22
TC	1.56	1.18	3.12	3.97	1.42 - 1.51	1.61
QC	1.80	1.13	2.60	3.00	1.37 - 1.57	1.20
7L	1.85	1.26	3.24	4.93	1.31 - 1.66	1.15

- the units for cutoff wavelength λ_c are μm.
- the units for mode-field radius ω are μm.

Table 7. Cladding materials for DC, TC, QC, and 7-layer fiber

Fiber	*layer 1*	*layer 2*	*layer 3*	*layer 4*	*layer 5*	*layer 6*	*layer 7*
DC	M16	M1	M7				
TC	M8	M13	M2	M10			
QC	M14	M1	M15	M10	M3		
7L	M3	M12	M10	M12	M10	M12	M1

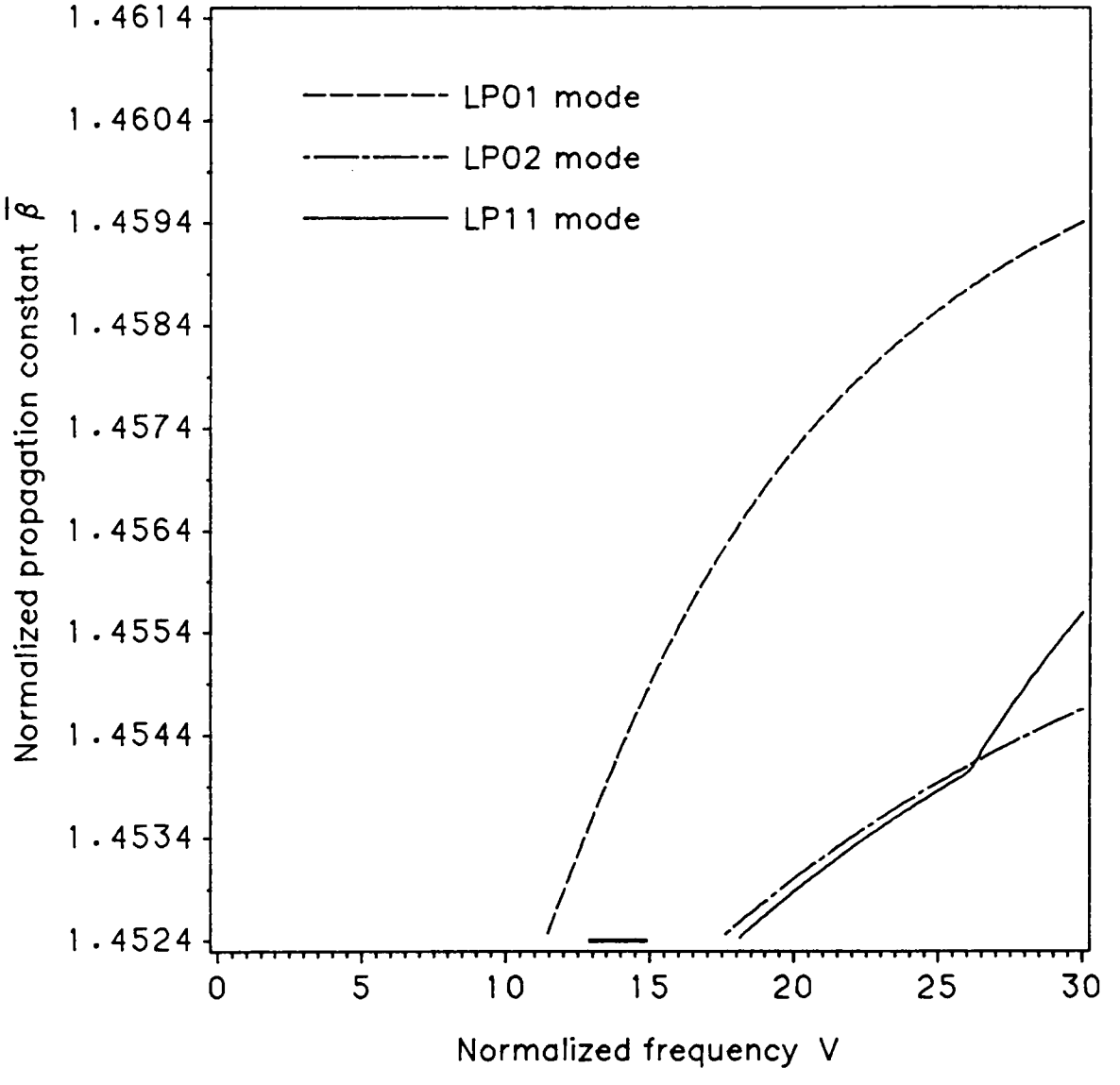

Figure 18. $\overline{\beta} - V$ curves for the LP_{01}, LP_{02}, and LP_{11} modes of QC fiber.

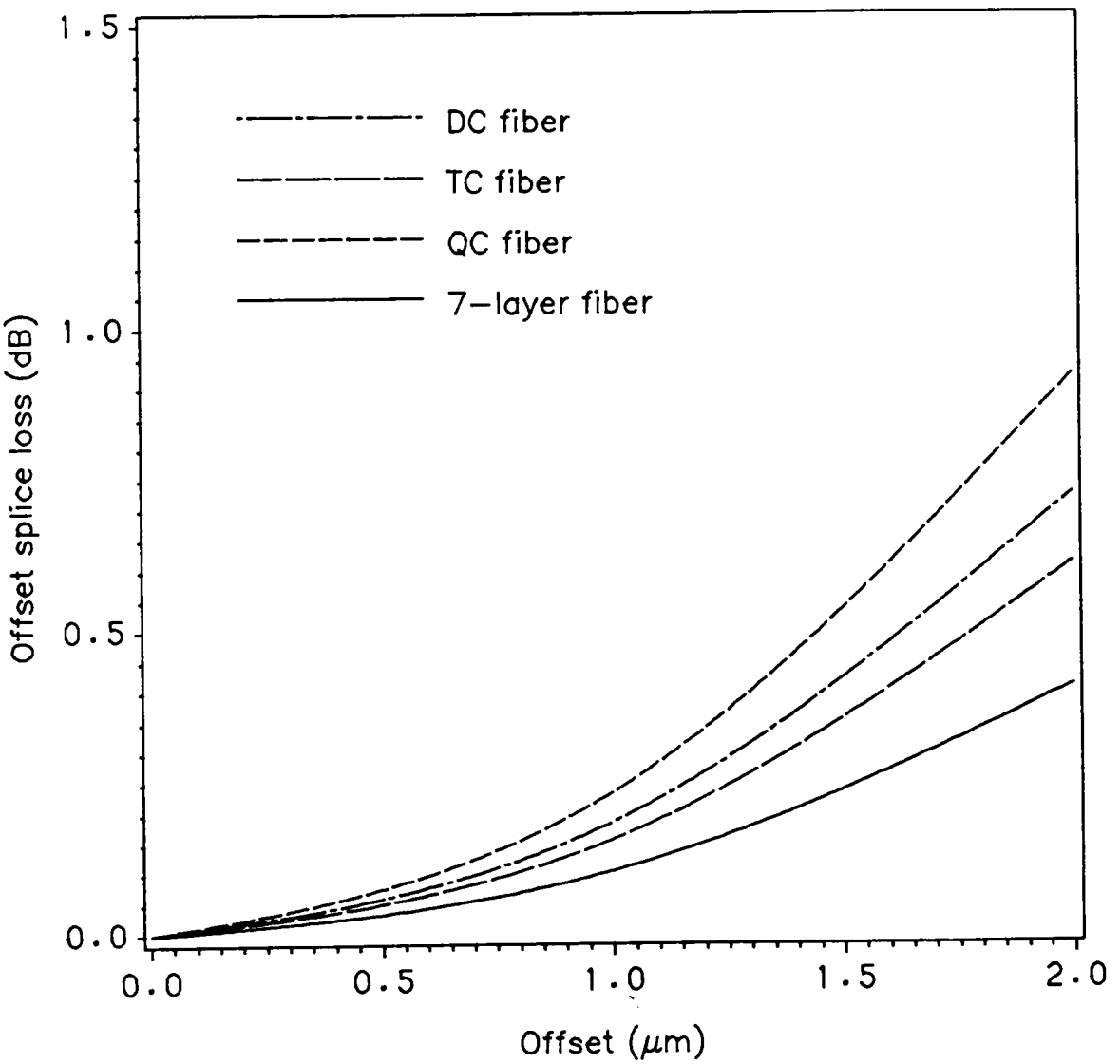

Figure 19. Lateral offset loss comparison for DC, TC, QC, and 7-layer fiber for the LP_{01} mode at 1.55 μm.

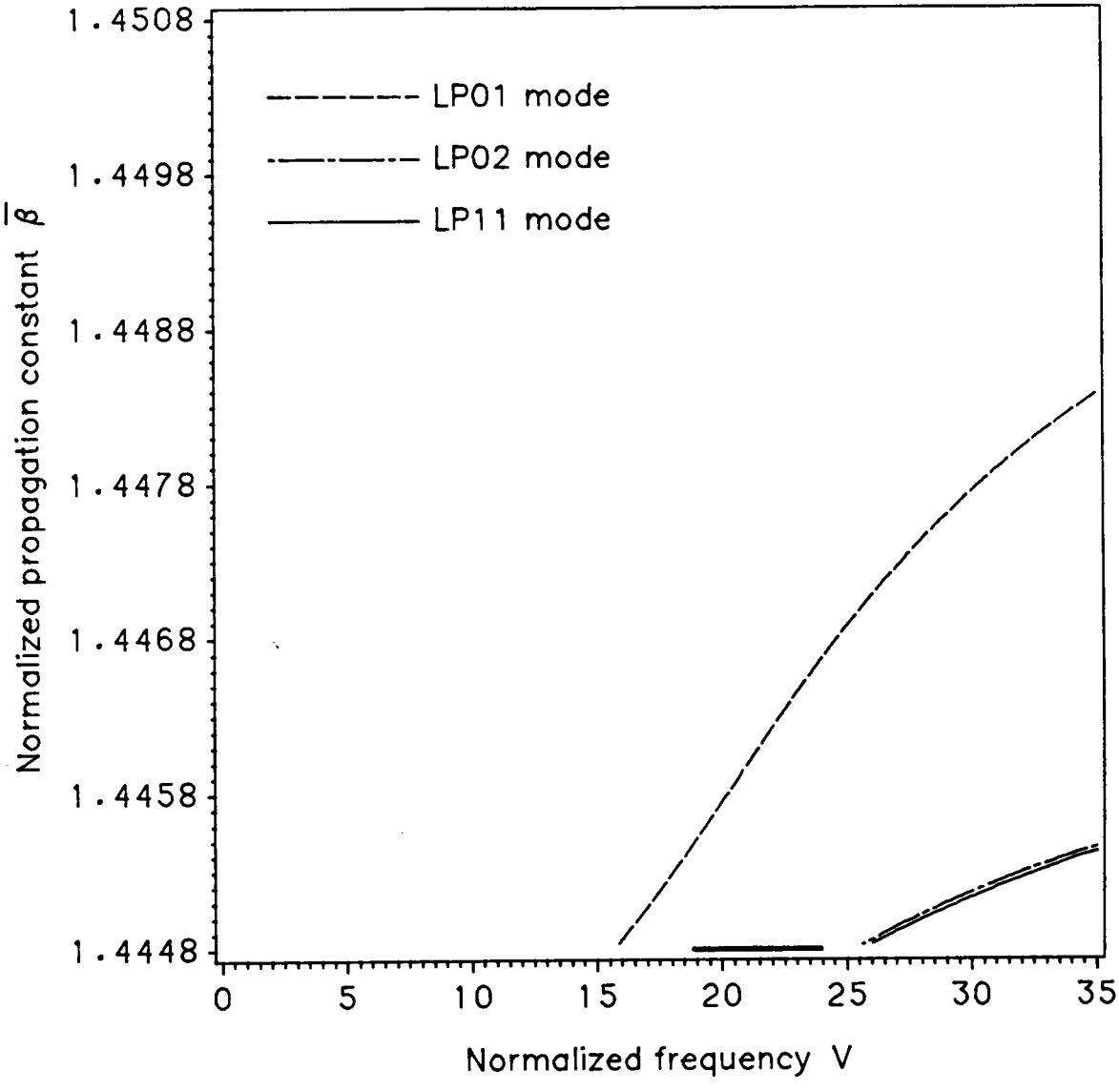

Figure 20. $\overline{\beta} - V$ curves for the LP_{01}, LP_{02}, and LP_{11} modes of 7-layer fiber.

Chapter 6. Optimization of Waveguide Parameters

This Chapter presents optimum solutions for the refractive index profile of DFSM fibers which support LP modes with prescribed dispersion characteristics. Basically, this is an inverse waveguide synthesis problem. It is a time consuming and tedious task. Several authors have reported optimized data for DFSM fibers, but little information is given about the optimization procedures [36]. In reference [64] the author used a modified interpretation of the eigenvalue problem to synthesize a waveguide. This method requires a highly accurate initial approximation of the roots to solve a system of nonlinear equations, and these roots are calculated by the halving recurrent method. After finding these roots one goes back to solve the system of nonlinear equations. With this method, the solution yields an index profile which is difficult to manufacture. In this section a new CAD method is discussed. The initial data for this synthesis procedure are layer indices, layer thickness ratios, and total core radius.

6.1. Requirements for Optimum Index Profile

To determine an optimum DFSM fiber profile, the following requirements need to be met:

1. The Rayleigh scattering loss should be kept as low as possible.
2. Splice and bend losses should be kepted as low as possible.
3. Single-mode operation should be maintained in the whole dispersion-flattened range and the dispersion-flattened window should lie between λ_{c01} and λ_{c11} and be sufficiently far from λ_{c01} and λ_{c11}. Single-mode operation should also be satisfied after cabling.
4. The production tolerances for a given dispersion spectrum should be not critical.
5. For the same amount of dispersion, the dispersion-flattened window should preferably be larger than that of DC, TC, and QC fibers, and have more than two zero-dispersion wavelengths.
6. The production cost should be minimized.

To meet requirement (1), the fiber profile index range should be less than 0.8%. Also, the core should be either pure silica or slightly germanium doped and the cladding should be depressed with fluorine dopant. The pure silica core and F-doped cladding fibers would have lower transmission loss than the conventional Ge-doped core fibers because of the reduction of Rayleigh scattering loss and because there is no increase in *OH* absorption loss [65]. To have requirement (2) satisfied, mode field-radius should be increased significantly by reducing the layer index differences and by increasing the fiber core radius. This can be done by increasing r_6 and by reducing layer thickness ratios. Bend loss is reduced by reducing power in the

cladding range. Thus, there is a trade off between bend loss and splice loss. Increasing the effective cutoff wavelength can improve the microbend loss without increasing the fiber's intrinsic loss. For requirement (3), by properly choosing core radius, layer index differences and layer thicknesses, the dispersion-flattened window can be made to lie between λ_{c01} and λ_{c11}. To meet requirements (4) and (5), layer production tolerance is achieved by making the dispersion curve sinusoidal instead of quadratic. For requirement (6), lower production cost is achieved by a small percentage of dopant, minimum number of layers, and a small number of different materials. Conventional QC fibers need five different materials, 7-layer fiber needs only four different materials although the number of layers is increased.

6.1.1. Material Consideration

A fiber composed of a GeO_2-doped SiO_2 core and a F/P_2O_5-doped cladding seems to be the best candidate for zero-dispersion in the 1.55 μm ultralow loss transmission window. Therefore, these materials are used to design most of the 7-layer fibers in this study. With the MCVD technique, a small germanium concentration and a low drawing temperature are the two key conditions to achieve low loss fibers. Fluorine doping creates depressed inner-claddings and this allows zero-dispersion to be obtained with a reduced amount of germanium in the central core layer and raised-index layers. Fluorine allows low transmission loss over a wavelength range of 1 μm to 1.8 μm to be achieved. P_2O_5 allows a reduction of the drawing temperature and is introduced in non-radiation hardened fibers in very small quantities (<0.2 mole precent). Therefore, the effects of P_2O_5 in the calculation of dispersion is neglected [62]. B_2O_3 is a suitable dopant, but the IR absorption edge limits the operation wavelength to less than 1.3 μm [66].

6.1.2. Optimum Index Profile

To make a strictly DFSM fiber, the dispersion-flattened window must be above the cutoff wavelength of the LP_{01} mode. An average layer thickness and a single-mode operation range should be predetermined. Figures 21 and 22 illustrate alternatives for making waveguide dispersion larger or smaller at particular frequencies simply by adding layers. They show waveguide dispersion versus the number of step-index layers. In Fig. 21, $\Delta n_1 = 0.33\%$, $\Delta n_2 = 0.00\%$, $\Delta n_3 = 0.33\%$, the average layer thickness ratio is 1, and $r_6 = 28\ \mu m$. When the number of layers is increased the waveguide dispersion window widens and moves toward larger frequency. In Fig. 22, as the layer thickness is further increased to 2 and r_6 is increased to 38 μm, with the same waveguide profile parameters mentioned above, the waveguide dispersion window becomes narrower as frequency increases. This implies that there exists an optimum layer thickness and an optimum number of layers which can be used to produce a certain waveguide dispersion which cancels the material dispersion. A test calculation reveals that the average layer thickness ratio of 1.6 μm and seven layer fiber can offer a sufficiently large spectral width for single-mode operation. A test calculation also shows that the lower and upper bounds of the approximate layer thickness ratios are 0.5 - 4.0. By choosing large values for r_6 a larger mode-field radius can be obtained. Layer index differences are chosen to be $< 0.8\%$. The seven layer fiber profile data can be optimized after the design limits have been established. An average layer thickness value 1.6 μm is selected as a starting value in the optimization program.

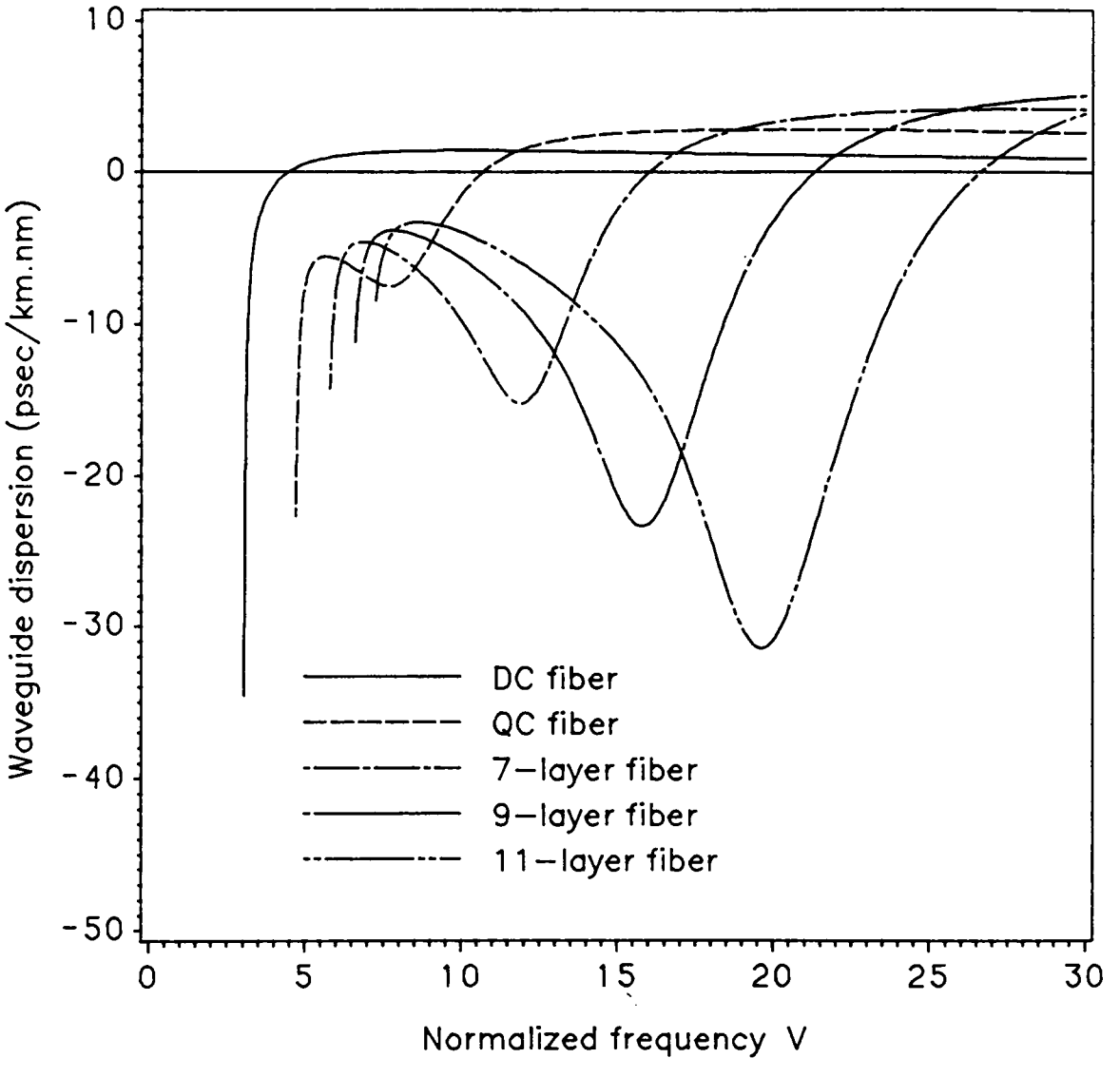

Figure 21. Waveguide dispersion spectra as a function of the number of layers for $\Delta n_1 = 0.33\%$, $\Delta n_2 = 0.00\%$, $\Delta n_3 = 0.33\%$, $\eta_1 = \eta_2 = \alpha = \gamma = 1.8$, $r_6 = 28\ \mu m$.

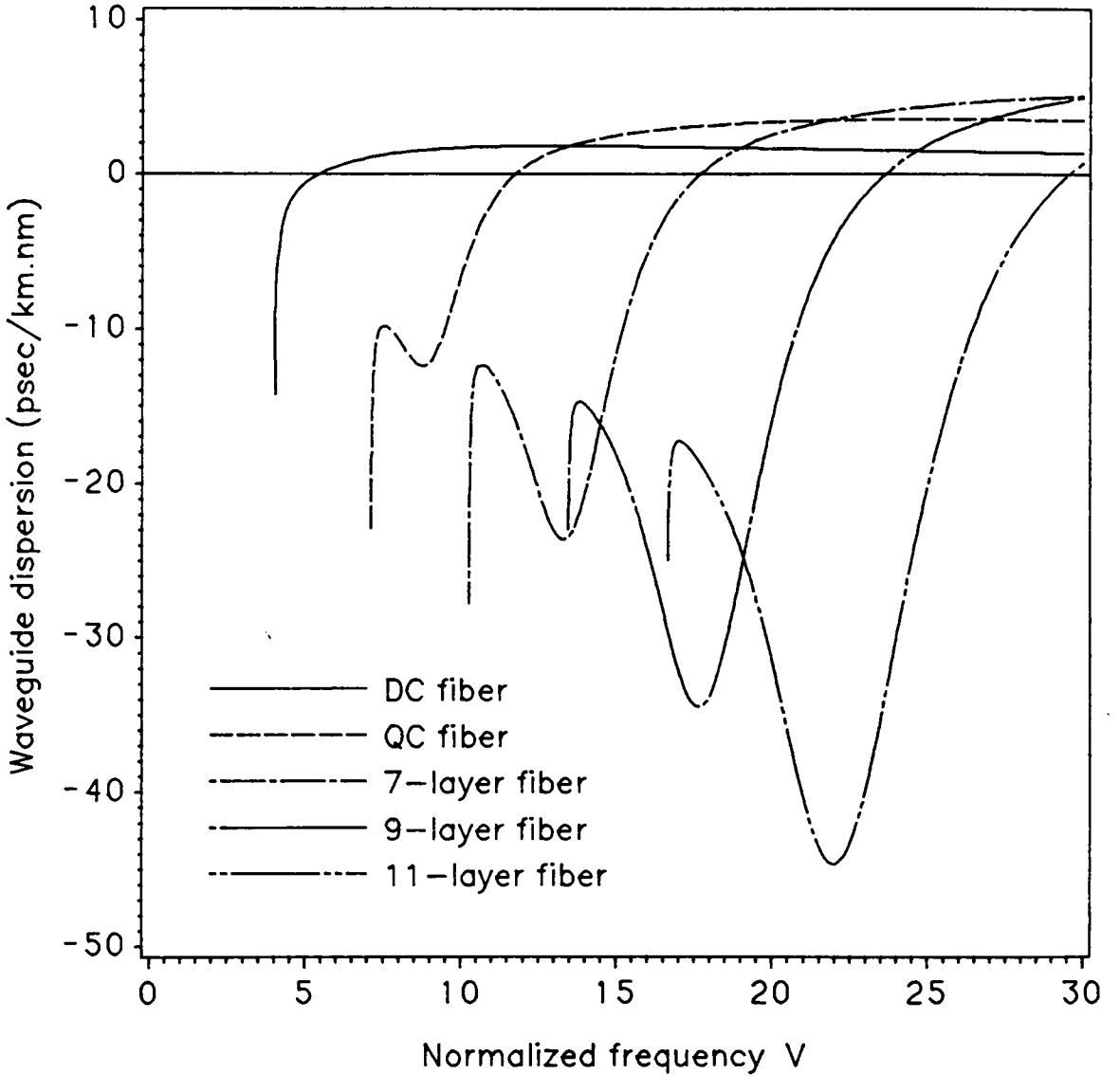

Figure 22. Waveguide dispersion spectra as a function of the number of layers for $\Delta n_1 = 0.33\%$, $\Delta n_2 = 0.00\%$, $\Delta n_3 = 0.33\%$, $\eta_1 = \eta_2 = \alpha = \gamma = 2.2$, $r_6 = 38\ \mu m$.

6.2. Objective Function

The refractive index profile to be optimized here is shown in Fig. 1. A program called DFSM is developed to optimize the refractive index profile with respect to: (1) minimum dispersion, (2) the wavelengths of the zero-dispersion, (3) the width of the dispersion-flattened window, (4) small index differences between the layers, and (5) reasonable layer thickness. This is a minimization problem with simple bounds. The problem is stated as follows: over a wavelength range of 1.3 μm to 1.7 μm, it is desired to minimize the total dispersion $D_{total}(\lambda, x_i)$, subject to the condition $l \leq x_i \leq u$. Based on the design considerations discussed above, the index differences are restricted to the range of $1.4460 \leq x_i \leq 1.4580$, and the thickness ratios of the layers are chosen within the range of $0.5000 \leq x_i \leq 4.0000$. The IMSL (International Mathematical and Statistical Library) optimization subroutine DBCONF [67] is used. This subroutine uses the quasi-Newton method and an active set strategy to solve minimization problems subject to simple bounds on the variables. The DBCONF subroutine can effectively determine the minimum total dispersion. Vectorization is applied to the program which is run on the IBM 3090 vector facility. The IMSL SFUN/LIBRARY is used for the Bessel and modified Bessel functions to save CPU time.

Also, two of the zero-dispersion points can be adjusted to any desired wavelengths through an objective function, as shown in Figs. 23 to 26. A sine objective function is used to achieve a total zero-dispersion at the wavelengths of $Zero_1$ and $Zero_2$ in the form

$$O(\lambda) = A \sin\left[2\pi \frac{\lambda - Zero_1}{Zero_2 - Zero_1}\right] + B , \tag{6.1}$$

where A is the amplitude of the desired total dispersion (in this paper A = 0.96 ps/km-nm), λ is the operation wavelength, and B is the dispersion vertical shift parameter. The purpose of B is to move $Zero_1$ to a lower wavelength and to minimize dispersion in the 1.5 μm to 1.6 μm range. $Zero_1$ is the wavelength corresponding to a zero-dispersion point at the lowest wavelength, and $Zero_2$ is the wavelength corresponding to a zero-dispersion point at the longest wavelength.

According to design requirements for optical communication systems, $Zero_1$ could be defined within the wavelength range of 1.29 μm to 1.35 μm, and the range of $Zero_2$ would be within the wavelength range of 1.50 μm to 1.65 μm. The minimization problem can then be stated as:

$$\min f(\lambda, x_i) = \sum_{\lambda = Zero_1}^{Zero_2} |D_{\text{total}}(\lambda, x_i) - O(\lambda)| \tag{6.2}$$

If only two zero-dispersion points are needed, one can use a quadratic function as an objective function; if only one zero point is needed one can use a point-slope form of line function as an objective function. In order to meet the CCITT dispersion recommendations, a design safety factor of 2.8 is applied to all the dispersion-flattened fibers, as shown in Table 2. In a 7-layer structure, extending the lower dispersion range below 1.3 μm presents a problem if only materials with known Sellmeier parameters are to be used [49]. Also there are difficulties below this range with QC fibers [36]. Table 3 shows the cutoff wavelengths for the LP_{01} and LP_{11} modes, the mode-field radii, and the dispersion-flattened wavelength ranges for the fibers listed in Table 2.

A 7-layer fiber, as illustrated in Fig. 1, has thirteen parameters to be optimized: seven layer indices, five layer thickness ratios, and a total core radius. After exam-

ining a variety of index profiles, it was found that the raised-index rings have nearly identical indices. The same was found to be the case for the depressed-index rings. Repeated tests also demonstrated that the thicknesses of the raised-index rings were nearly the same. The thicknesses of the depressed-index rings were also found to be nearly indentical. This suggests that the thirteen design parameters mentioned above could be reduced to only nine.

6.3. CAD Optimized Index Profiles

The capability to set the zero-dispersion point at an arbitrary wavelength is the major advantage of this optimization program. This is demonstrated in Figs. 23 to 26.

Figure 23 shows the dispersion spectrum for fiber no. 6 in Table 2, in which a dispersion of 0.97 ps/km-nm between 1.31 μm to 1.66 μm with the zero-dispersion wavelengths at 1.34 μm, 1.50 μm, and 1.63 μm is achieved. This is the lowest dispersion with the widest dispersion-flattened window reported to date. Since Sellmeier coefficients are available in reference [49] for only a limited number of doped glasses, the dispersion curves in Figs. 24, 25, and 26 are constructed by linear interpolations of Sellmeier expressions [62] and by using approximate method b in Chapter 8. The interpolations are made between the values of index (at wavelength λ = 1.3 μm) corresponding to pure silica, 3.1 mole percent GeO_2 -doped silica, and 1.0 mole percent F-doped silica [49]. In Fig. 24 zero-dispersion wavelengths are located at 1.3 μm, 1.48 μm, and 1.56 μm by defining $Zero_1$ = 1.3, $Zero_2$ = 1.56, A = 1, and B = 0.50. If B =0.85, then we obtain values for $Zero_1$ and $Zero_2$ exactly equal to 1.3 μm and 1.55 μm respectively, as shown in Fig. 25. We wish to design fibers with zero-dispersion wavelength within $\pm$1 ps/km-nm of the 1.55 μm center wavelength in

order to guarantee minimum dispersion in the vicinity of 1.55 μm. In Fig. 26, by setting $Zero_1$ = 1.34, $Zero_2$ = 1.67, A = 1.3, and B = 0.5, zero-dispersion wavelengths at 1.34 μm, 1.55 μm, and 1.67 μm are found.

The optimized parameters are listed in Table 2 and the corresponding fiber performance data are summarized in Table 3. These data show that 7-layer fibers have wider dispersion-flattened windows (for a total dispersion of 0.97 ps/km-nm) with larger mode-field radii than the QC fibers in the reference [36]. The normalized propagation constant $\overline{\beta}$ is plotted against the normalized frequency V in Fig. 5 for the LP_{01} , LP_{11}, and LP_{02} modes for the fibers listed in Table 2. These curves indicate that the multi-clad fiber's dispersion-flattened wavelength range of 1.3 μm to 1.7 μm is in the single-mode operation region. Hence, the proposed multi-clad fibers are strictly single-mode fibers. The dispersion curves for these fibers are presented in Fig. 4. The magnitudes of all these dispersion curves are $\pm$0.97 ps/km-nm.

Figures 27 to 29 show several final steps approaching the objective functions, in these dispersion curves only layer ratios η_1 , α, γ, and η_2 are varied, the layer indices and total core radius r_6 are fixed. Figure 27 shows optimization processes for fiber no. 6. The dispersion curves approach the horizontal axis with a sinusoidal form. The maximum dispersion is 0.97 ps/km-nm in the range of 1.31 μm to 1.66 μm with zero-dispersion wavelengths at 1.34 μm, 1.50 μm and 1.63 μm respectively. The range of minimum dispersion of the second curve lies within the wavelength range of 1.5 μm to 1.65 μm, with zero-dispersion wavelengths at 1.33 μm, 1.56 μm and 1.61 μm, respectively. Figure 28 shows optimization processes for a QC fiber. The dispersion curves move toward the horizontal axis in a form of a parabola. The maximum dispersion is 0.97 ps/km-nm in the range of 1.37 μm to 1.58 μm with zero-dispersion wavelengths at 1.40 μm and 1.55 μm. In the two examples above, the dispersion amplitude parameter A in Eq. (6.1) is defined as 0.96 ps/km-nm and B is

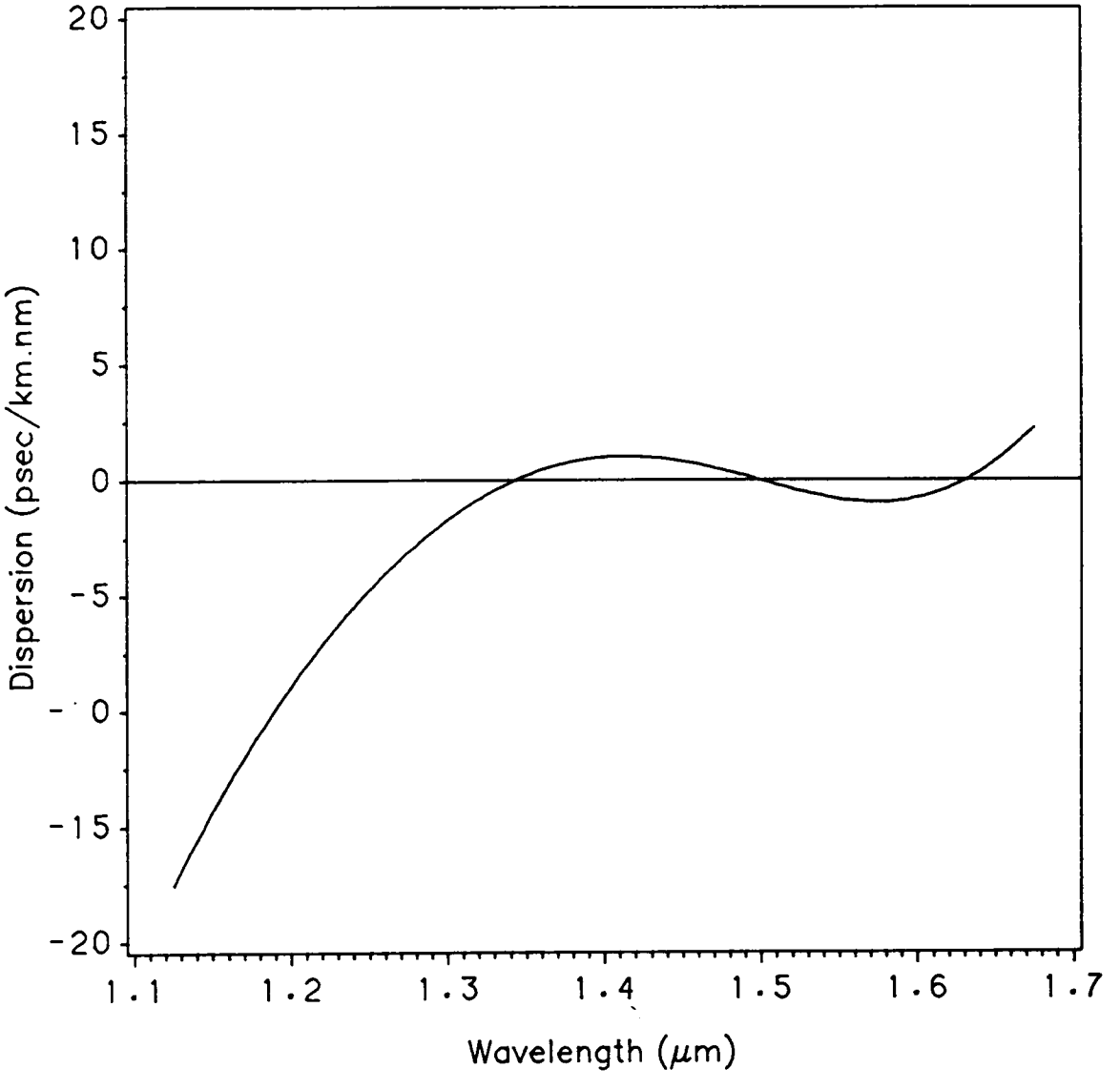

Figure 23. Chromatic dispersion spectrum of fiber no. 6.

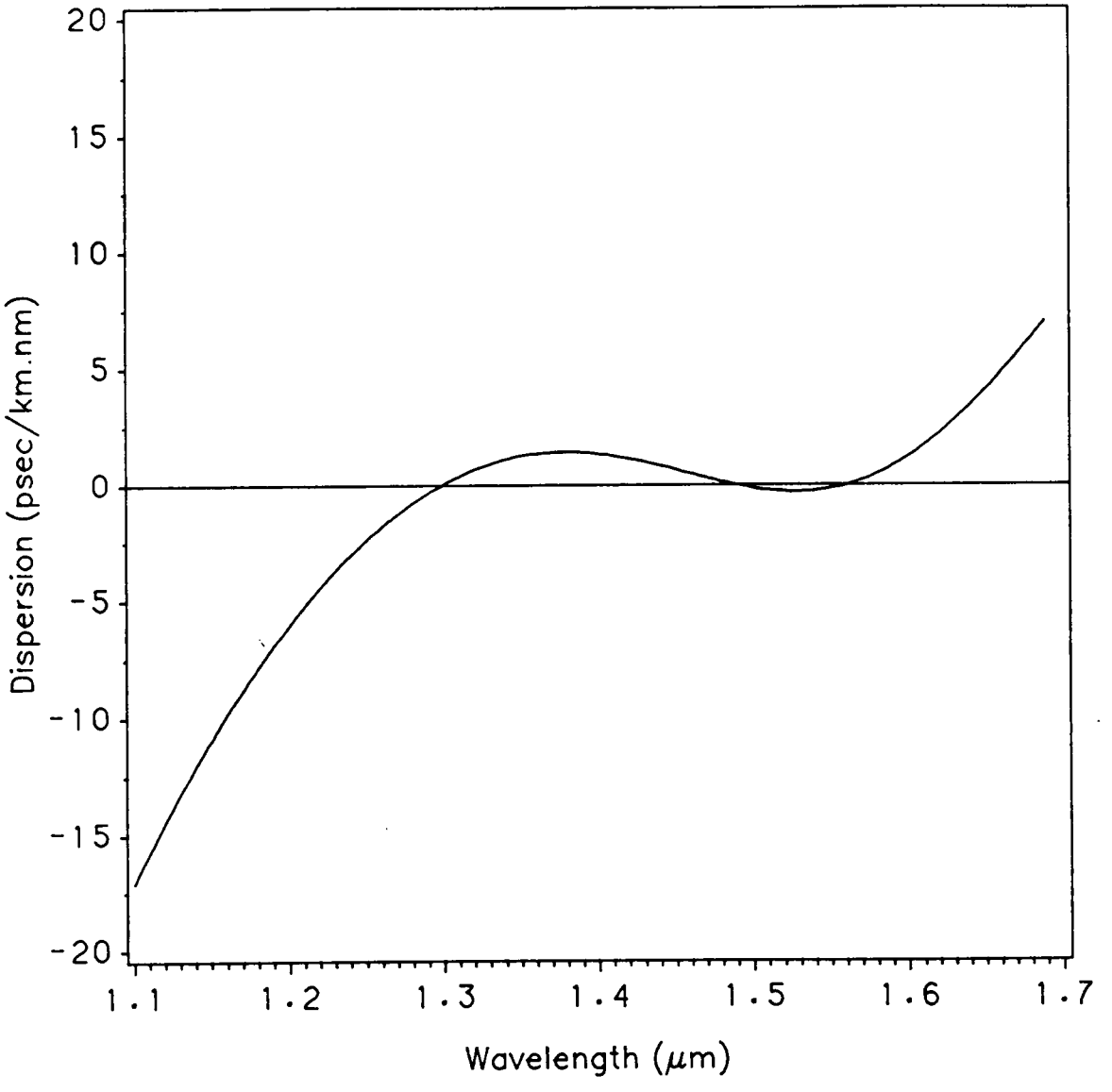

Figure 24. Chromatic dispersion spectrum with zero-dispersion wavelengths at 1.3 μm and 1.56 μm.

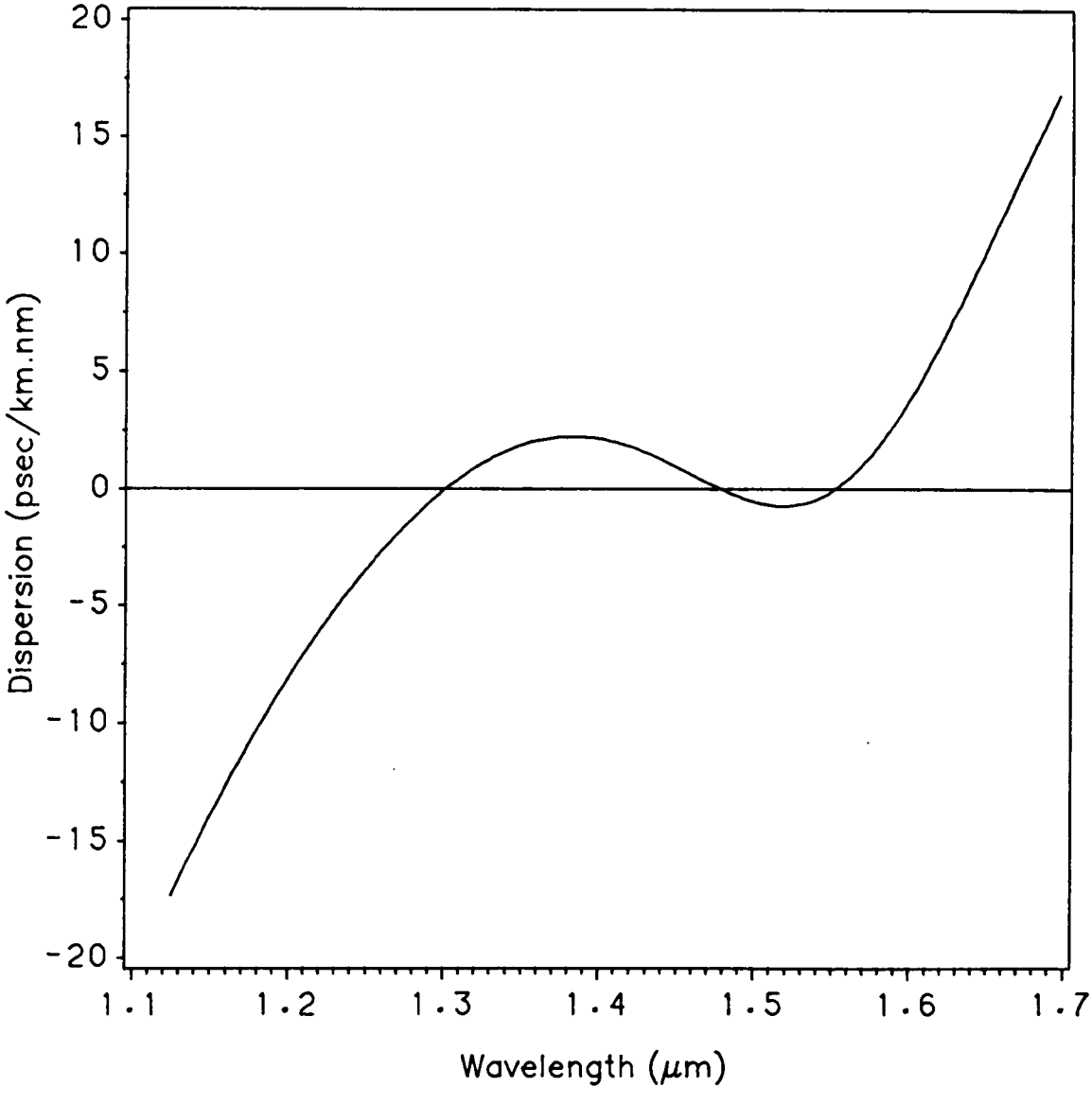

Figure 25. Chromatic dispersion spectrum with zero-dispersion wavelengths at 1.3 μm and 1.55 μm.

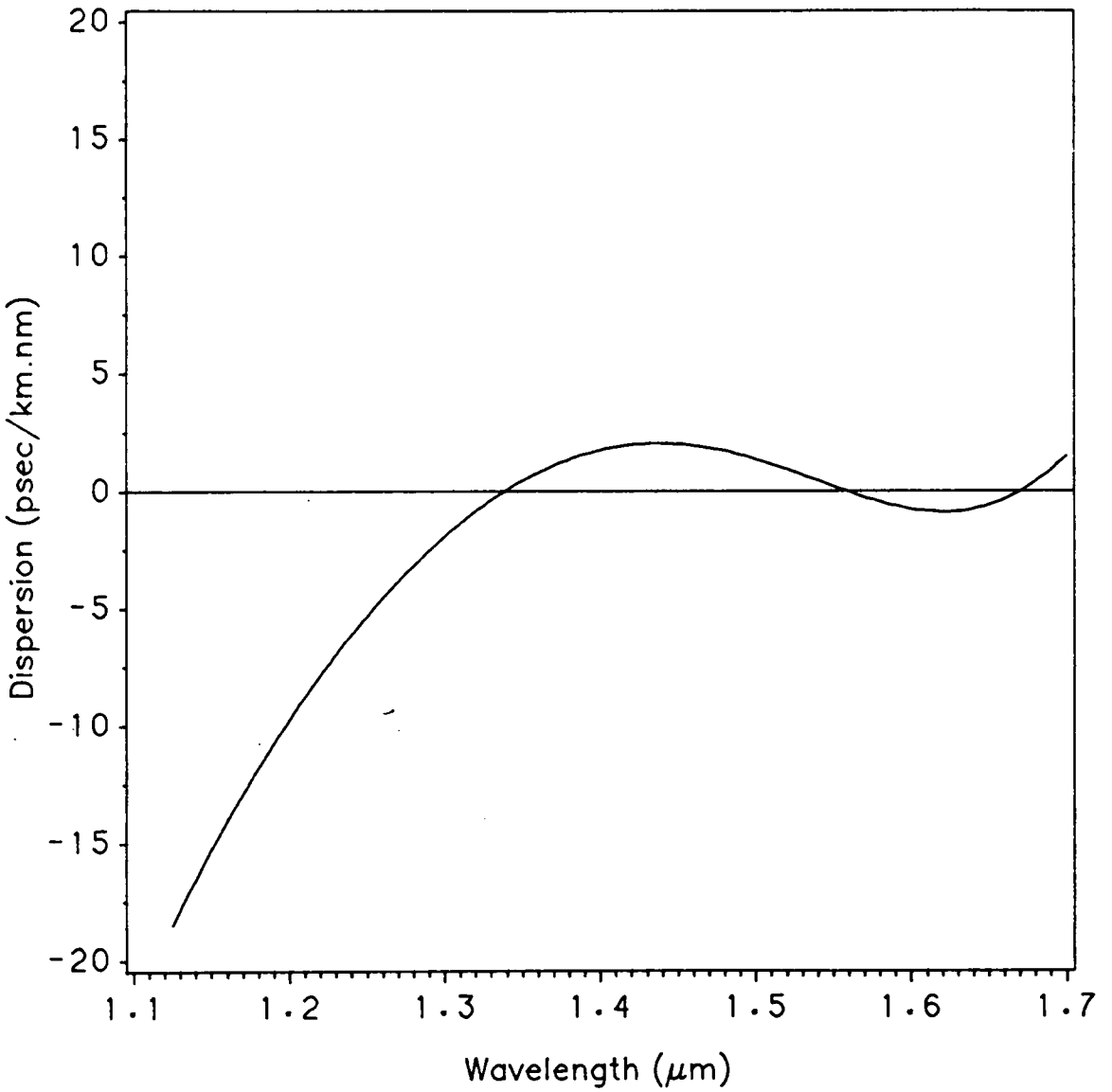

Figure 26. Chromatic dispersion spectrum with the center zero-dispersion wavelength at 1.55 μm.

defined as zero in the program. As a third example, Fig. 29 shows optimization processes for a 7-layer fiber. If the A is defined as 0.001 ps/km-nm, and $Zero_1$ = 1.45 μm, $Zero_2$ = 1.55 μm, and Eq. (6.1) is used as an objective function, the dispersion curves migrate toward the horizontal axis with a sinusoidal form as shown in Fig. 29. In Fig. 29 the minimum dispersion is 0.02 ps/km-nm in the range of 1.45 μm to 1.56 μm with zero-dispersion wavelengths at 1.45 μm, 1.50 μm, and 1.55 μm. This is an example in which DBCONF is used to determine a waveguide dispersion which is almost the negative of the material dispersion, resulting in a very low total dispersion within the 1.44 μm to 1.58 μm wavelength range. If A assumes a value equal to 10^{-4}, and the program is allowed to proceed, the dispersion curve can be pushed to become tangent to the axis as shown in Figs. 31, 32, and 33 in Chapter 7. The field distributions for fiber no. 4 and fiber no. 6 in table 2 are plotted in Fig. 30. By increasing total core radius r_6 and decreasing layer thickness ratios, the mode-field radius can be made larger.

Since we are trying to design real fibers, the glass materials in reference [49] for which Sellmeier coefficients are available are used. The results show that with these index combinations it is very difficult to achieve a single-mode fiber which has zero-dispersion wavelengths at 1.3 μm and 1.55 μm simultaneously with dispersion less than 1 ps/km-nm. For all fiber designs in Tables 2, 5, and 9 the layer indices, which are calculated based on Sellmeier coefficients [49], are used in the optimization program as input parameters, i.e., the lower limit and the upper limit of the index data are the same, only layer ratios are varied within their lower and upper limits. So the optimum output data are η_1, α, γ , and η_2.

If layer indices are allowed to vary, the more design freedom we have, the more efficient the program would be. Then the output data would include layer indices. At that point the fiber design would involve a chemical synthesis task, that of finding

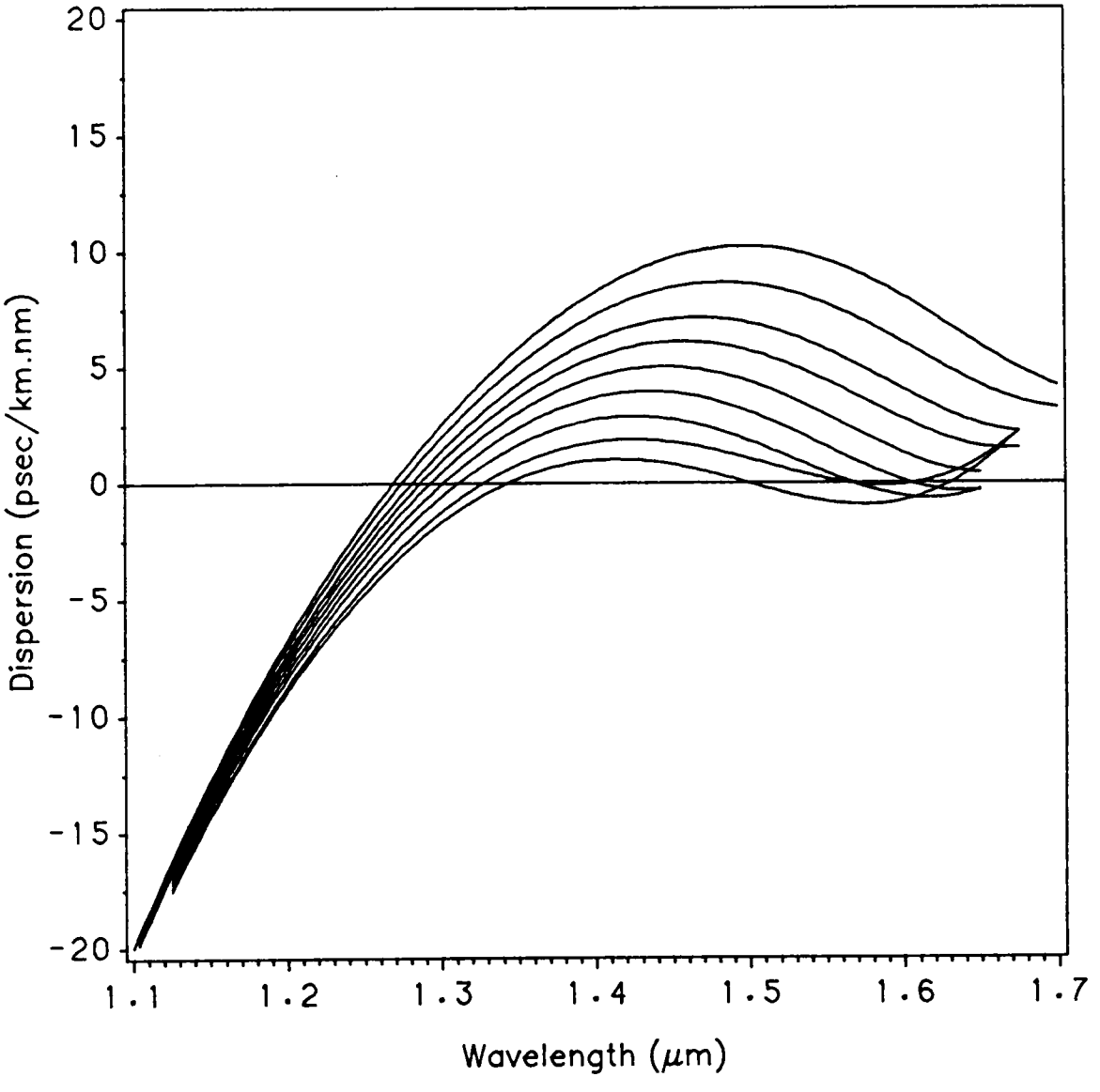

Figure 27. 7-layer fiber optimization processes (example one).

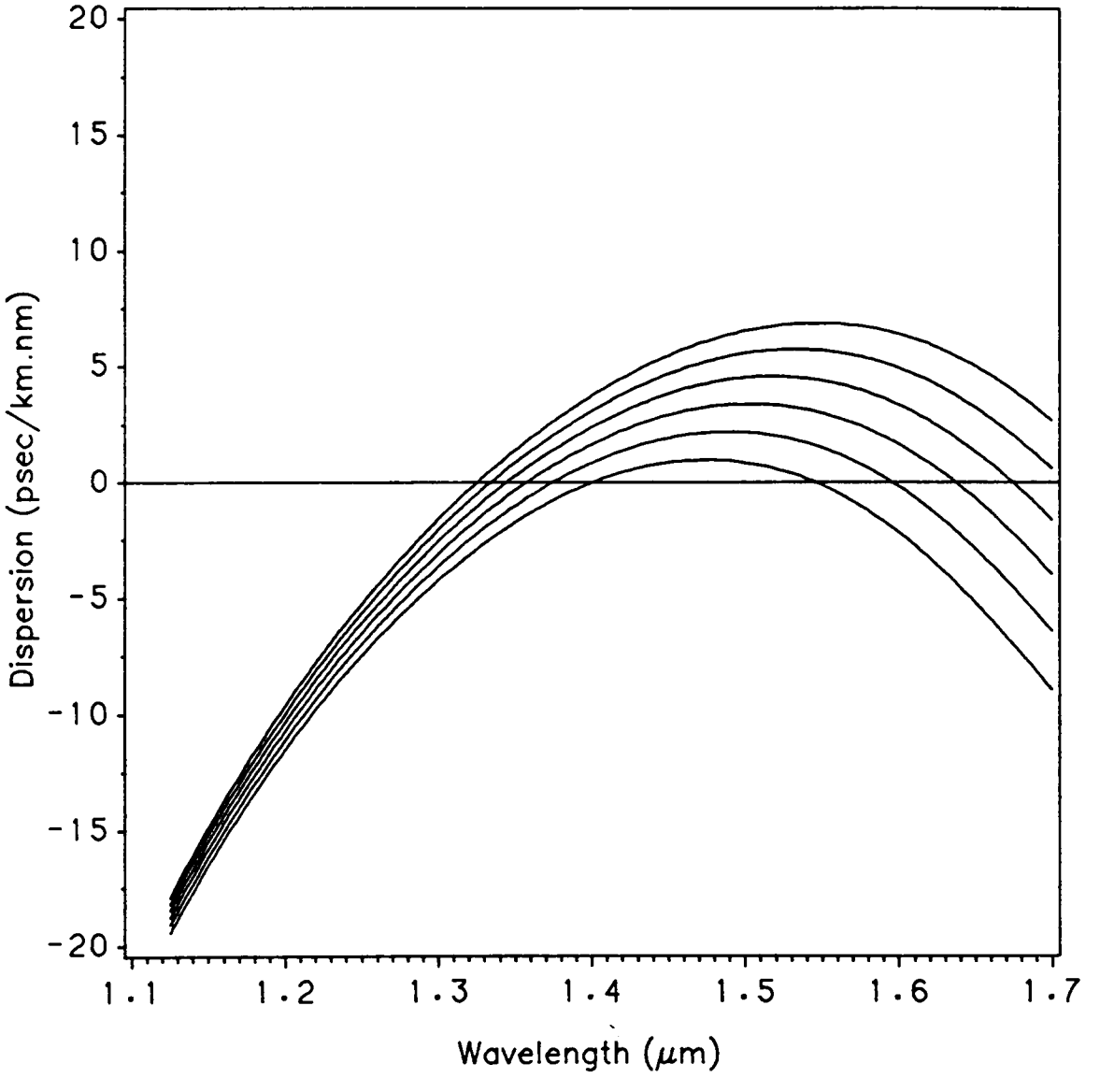

Figure 28. QC fiber optimization processes (example two).

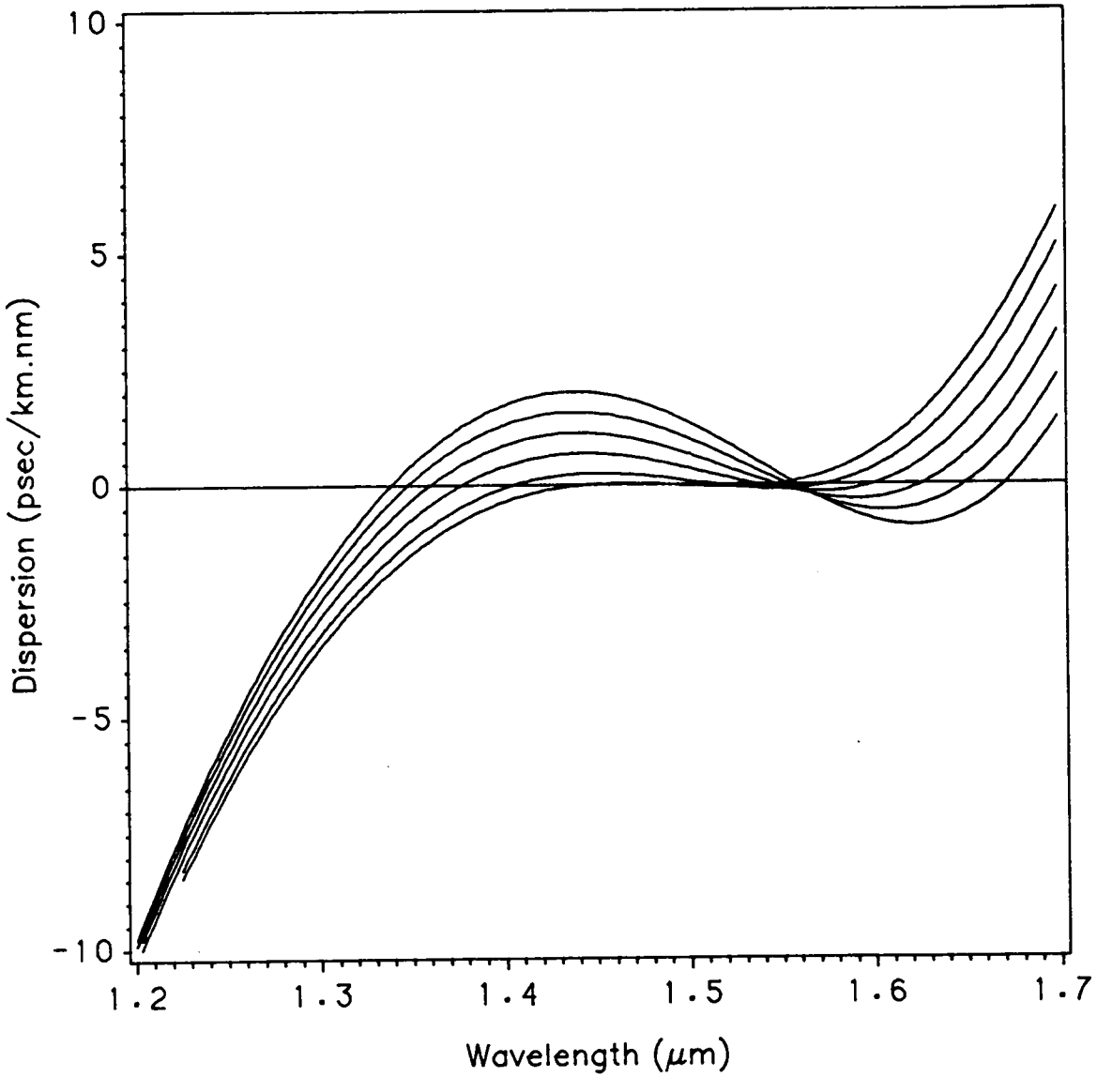

Figure 29. 7-layer fiber optimization processes (example three).

proper dopant material and the mole percentage of dopant concentrations to produce glass with specific layer indices at a specific wavelength.

Convergence and accuracy are important factors for any optimization technique. The convergence for this optimization program is very rapid, as long as $Zero_1$ and $Zero_2$ are within the ranges mentioned above. Beyond this range, the amplitude of the objective function must increase to allow for zero-dispersion adjustment. Nevertheless this program will give an optimized solution provided the requested fiber properties are not physically inconsistent. The matrix method is fast and accurate when the matrix inversion is prearranged and transfer matrices are written in a closed form. Average CPU time for optimizing a 7-layer fiber is 22 seconds for achieving a total dispersion below 3 ps/km-nm, and 45 seconds for achieving a total dispersion below 1 ps/km-nm.

In attempting to find more than three zero-dispersion points within the 1.3 μm to 1.7 μm wavelength range, a variety of profiles with step-index structures and graded-index structures were tested. Our results show that three zero-dispersion wavelengths are seemingly the maximum number of wavelengths attainable.

Table 8. Index profile parameters for 7-layer fibers

Fiber	Δn_1	Δn_2	Δn_3	η_1	α	γ	η_2	r_6
1	0.273%	0.153%	0.322%	0.874	1.144	2.500	2.500	39.25
2	0.431%	0.346%	0.153%	1.255	1.315	2.000	2.800	35.0
3	0.431%	0.346%	0.153%	1.300	1.316	2.000	2.750	35.0
4	0.418%	0.200%	0.145%	1.400	1.400	3.500	3.510	38.0

In Table 8, fiber no. 1 corresponds to fiber no. 6 in Table 2. The dispersion curve for fiber no. 2 appears in Fig. 24. The curve for fiber no. 3 appears in Fig. 25, and the curve for fiber no. 4 appears in Fig. 26.

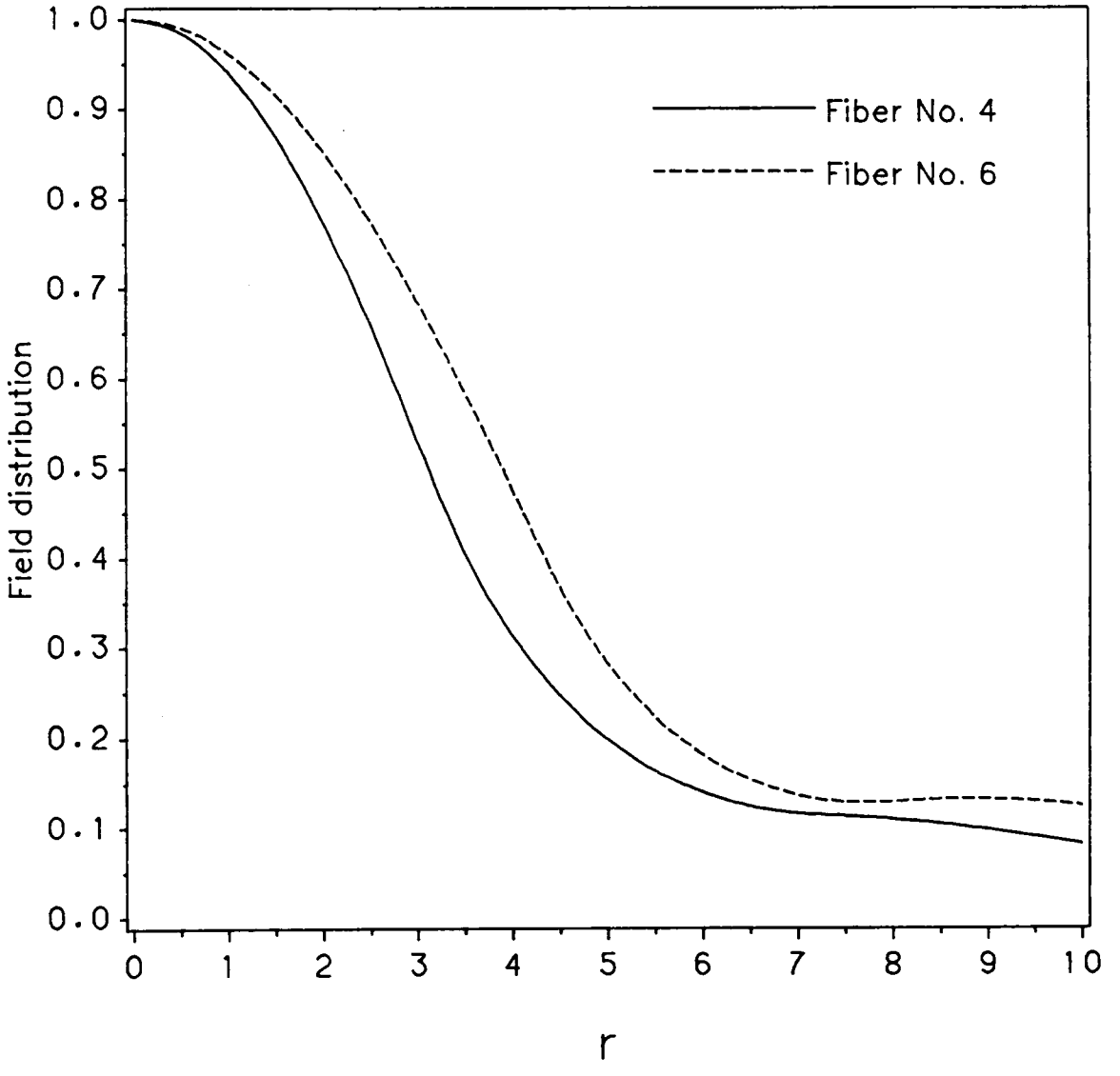

Figure 30. Field distributions for the LP_{01} mode as a function of radial coordinate.

Chapter 7. Novel Dispersion-Shifted Fibers

The 1.55 μm transmission window is very promising for long distance optical fiber communications, because in this wavelength region silica fibers have minimum transmission loss and low splice loss due to relatively larger mode-field radius. Also, the excess losses caused during the cabling process, installation, and long-term use in the field are lower for longer wavelengths. However, single-mode fibers with a conventional design have about 20 ps/km-nm dispersion at 1.55 μm [68]. Reduction of chromatic dispersion in the 1.55 μm transmission window can be achieved by dispersion-shifted single-mode fiber, but values as high as 8 ps/km-nm are still apparent at 1.45 μm and 1.65 μm for zero-dispersion at 1.55 μm [69].

Dispersion-shifted fibers have been produced before by using single-clad structures with GeO_2-doped silica cores, but these fibers exhibited higher losses than had been expected due to an increase in Rayleigh scattering by higher germanium concentrations. A later development came in the form of a graded-index profile which allowed the excess loss to be greatly reduced. One disadvantage of this design is its sensitivity to bending. To overcome this problem there must be an increase in the peak dopant level or core diameter, both of which shift the LP_{11} mode cutoff to longer

wavelengths. The former leads to higher excess loss while the latter causes the zero-dispersion point to assume a wavelength shorter than 1.55 μm.

The total dispersion can be reduced to zero only at one wavelength. It increases as the wavelength departs from the optimum wavelength for the dispersion-shifted fibers. This restricts the choice of laser sources and limits wavelength multiplexing potential. It is desirable that the total dispersion of a single-mode fiber be minimized over an extended spectral range covering the low-loss window. We report, for the first time, ultralow dispersion single-mode (ULDSM) fiber with zeroth-order dispersion $< 10^{-2}$ ps/km-nm throughout a 1 μm range centered about 1.5 μm or 1.55 μm wavelength. The first-order and second-order derivatives of the dispersion are zero at 1.5 μm or 1.55 μm. This effectively increases the laser emission tolerance. ULDSM fibers open the way to wavelength multiplexing with inexpensive available multifrequency lasers for either local or long distance network application.

7.1. Maximum Information Capacity of Single-Mode Fiber

Pulse spreading in single-mode fibers is caused by the material dispersion and waveguide dispersion of the fiber and the spectral width of the source. In this section we analyze the cancellation between material and waveguide dispersion and predict an optimum fiber for which the zeroth-order total dispersion as well as the first and second-order residual dispersion are zero at 1.5 μm or 1.55 μm. If a source spectrum spreads about the minimum dispersion, higher-order dispersion terms become important. The group delay τ is given by [70]

$$\tau = \frac{L}{c} N, \tag{7.1}$$

where L is the length of the fiber and N is the group index. If a signal is simultaneously impressed on the two wavelengths, say, λ, $\lambda + \Delta\lambda$, the arrival time after traveling a distance L differs by an amount

$$\Delta\tau = \frac{L}{c}[N(\lambda) - N(\lambda + \Delta\lambda)]. \tag{7.2}$$

If $\Delta\lambda/\lambda \ll 1$, this pulse spreading in group delay, $\Delta\tau$, can be obtained by means of a Taylor series expansion of the pulse propagation time, τ, about λ_0 [70]

$$\Delta\tau = \frac{L}{c}\left[\frac{dN}{d\lambda}\Delta\lambda + \frac{1}{2}\frac{d^2N}{d\lambda^2}\left(\frac{\Delta\lambda}{2}\right)^2 + \ldots\right], \tag{7.3}$$

here N is the group index including both material and waveguide dispersion. The neglected higher-order terms would become significant if the zeroth-order dispersion vanishes at λ_0. The residual first-order pulse spreading for a source of width $\Delta\lambda$ centered at λ_0 is proportional to $(\Delta\lambda/2)^2$ as shown in Eq. (7.3). This represents the slope of chromatic dispersion and has the value of 2.50×10^{-2} ps/km-nm^2 for fused silica at 1.273 μm. The carrier frequency limited pulsewidth is about 2×10^{-3} ps [71].

7.2. Dispersion Minimum at 1.55 μm

For a fiber with zero-dispersion wavelength shifted to 1.55 μm,

$$\left.\frac{dN}{d\lambda}\right|_{\lambda_0 = 1.55} = 0. \tag{7.4}$$

At λ_0, the first-order residual dispersion limits the information capacity of the single-mode fiber [71]. The information capacity may be further increased if $d^2N/d\lambda^2$

is also zero at λ_0. Again, the Fig. 1 index profile is used to achieve this goal. One should run the optimization program DFSM and set the objective function as

$$O(\lambda) = \lambda_0 + \lambda^3, \tag{7.5}$$

where λ_0 is a shifted center wavelength. The optimum results in Figs. 31-33 correspond to the data in Table 9 and Table 10. Dispersion spectra for fiber no. 1 and fiber no. 2 are achieved by using the objective function of Eq. (7.5) and setting λ_0 = 1.51 μm. The maximum dispersion is < 0.01 ps/km-nm within the wavelength range of 1.45 μm to 1.59 μm for both fibers. The zeroth-order total dispersion as well as the first and second-order residual dispersion for fiber no. 1 are zero at 1.515 μm wavelength, and 1.510 μm for fiber no. 2. Dispersion spectra for fiber no. 3 are achieved by using the sinusoidal objective function of Eq. (6.1) and setting $A = 10^{-4}$, $B = 0$, $Zero_1$ = 1.5, and $Zero_2$ = 1.6. The results are shown in Fig. 33, where zero-dispersion wavelengths are at 1.5 μm, 1.55 μm, and 1.6 μm respectively, and the maximum dispersion is < 0.01 ps/km-nm in the wavelength range of 1.49 μm to 1.61 μm. The first and second-order residual dispersion are zero at 1.55 μm wavelength.

Normalized propagation constant $\bar{\beta}$ versus normalized frequency V for LP_{01}, LP_{02}, and LP_{11} modes has been ploted for fiber no. 1 as presented in Fig. 34. The short horizontal line along the frequency axis in Fig. 34 corresponds to the ultralow dispersion wavelength range of the fiber no. 1. It implies that fiber no. 1 is a true single-mode fiber.

Again, Eq. 3.2 is used to analyze splice loss of the ULDSM fiber. Splice loss for fiber no. 1 is presented in Fig. 35. It has been noticed that the splice loss for ULDSM fiber is smaller than DC, TC, and QC fibers with the same lateral offset. The field distribution for the LP_{01} mode of fiber no. 1 is shown in Fig. 36.

All three examples in Table 9 are calculated using reported Sellmeier parameters [49], therefore, index tolerance effects are ignored here, only geometric imperfections are considered.

Figures 37 to 42 demonstrate that the production tolerance would be very tight. These figures are produced in the same way as in Section 4.2. Tolerance analysis is not repeated here, only an estimate of tolerance variations in layer radii is given. It can be shown from Eq. (4.3) that one also can have very tight a and Δ values, since σ_D is less than 0.01 ps/km-nm.

The absolute tolerance value of δr_1 is then ± 0.06 μm for the value of $\partial D/\partial r_1$ = 33.3 ps/km-nm-μm as shown in Fig. 37. The absolute tolerance value of δr_2 is then ± 0.16 μm for the value of $\partial D/\partial r_2$ = 12.5 ps/km-nm-μm as shown in Fig. 38. The absolute tolerance value of δr_3 is then ± 0.24 μm for the value of $\partial D/\partial r_3$ = 8.3 ps/km-nm-μm as shown in Fig. 39. Figure 40 shows that the values of $\partial D/\partial r_4$ are always small if the tolerance values of δr_4 are positive. By contrast, Fig. 41 shows that the values of $\partial D/\partial r_5$ are always small if the tolerance values of δr_5 are negative. Again, possible tolerance cancellations can occur between r_1 and r_3, r_2 and r_3, and r_4 and r_5.

The fiber profile data and fiber performance data of Figs. 31 to 33 are listed in Table 9 and Table 10. The index differences have been calculated at a wavelength $\lambda = 1.3 \mu m$, and the index of the reference layer $n_0 = 1.450815$ for fiber no. 1, $n_0 = 1.449128$ for fiber no. 2, and $n_0 = 1.446918$ for fiber no. 3. Core and Cladding materials for the fibers are presented in Table 11. The material compositions are shown in Appendix B.

Table 9. Index profile parameters for novel dispersion-shifted fibers

Fiber	Δn_1	Δn_2	Δn_3	η_1	α	γ	η_2	r_6
1	0.338%	0.158%	0.273%	1.320	1.265	1.860	2.000	30.0
2	0.458%	0.171%	0.297%	1.340	1.470	1.934	2.810	30.0
3	0.431%	0.153%	0.322%	1.384	1.420	1.998	2.523	30.0

Table 10. Fiber performance data for novel dispersion-shifted fibers

Fiber	λ_{c01}	λ_{c11}	$\omega_{1.3}$	$\omega_{1.55}$	DF (< 0.01 ps/km-nm)
1	1.72	1.21	----	3.74	1.45 - 1.59
2	1.86	1.22	----	4.28	1.45 - 1.59
3	1.75	1.13	----	3.77	1.49 - 1.61

- the units for cutoff wavelength λ_c are μm.
- the units for mode-field radius ω are μm.

Table 11. Cladding materials for novel dispersion-shifted fibers

Fiber	*layer 1*	*layer 2*	*layer 3*	*layer 4*	*layer 5*	*layer 6*	*layer 7*
1	M8	M1	M2	M1	M2	M1	M3
2	M8	M5	M6	M5	M6	M5	M10
3	M2	M12	M10	M12	M10	M12	M1

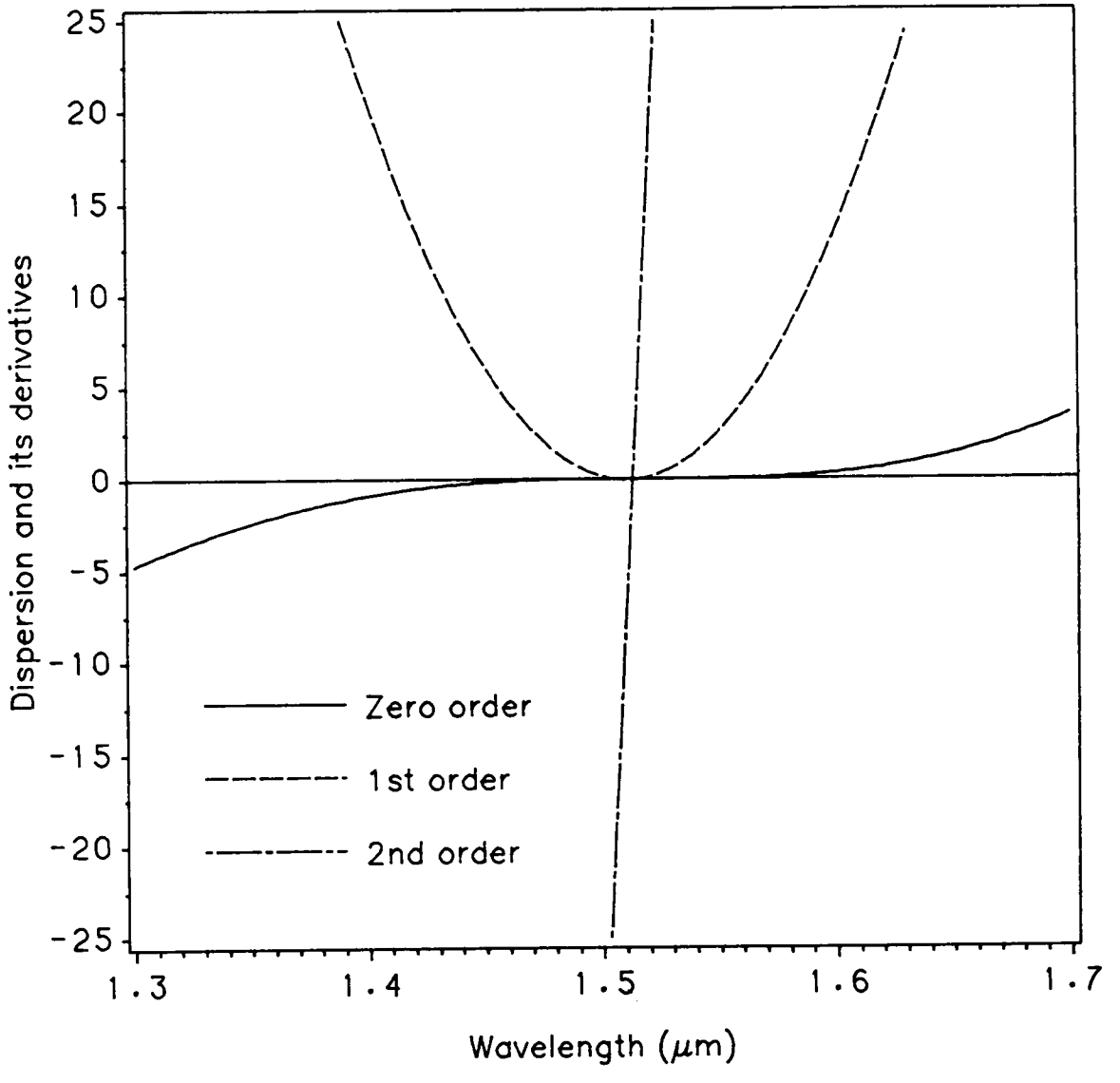

Figure 31. Chromatic dispersion and its 1st-order and 2nd-order derivatives versus wavelength for fiber no. 1.

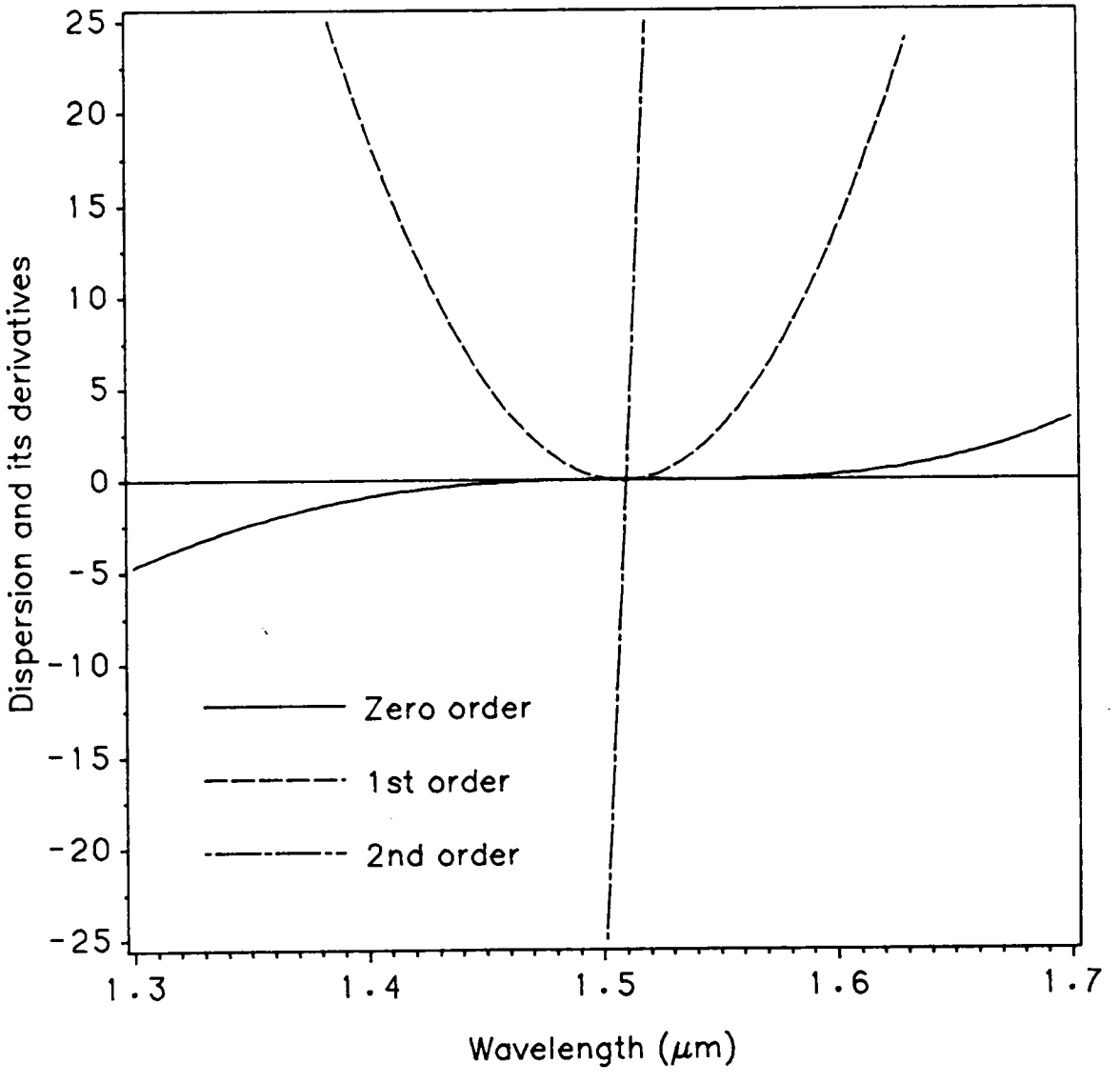

Figure 32. Chromatic dispersion and its 1st-order and 2nd-order derivatives versus wavelength for fiber no. 2.

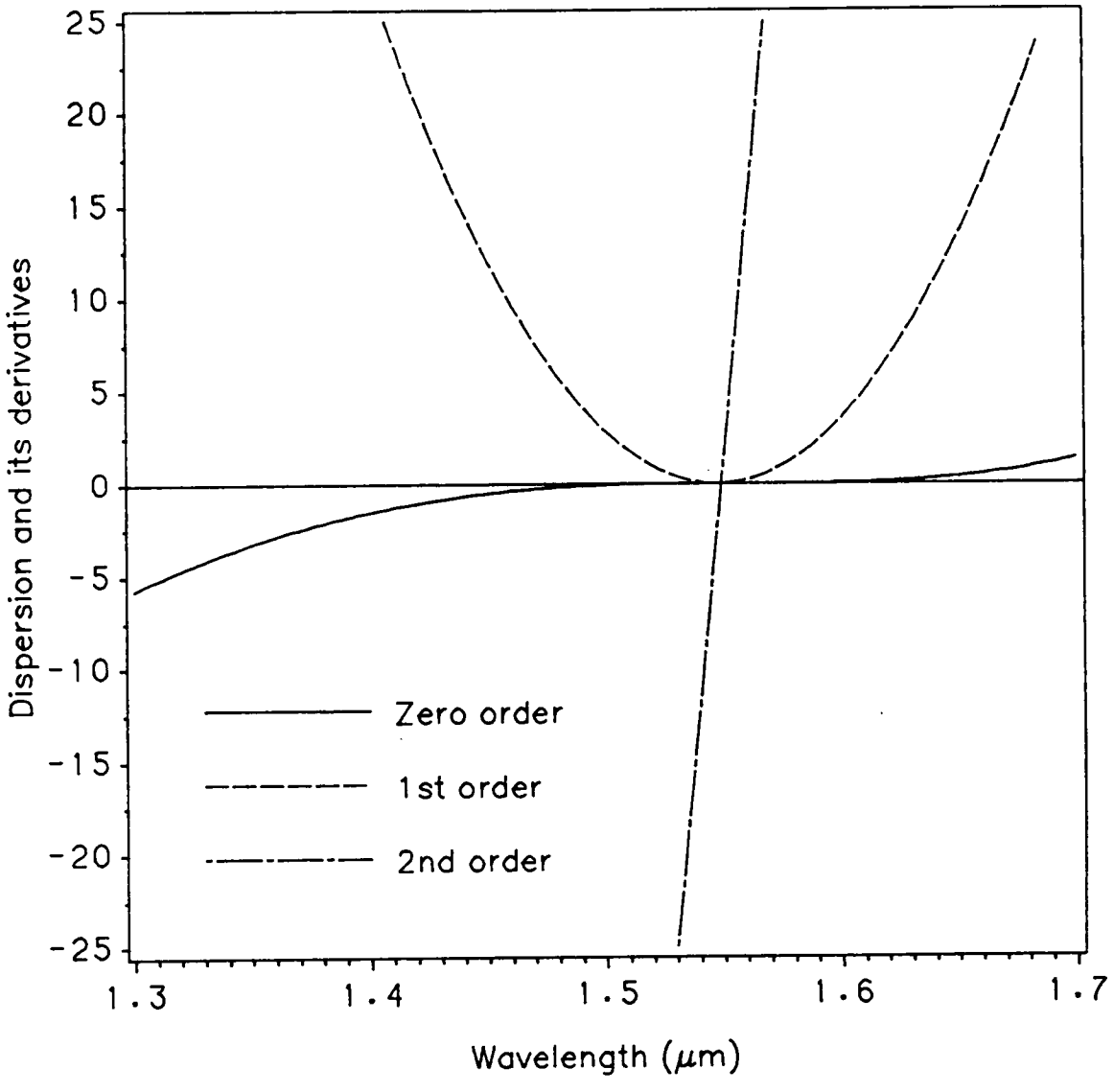

Figure 33. Chromatic dispersion and its 1st-order and 2nd-order derivatives versus wavelength for fiber no. 3.

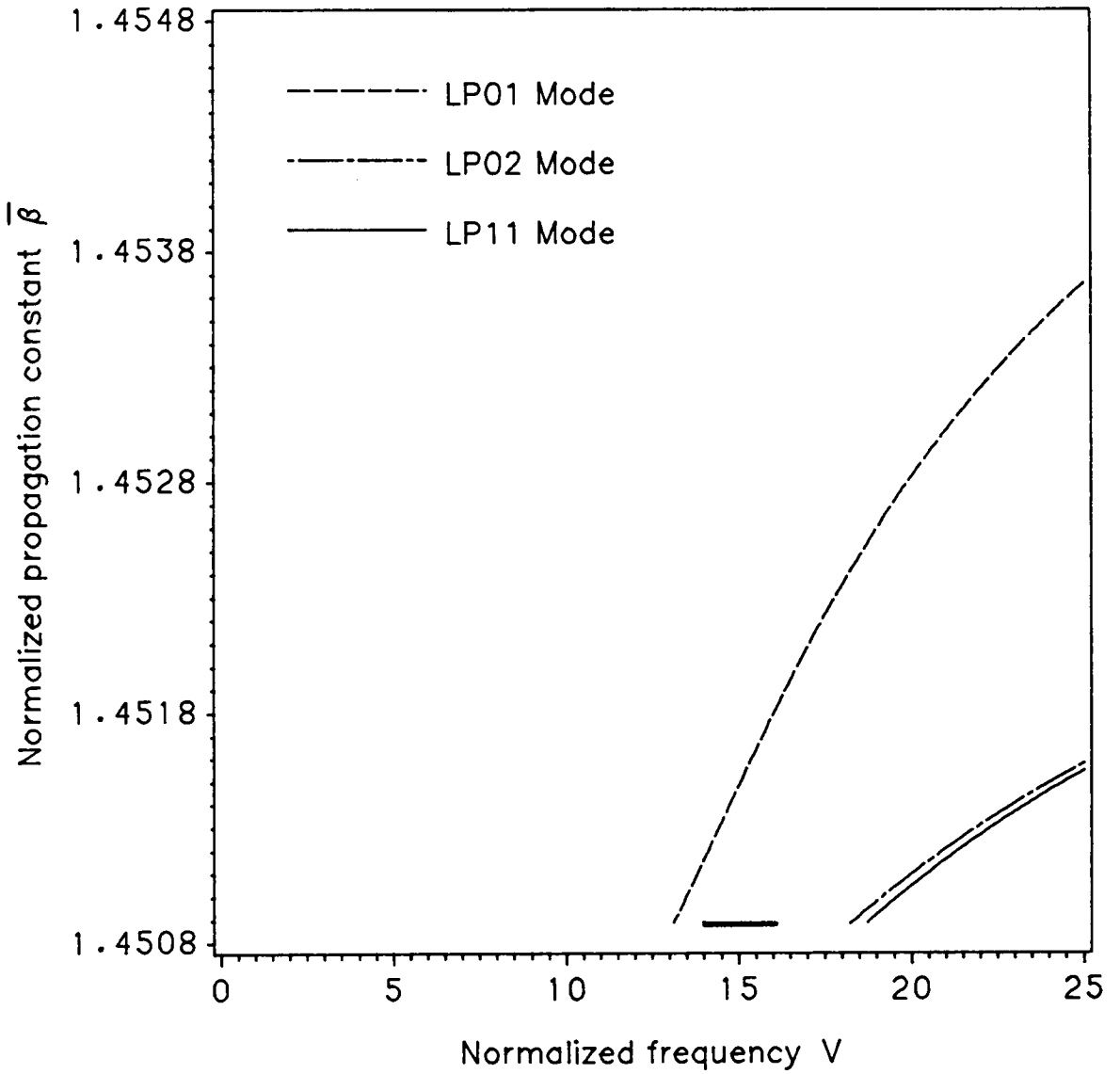

Figure 34. $\bar{\beta} - V$ curves for the LP_{01}, LP_{02}, and LP_{11} modes of fiber no. 1.

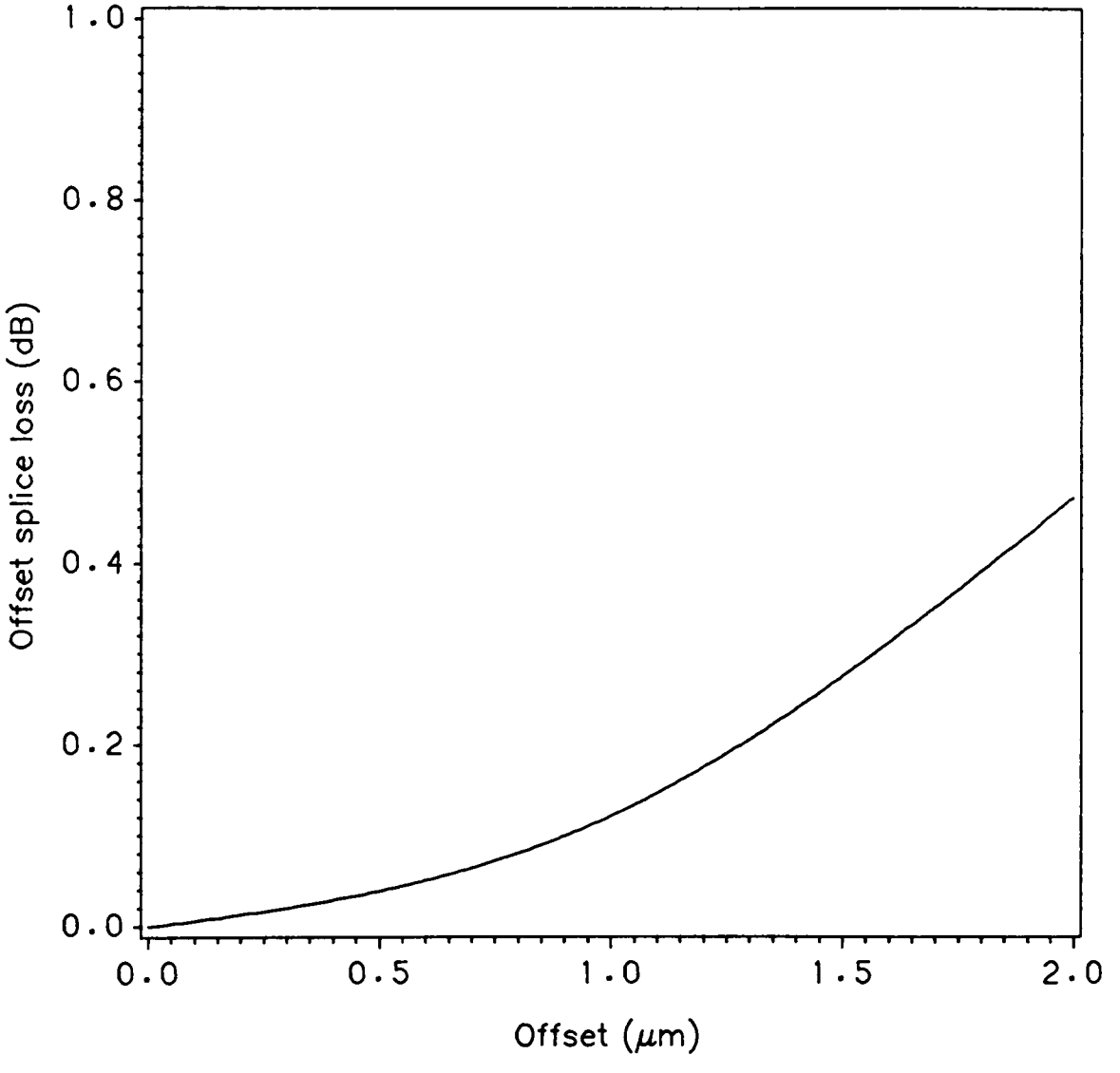

Figure 35. Lateral offset loss for fiber no. 1 (for the LP_{01} mode at 1.55 μm).

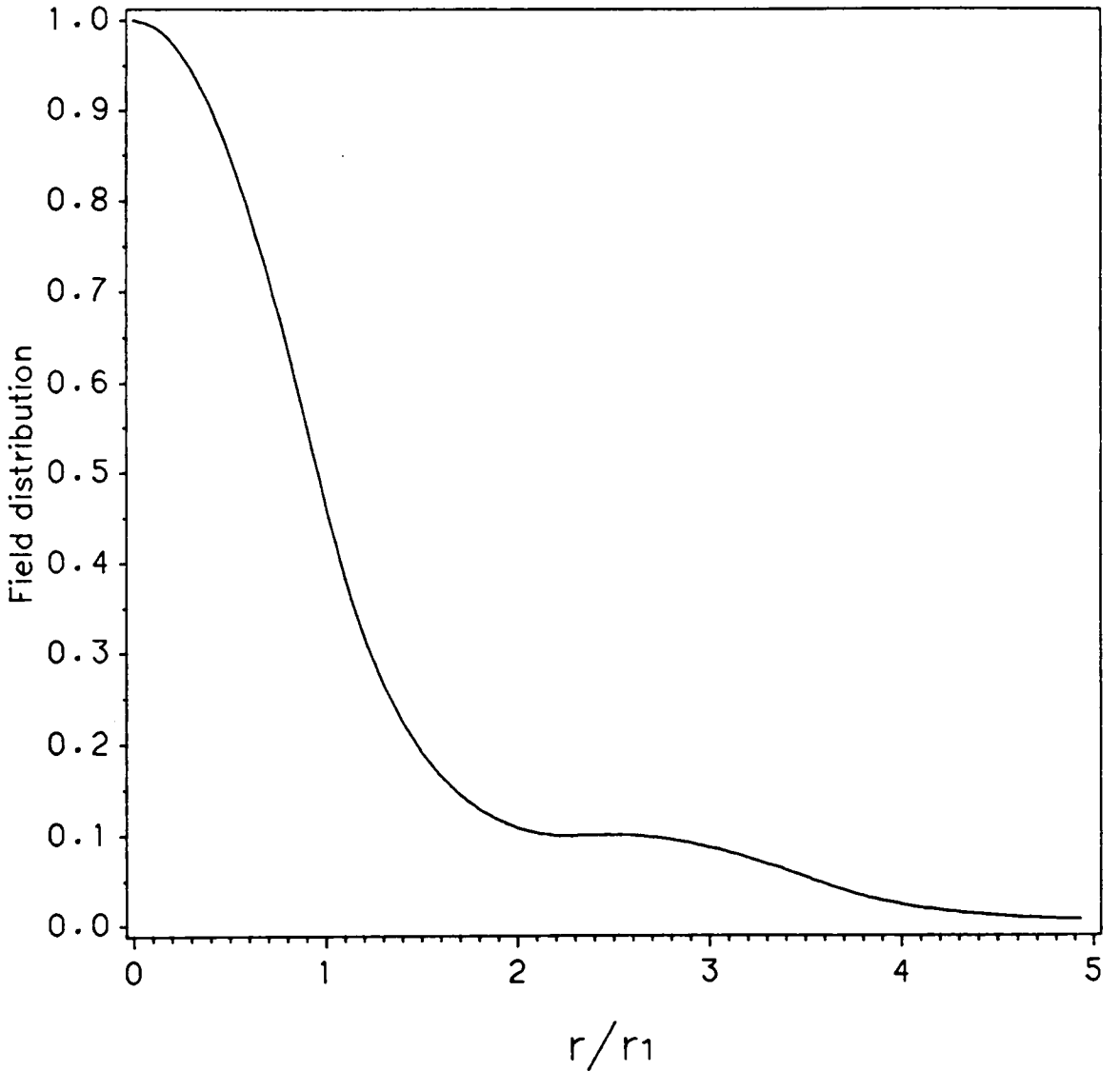

Figure 36. Field distribution for the LP_{01} mode of fiber no. 1 as a function of radial coordinate.

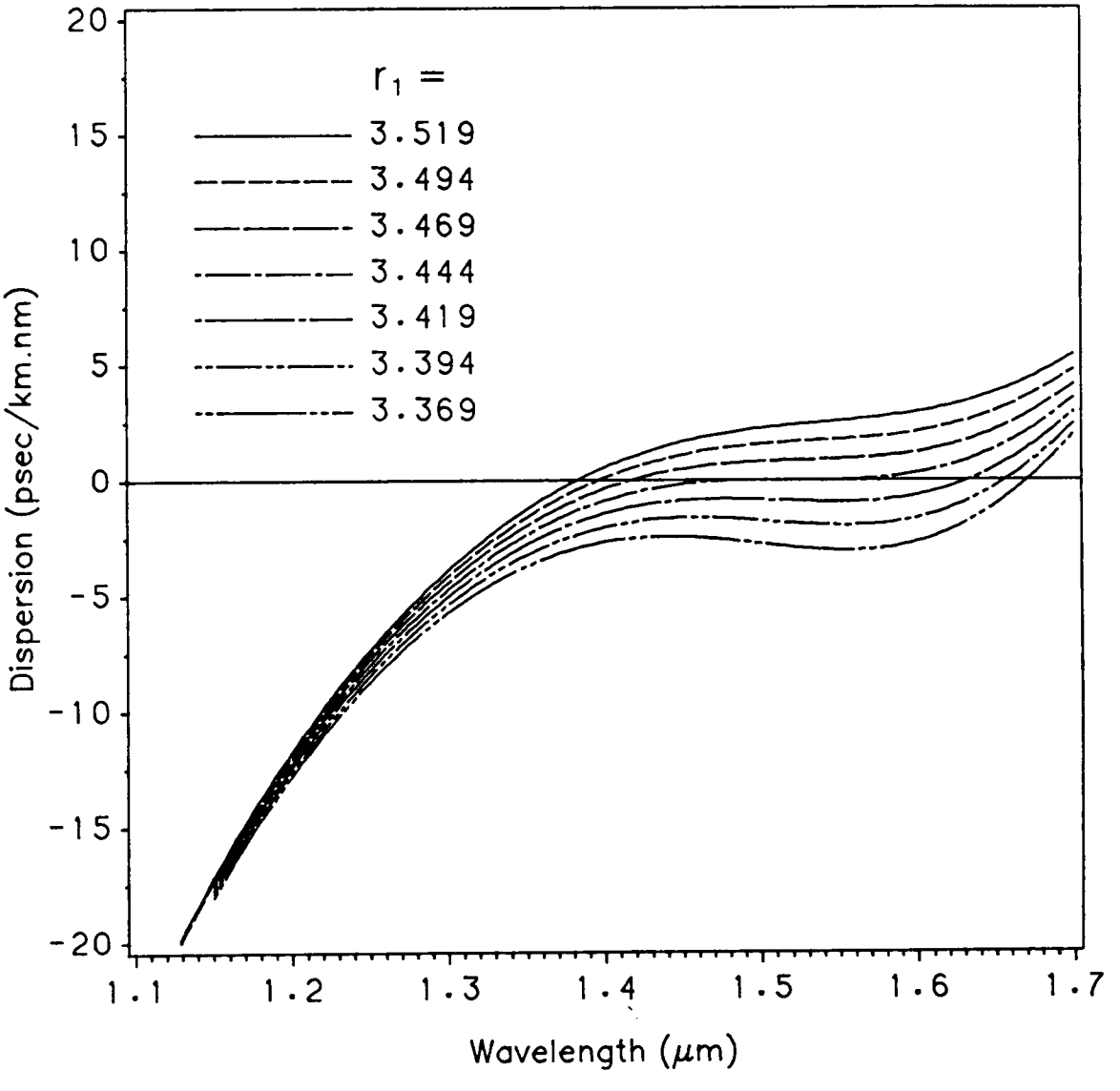

Figure 37. Variations of dispersion for fiber no. 1 as a function of r_1 for constant r_2, r_3, r_4, r_5, and r_6.

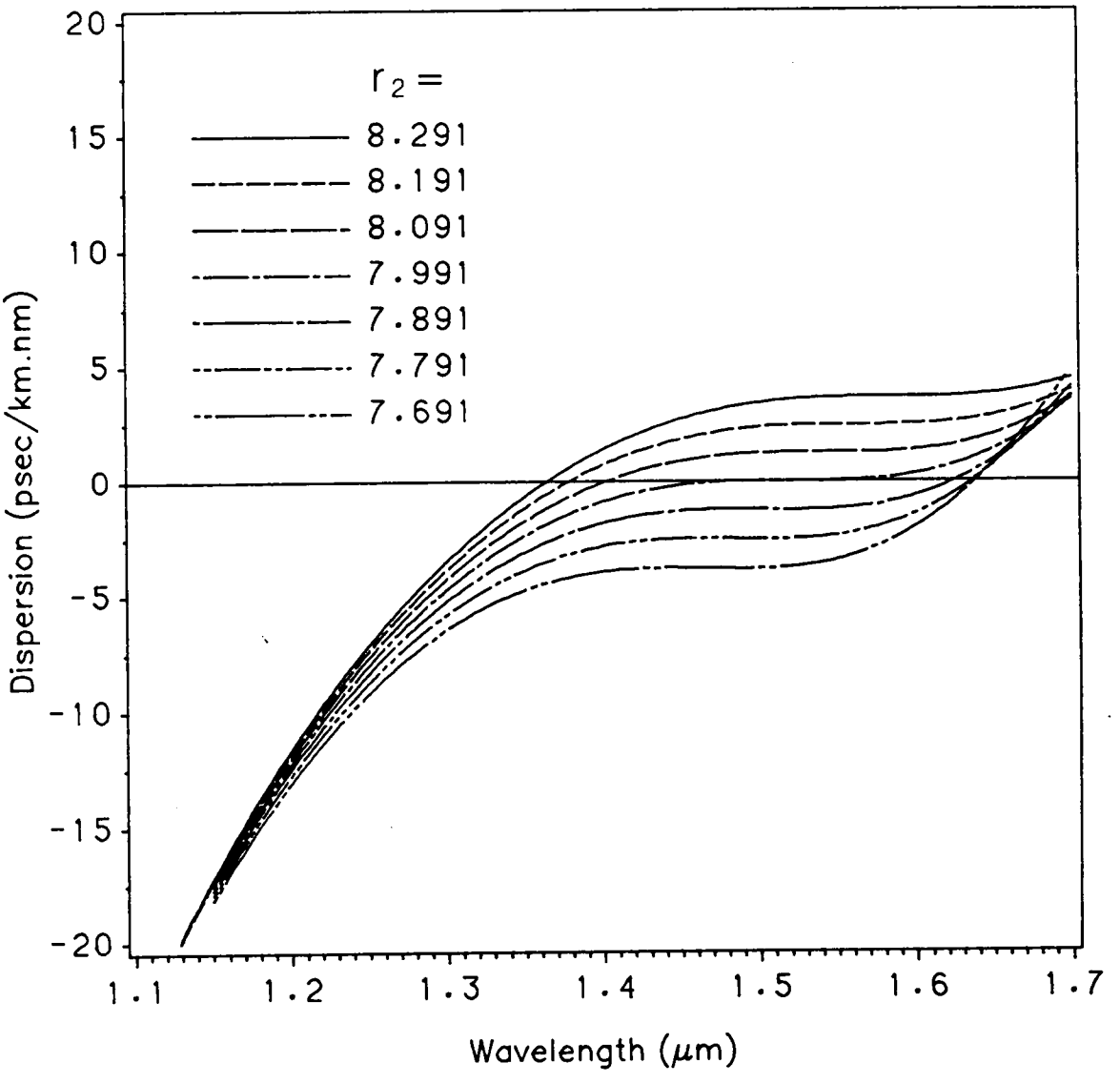

Figure 38. Variations of dispersion for fiber no. 1 as a function of r_2 for constant r_1, r_3, r_4, r_5, and r_6.

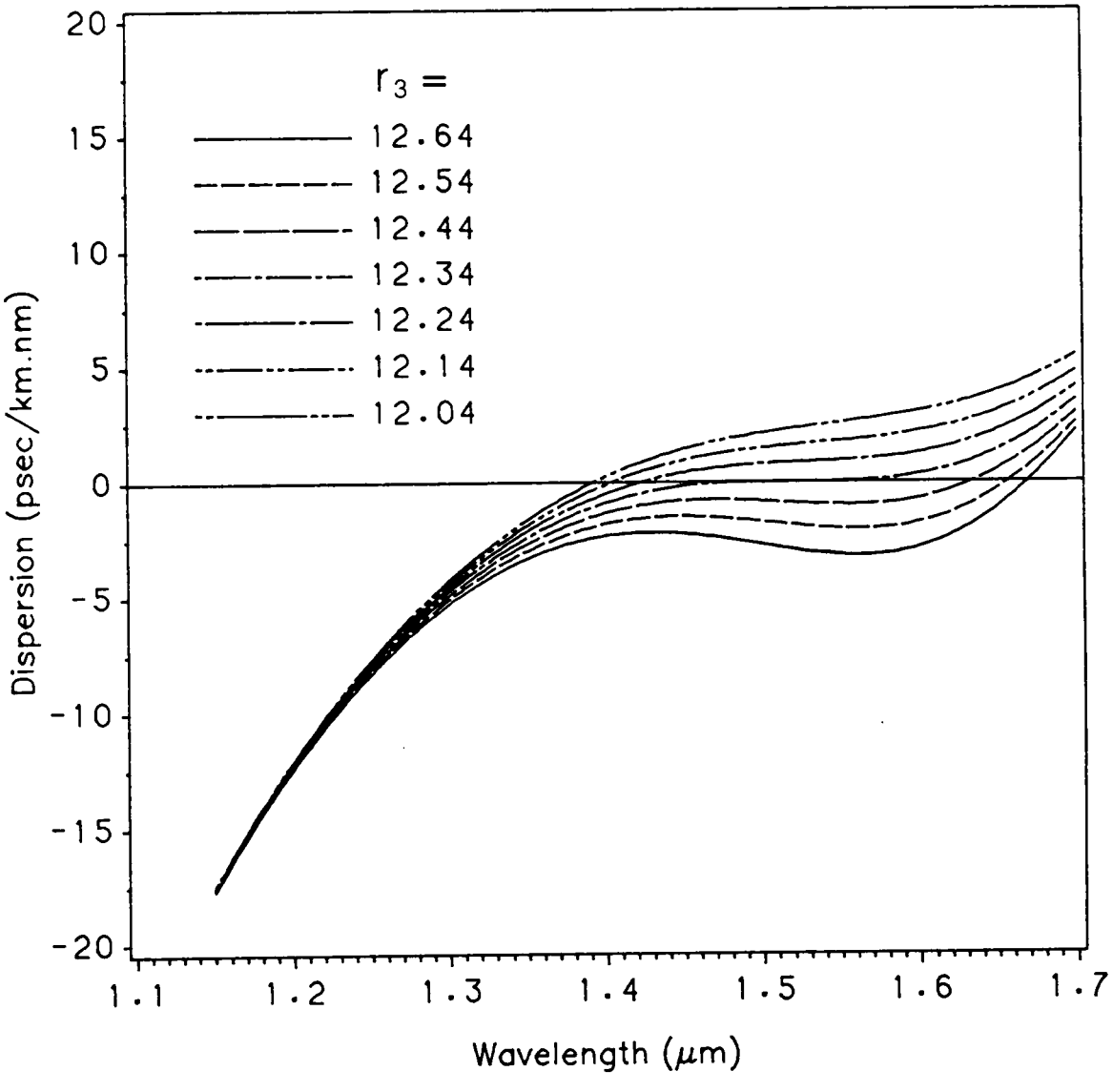

Figure 39. Variations of dispersion for fiber no. 1 as a function of r_3 for constant r_1, r_2, r_4, r_5, and r_6.

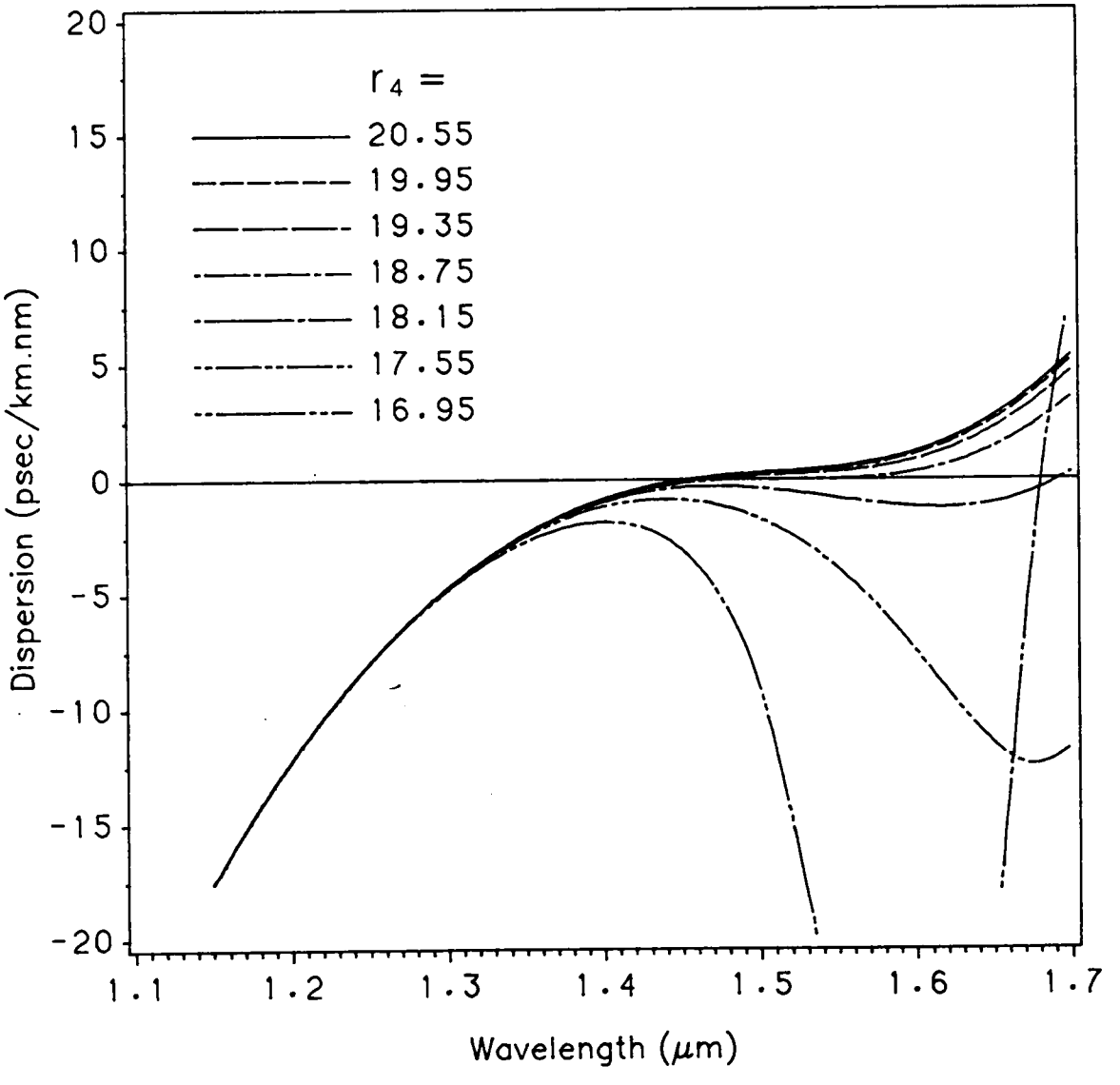

Figure 40. Variations of dispersion for fiber no. 1 as a function of r_4 for constant r_1, r_2, r_3, r_5, and r_6.

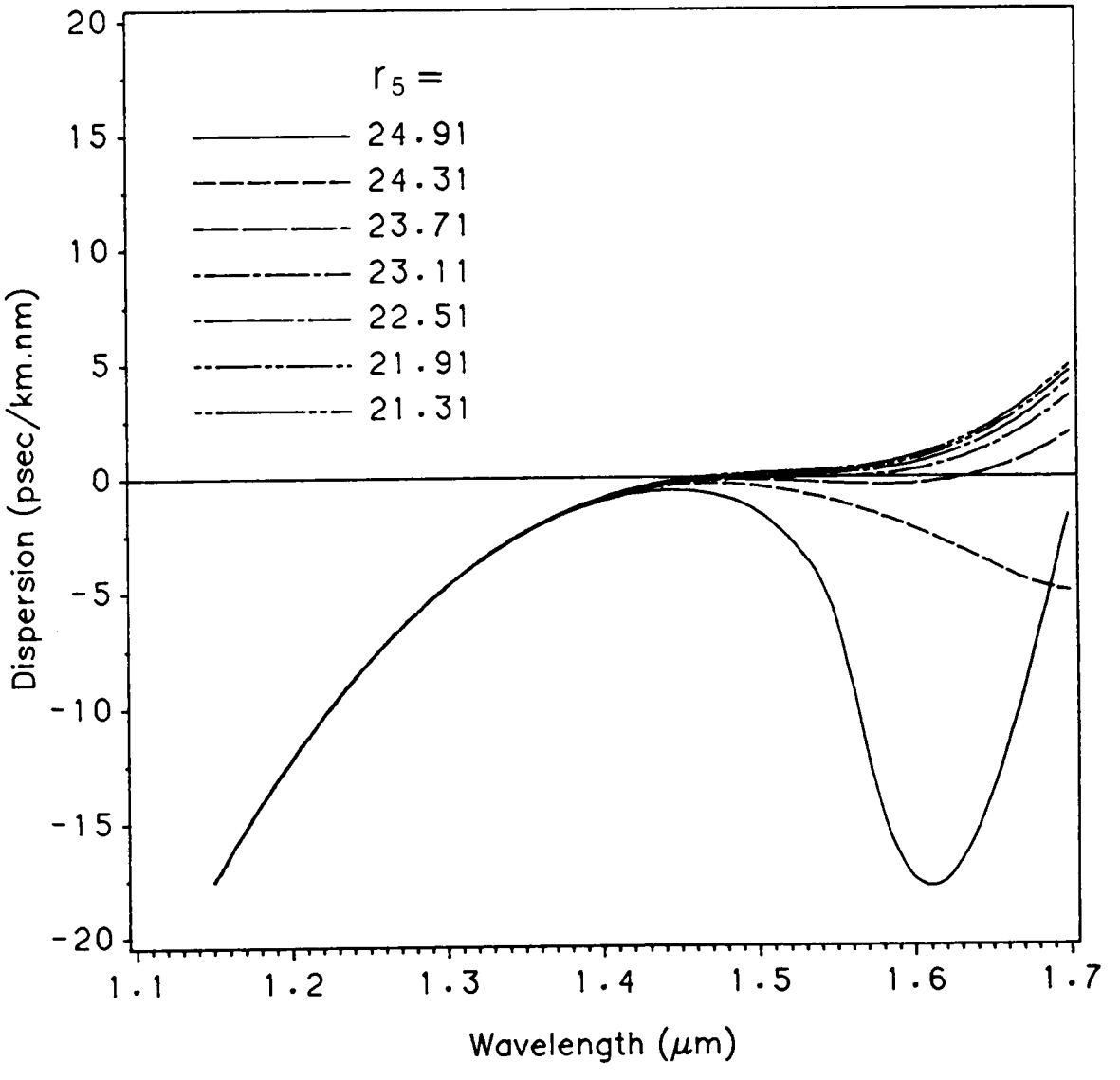

Figure 41. Variations of dispersion for fiber no. 1 as a function of r_5 for constant r_1, r_2, r_3, r_4, and r_6.

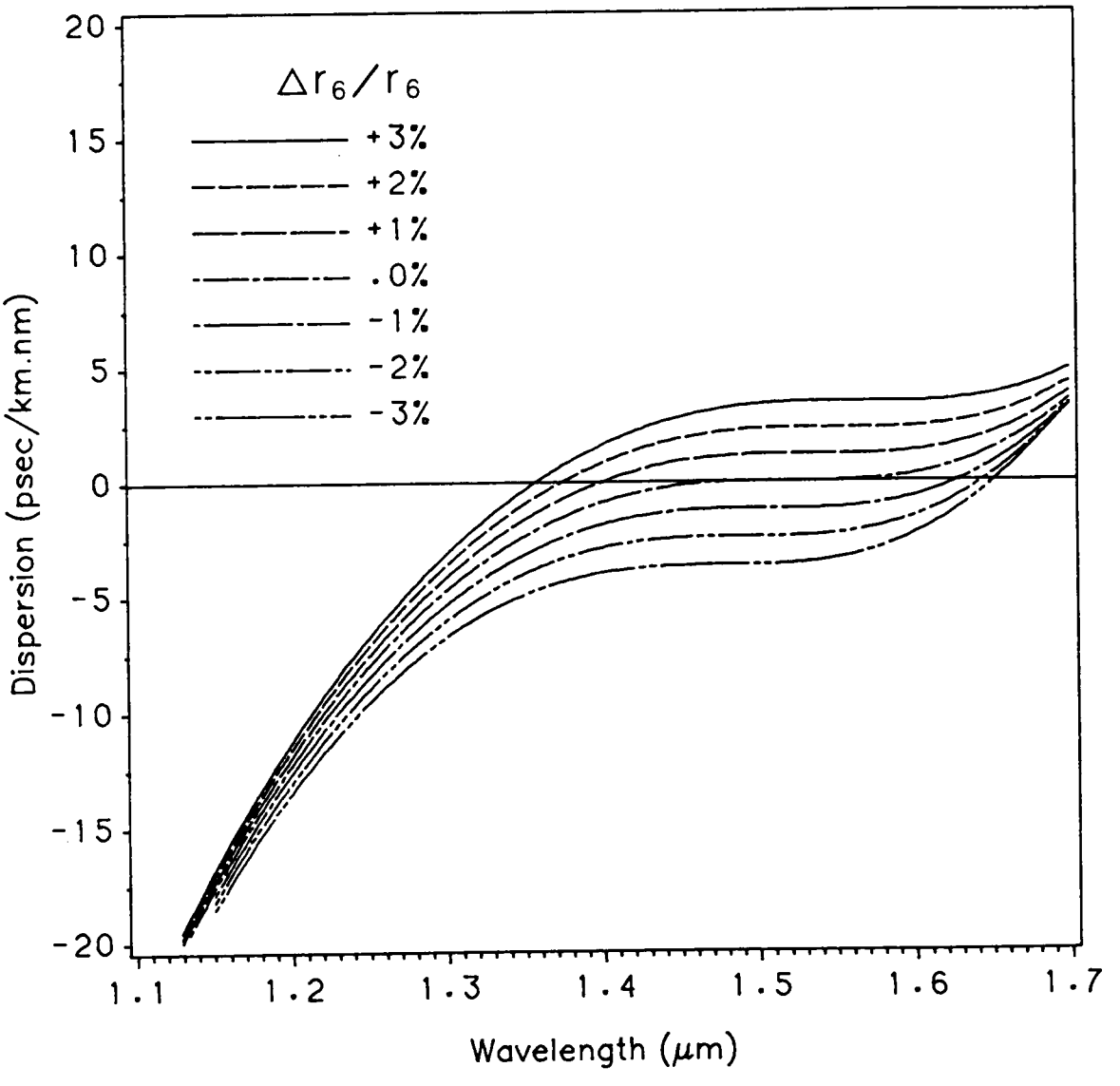

Figure 42. Variations of dispersion for fiber no. 1 as a function of r_6 for constant layer thickness ratios η_1, η_2, α, and γ.

Chapter 8. Accuracy of Approximate Methods for the Evaluation of Chromatic Dispersion in Dispersion-Flattened Fibers

The approximation based on the assumption that waveguide and material dispersion are additive effects leads to a reasonably accurate estimate of chromatic dispersion in ordinary step-index fibers. However, whether this approximation is also adequate for ultralow dispersion fibers is questionable. This chapter examines the accuracy of approximate methods for estimating chromatic dispersion in dispersion-flattened fibers. With these methods, the material dispersion of fiber is approximated by (*a*) the dispersion of pure fused silica, (*b*) the dispersion of the core material, and (*c*) the weighted average of material dispersion of various layers of the fiber. Actual and three approximate dispersions are calculated and compared for fibers with two, three, four, and six cladding regions. Examples for both satisfactory and poor accuracy are given. Generally, for fibers with index differences larger than 0.8% - 1%, the errors in approximate dispersion, relative to the actual dispersion, are substantial at

most wavelengths in the dispersion-flattened window. It is shown that the accuracy of approximate methods depends on the index differences and their first and second-order derivatives with respect to wavelength. The smaller the index differences and their derivatives, the smaller the errors in the approximate dispersion. Small index differences alone do not guarantee small errors. For GeO_2-doped fibers, the accuracy of approximate methods *b* and *c* is much better than that of method *a*.

The question may be asked that, if it is possible to calculate the actual dispersion, why should an approximate method be used, so that one must be concerned about its accuracy. In designing a fiber, the indices of most layers are initially unknown and an actual analysis of dispersion requires the Sellmeier coefficients of all indices, which are only available for a limited number of glass materials. Thus, in most fiber design work, approximate methods are important means of estimating chromatic dispersion and their accuracy should be of concern to the designers.

8.1. Calculation of Dispersion

Let us consider an optical fiber consisting of k circularly cylindrical regions. The jth region, $j = 1, 2, \ldots k$, is characterized by a refractive index n_j. Figure 43 illustrates the index profiles and parameters for fibers with a central core and two, three, and four claddings. The outer cladding region is assumed to extend to infinity. The scalar field in each region is expressed in terms of the Bessel and modified Bessel functions as was discussed in Chapter 2. Imposing boundary conditions, an eigenvalue equation is obtained which, for convenience, is expressed as

$$f(\lambda,\ \beta,\ n_j;\ j = 1, 2, \ldots k) = 0, \tag{8.1}$$

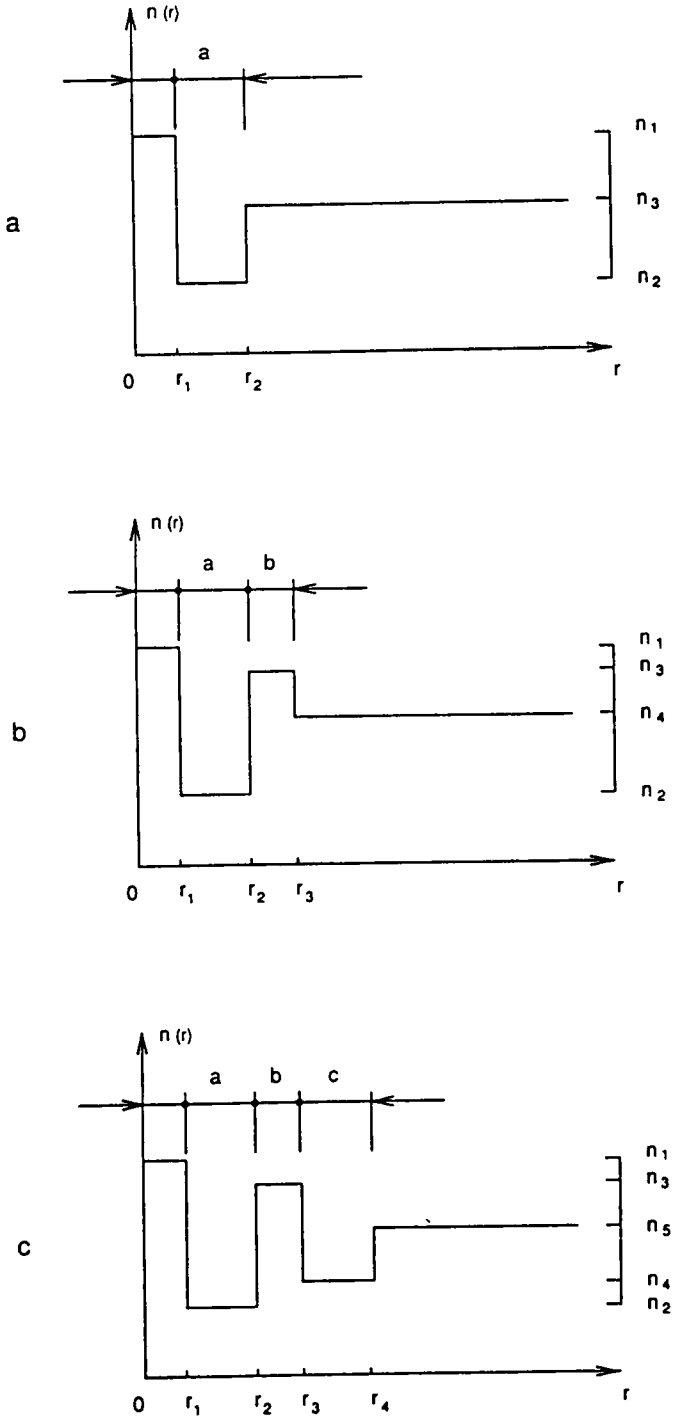

Figure 43. Index profiles and parameters for, (a) double-clad fiber, (b) triple-clad fiber, and (c) quadruple-clad fiber.

where β is the propagation constant and λ is the free-space wavelength. The dependence of β on λ determines the dispersive properties of the fiber. The function f in Eq. (8.1) also includes other variables such as core and cladding radii. These variables do not depend upon wavelength and thus are not shown explicitly in Eq. (8.1). Assuming that only the dominant LP_{01} mode propagates in the fiber, the chromatic dispersion is obtained from Eq. (2.14b). This equation is used to calculate both approximate and actual chromatic dispersion as described below.

8.1.1. Approximate Dispersion

An estimate of chromatic dispersion is obtained by adding the waveguide and material dispersion calculated separately. The waveguide dispersion, D_{wg}, is obtained from Eq. (2.14b) when β is the solution of Eq. (8.1) with constant (no variation with λ) indices n_j. The material dispersion in the jth layer, $(D_{mat})_j$, is also obtained from Eq. (2.14b) using $\beta = (2\pi/\lambda)n_j(\lambda)$ which is the propagation constant of a uniform plane-wave in an infinite homogeneous medium with refractive index n_j . For glass materials n_j is expressed in terms of Sellmeier equation [49] given by Eq. (2.19b). Using Eq. (2.19b) in Eq. (2.14b) in conjunction with $\beta = (2\pi/\lambda)n_j(\lambda)$, yields Eq. (2.19a). The total material dispersion in silica-based fibers may be approximated by the dispersion of the pure fused silica,

$$D_{mat} = (D_{mat})_{silica} , \tag{8.2a}$$

by the dispersion of the core material on the basis that much of the power flows in the core region,

$$D_{mat} = (D_{mat})_{core} , \tag{8.2b}$$

or by the weighted average of dispersion of the materials constituting the fiber,

$$D_{mat} = \sum_{j=1}^{k} \Gamma_j (D_{mat})_j , \tag{8.2c}$$

where

$$\Gamma_j = \int_{r_j}^{r_{j+1}} |\Psi_j|^2 r dr / \int_0^{\infty} |\Psi|^2 r dr , \tag{8.3}$$

with Ψ_j being the field in the jth region. Having calculated D_{wg} and D_{mat} , the total dispersion is obtained from $D_{total} = D_{wg} + D_{mat}$.

8.1.2. *Actual Dispersion*

Substituting for n_j in Eq. (8.1) from Eq. (2.19b), the eigenvalue equation becomes a function of β and λ only. This equation now accounts for all dispersion effects simultaneously. Using numerical techniques β, $d\beta/d\lambda$, and $d^2\beta/d\lambda^2$ are readily determined from Eq. (8.1) and are put in Eq. (2.14b) to obtain the total dispersion. If the eigenvalue equation produces the actual eigenvalue, the chromatic dispersion obtained in this way will be actual dispersion. This analysis does not account for errors due to the scalar wave approximation of fields. Appendix A considers the possible magnitude of such errors.

8.2. Numerical Results

To assess the accuracy of the approximate methods discussed in the previous section, four types of dispersion-flattened fibers with two, three, four, and six claddings are examined. Furthermore, for each fiber type examples corresponding to small and large errors in the approximate dispersion are considered. For each fiber, approximate dispersion characteristics corresponding to Eqs. (8.2a), (8.2b) and (8.2c) are compared with the actual characteristic.

Table 12. Parameters for double-clad (DC) fibers

Fiber	*Data*	*Core*	*Clad* 1	*Clad* 2
	Δ	0%	1.403%	0.695%
DC1	η	1.000	1.250	
($r_2 = 5.6\mu m$)	M	$M17$	$M4$	$M15$
	Δ	0%	0.835%	0.461%
DC2	η	1.000	1.250	
($r_2 = 6.8\mu m$)	M	$M16$	$M1$	$M7$

Data for double-clad (DC) fibers are summarized in Table 12. In this Table, and in Tables 13 and 14 as well, Δ denotes the index difference with respect to the core index, η is the ratio of a layer thickness to the core radius, and M represents the material composition of the layer according to Table 15 in Appendix B. All index differences correspond to indices at $\lambda = 1.33\ \mu m$. These fibers are referred to as DC1 and DC2 and are intended as examples with low and high accuracy for the approximate dispersion, respectively. Figure 44 illustrates the actual and the approximate

dispersion characteristics for fiber DC1. It is observed that the actual method predicts a chromatic dispersion less than 2 ps/km-nm in the $1.3\ \mu m < \lambda < 1.58\ \mu m$ range. The approximate dispersion is, however, more than twice the actual dispersion at most wavelengths in the same range. Thus, errors in the approximate results are on the same order of magnitude as the dispersion itself. For $\lambda < 1.5\ \mu m$, the approximate characteristic *c* is in better agreement with the actual characteristic, but, in general, none of the approximations gives a good estimate of the chromatic dispersion. An accuracy analysis discussed later examines the causes of errors in the approximate dispersion and also gives recommendations as to when and which approximate method may be used.

Figure 45 compares the actual and approximate dispersion characteristics for DC2. It is noted that the agreement between the actual characteristic and the approximate characteristics *b* and *c* is excellent. However, the errors in the approximate dispersion based on Eq. (8.2a) are relatively large in the flattened dispersion window. In the short wavelength range, however, the accuracy of this approximate dispersion improves, simply because the chromatic dispersion itself is large in the short wavelength range. For this fiber, therefore, the approximate methods *b* and *c* can reliably predict the chromatic dispersion. This fiber, as may be seen from Table 12, has much smaller index differences than DC1. Apart from the index differences, their derivatives with respect to wavelength also influence the accuracy of the approximate methods as discussed later.

Next, dispersion characteristics of triple-clad (TC) fibers are examined. The data for these fibers, referred to as TC1, TC2 and TC3, are given in Table 13. Fibers TC1 and TC2 are examples for large and small errors in the approximate dispersion, respectively, while TC3 is an example with errors in between those of TC1 and TC2.

Figure 46 shows the actual and approximate dispersion characteristics for TC1. This fiber has been designed to offer an actual total dispersion of about 2 ps/km-nm in the 1.3 $\mu m < \lambda < 1.6\ \mu m$ range with zero-dispersion wavelengths close to 1.33 μm and 1.55 μm. We observe that all three approximate characteristics differ substantially from the actual one at most wavelengths in the desired range. As in the case of double-clad fibers, the errors of approximate dispersion are much less in the short wavelength range than those in the flattened dispersion window. In the long wavelength range, no approximate method is adequate, but for 1.3 $\mu m < \lambda < 1.48\ \mu m$, approximations *b* and *c* are better than *a*, while for 1.5 $\mu m < \lambda < 1.6\ \mu m$, approximation *a* is more accurate than *b* and *c*. It is also worth noting that the wavelengths of zero-dispersion in the approximate characteristics are shifted considerably or disappear completely.

Table 13. Parameters for triple-clad (TC) fibers

Fiber	*Data*	*Core*	*Clad 1*	*Clad 2*	*Clad 3*
	Δ	0%	1.403%	0%	0.695%
TC1	η	1.000	0.801	1.000	
($r_3 = 12.2\mu m$)	M	$M17$	$M4$	$M17$	$M15$
	Δ	0%	0.835%	0%	0.461%
TC2	η	1.000	0.990	0.898	
($r_3 = 12.5\mu m$)	M	$M16$	$M1$	$M16$	$M7$
	Δ	0%	0.628%	0.181%	0.457%
TC3	η	1.000	0.944	1.720	
($r_3 = 14.9\mu m$)	M	$M8$	$M13$	$M2$	$M10$

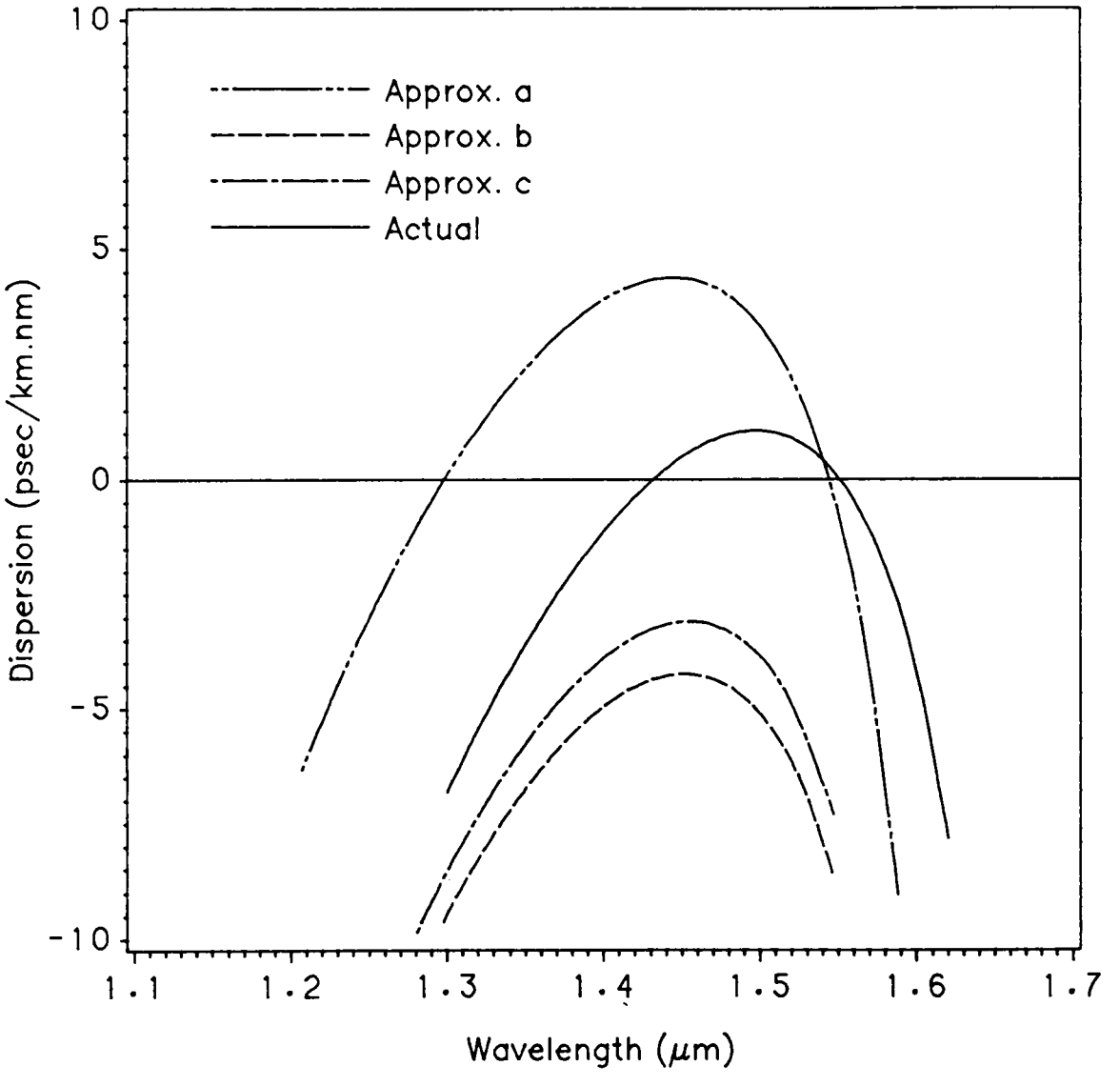

Figure 44. Comparison of actual and approximate dispersion characteristics for double-clad fiber DC1.

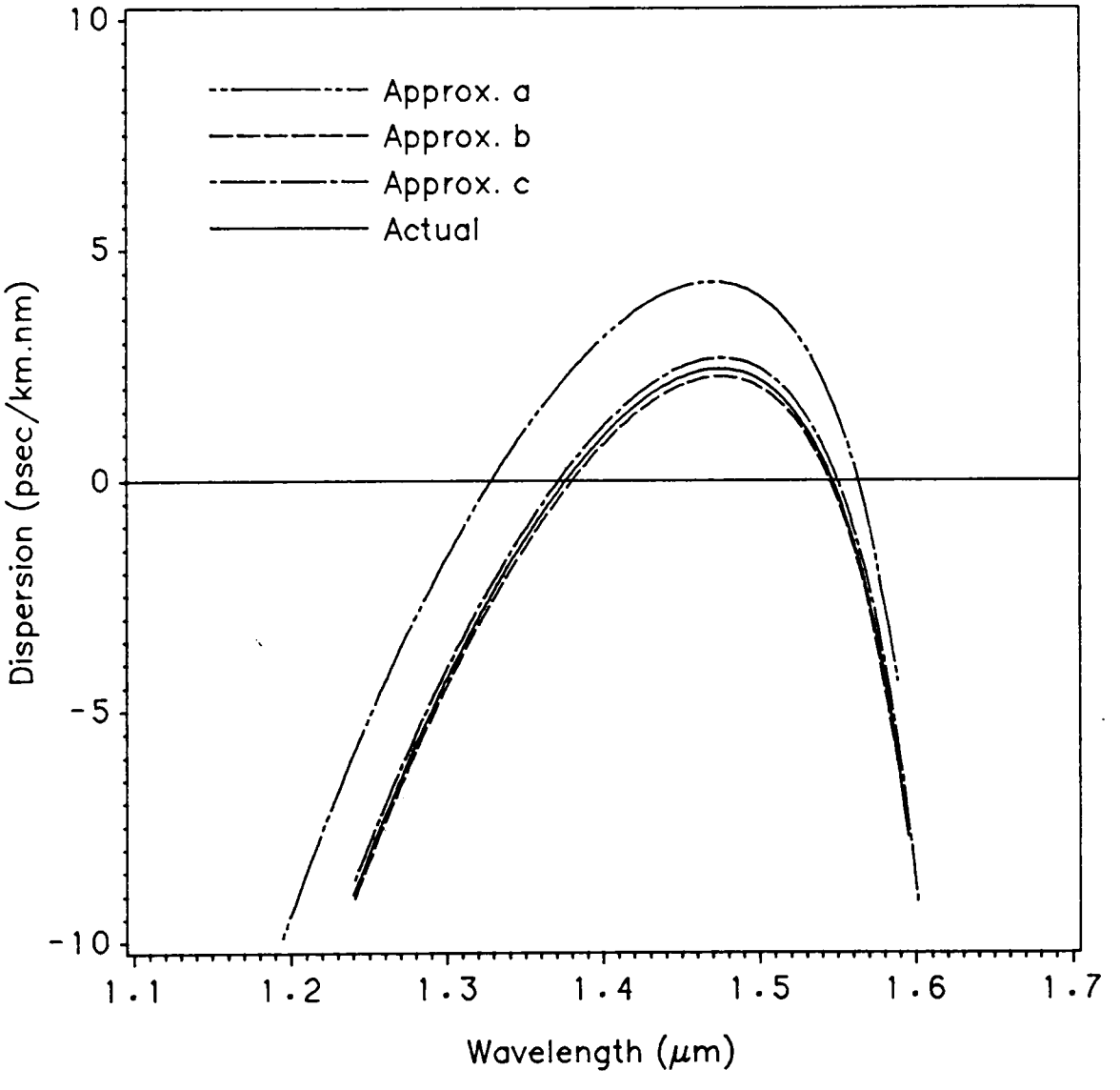

Figure 45. Comparison of actual and approximate dispersion characteristics for double-clad fiber DC2.

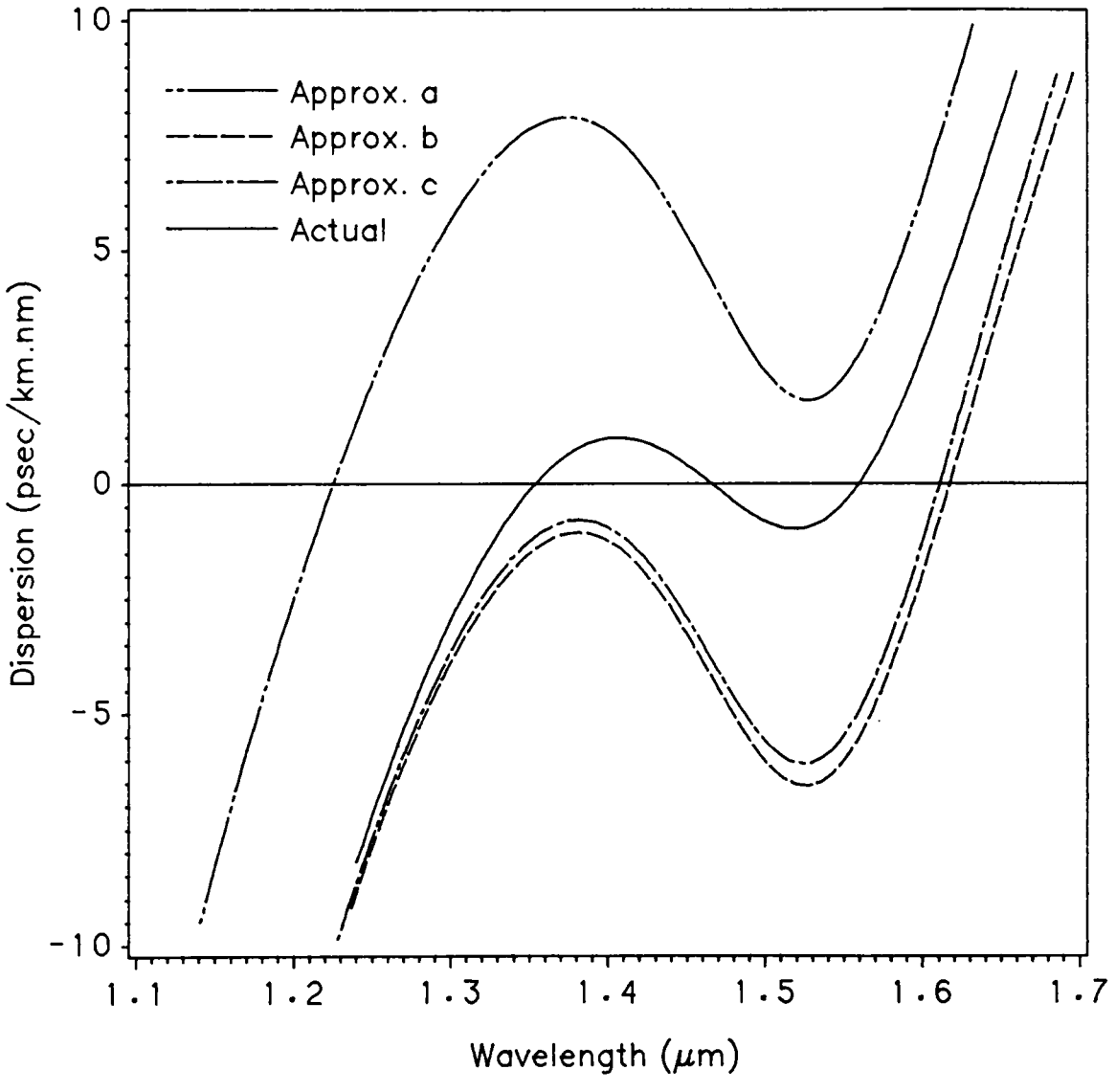

Figure 46. Comparison of actual and approximate dispersion characteristics for triple-clad fiber TC1.

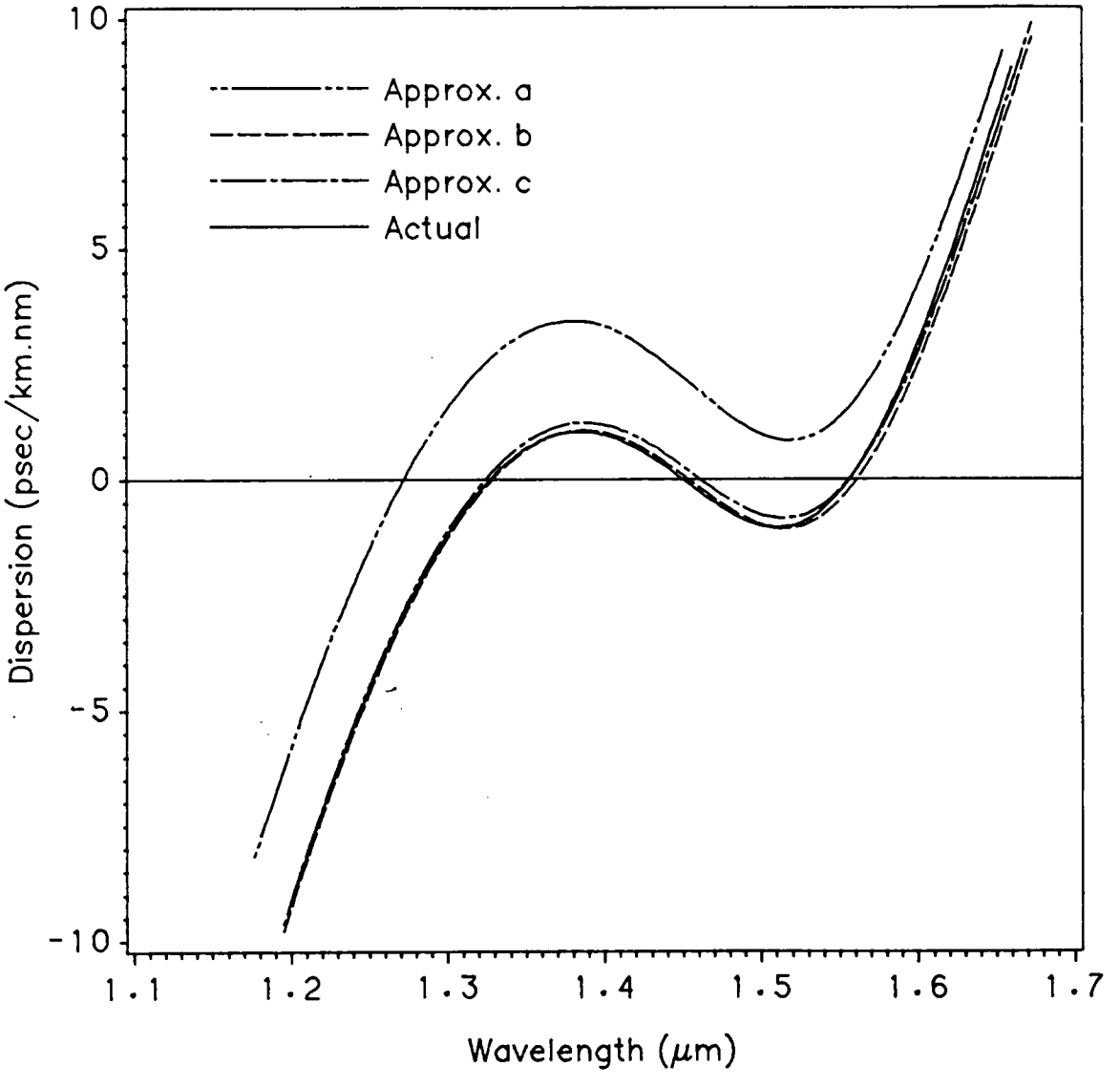

Figure 47. Comparison of actual and approximate dispersion characteristics for triple-clad fiber TC2.

Figures 47 and 48 illustrate the actual and approximate dispersion for fibers TC2 and TC3, respectively. Fiber TC2 has a chromatic dispersion less than 1 ps/km-nm in the 1.3 $\mu m < \lambda < 1.57$ μm range. The approximate characteristics *b* and *c* are in very good agreement with the actual one. The accuracy of the characteristic *a*, however, is not satisfactory. It is emphasized that errors relative to the actual dispersion and not the absolute errors are considered in this analysis. For fiber TC3 there is a fairly good agreement between the actual and approximate characteristics for $\lambda < 1.45$ μm, but errors in the approximate dispersion are quite large for $\lambda > 1.5$ μm. A notable difference between TC3 and other two TC fibers is that TC3 has four different indices, whereas TC1 and TC2 have only three different indices. A comparison of the characteristics of all three TC fibers reveals that: (1) when none of the fiber layers is pure silica and there is a large index difference as in TC1, characteristic *a* differs drastically from the other two approximate characteristics (Fig. 46), and (2) the approximate characteristics *b* and *c* in all cases differ only slightly from each other. The latter conclusion is because power in such single-mode fibers is largely confined to the central core. These conclusions are also valid in fibers with two, four, or more claddings.

Let us consider two quadruple-clad (QC) fibers with data given in Table 14. The parameters of QC1 are typical of a dispersion-flattened fiber with four claddings of different indices. The dispersion characteristics for QC1 and QC2 are shown in Figs. 49 and 50, respectively. Much of the discussion on TC2 and TC3 also applies to QC1 and QC2 and thus need not be repeated again. The dispersion analysis for the three types of fibers presented here may, in fact, be generalized to any single-mode fiber operating in the long wavelength range. From these examples, it has become clear

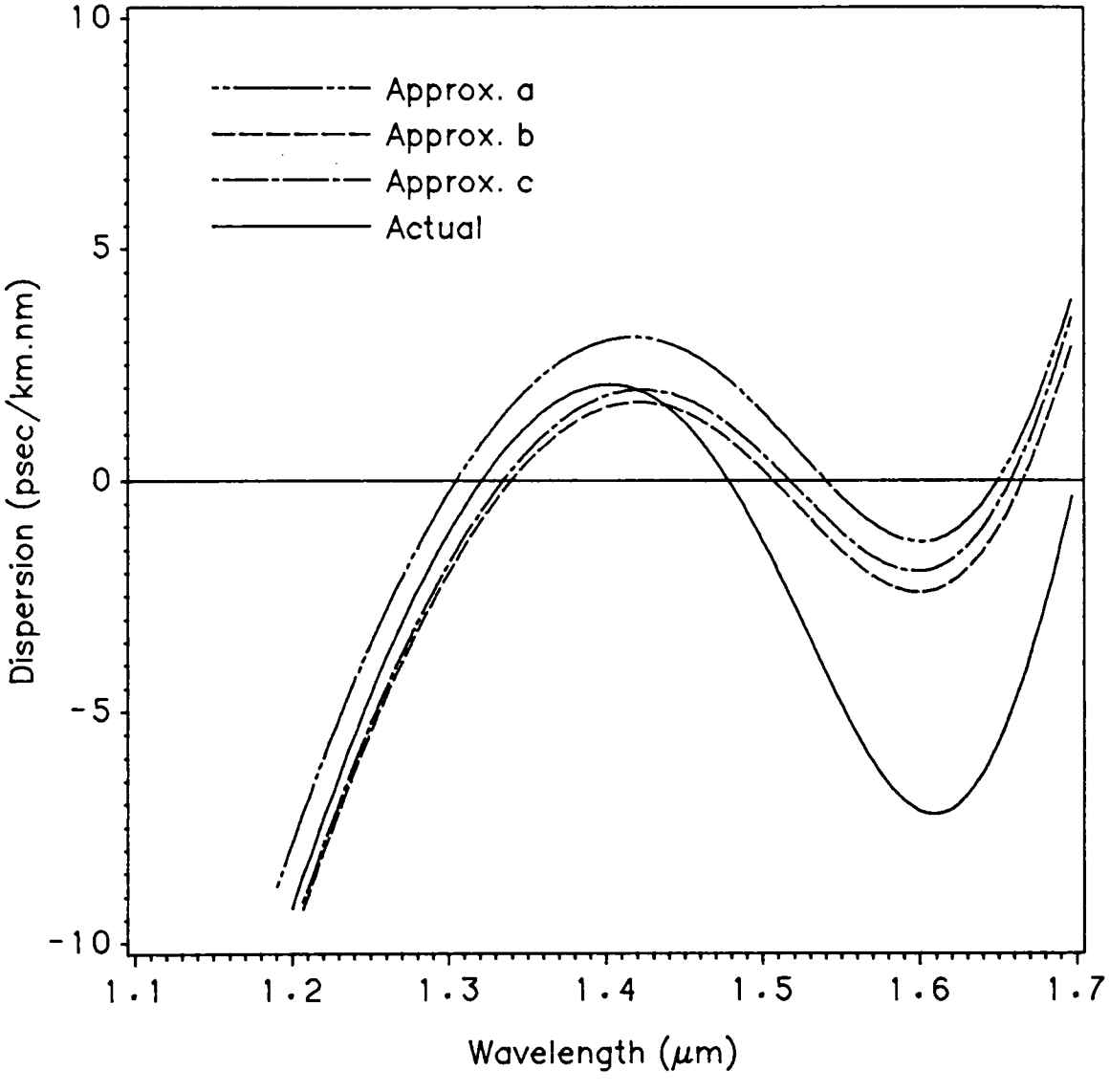

Figure 48. Comparison of actual and approximate dispersion characteristics for triple-clad fiber TC3.

that small index differences are necessary but not sufficient to achieve small errors in approximate dispersion b and c, because the errors are also influenced by the derivatives of index differences with respect to wavelength as discussed below.

Table 14. Parameters for quadruple-clad (QC) fibers

Fiber	*Data*	*Core*	*Clad 1*	*Clad 2*	*Clad 3*	*Clad 4*
	Δ	0%	1.022%	0.272%	0.873%	0.649%
QC1	η	1.000	0.905	1.500	2.600	
($r_4 = 19.4\mu m$)	M	$M14$	$M1$	$M15$	$M10$	$M7$
	Δ	0%	0.835%	0%	0.835%	0.461%
QC2	η	1.000	1.440	1.000	1.520	
($r_4 = 12.5\mu m$)	M	$M16$	$M1$	$M16$	$M1$	$M7$

8.3. Influence of Derivatives of Index Differences on the Accuracy of Approximate Methods

It is evident from Eqs. (2.14b) and (2.19b) that chromatic dispersion depends on the first and second-order derivatives of the refractive indices of various layers with respect to wavelength. Since all cladding indices may be expressed in terms of the core index and Δ_j defined as $\Delta_j = (n_1^2 - n_{j+1}^2)/2n_1^2$, $j = 1, 2, \ldots k-1$, it can be said that chromatic dispersion depends on Δ_j and their derivatives. The exact nature of the influence of derivatives of Δ_j on chromatic dispersion is very complicated. Here, we limit the analysis to a qualitative one and try to gain some insight into the significance of these derivatives and their effects on the approximate dispersion. There are many

different index differences for various fibers discussed in the previous section, and studying the first and second-order derivatives of all is laborious and perhaps unnecessary.

We, therefore, choose to study the largest index difference which generally belongs to the innermost cladding as a representative index difference. It is also intuitive that the influence of this index difference on material dispersion is stronger than that of other claddings.

Variations of $\Delta_1' = d\Delta_1/d\lambda$, and $\Delta''_1 = d^2\Delta_1/d\lambda^2$ versus wavelength are shown in Figs. 51 and 52, respectively. We note that these derivatives for DC1 and TC1 are much larger than those for DC2 and TC2. On the other hand, the errors in the approximate dispersion characteristics *b* and *c* are quite large for DC1 and TC1 (Figs. 44 and 46) and are appreciatively smaller for DC2 and TC2 (Figs. 45 and 47). Thus, larger values of Δ_1, Δ'_1, and Δ''_1 imply larger errors in the approximate dispersion. Let us next compare Δ'_1 and Δ_1'' for QC1 and QC2 fibers. For QC2, Δ_1' is small at all wavelengths and Δ_1'' decreases with wavelength. For this fiber, the approximate characteristics *b* and *c* are in very good agreement with the actual one at all wavelengths (Fig. 50). For QC1, in the short wavelength range, Δ_1'' is very small and Δ'_1 is nearly equal to that for QC2. Furthermore, both Δ_1' and Δ_1'' increase with wavelength. On the other hand, we recall that the accuracy of the approximate characteristics for QC1 (Fig. 49) is good in the short wavelength range and is poor in the long wavelength range, with the implication that larger values of Δ_1, Δ_1', and Δ_1'' are responsible for the lower accuracy.

Comparison of results for TC2 and TC3 fibers is quite revealing. It is noted from Figs. 47 and 48 that the accuracy of approximate dispersion *b* and *c* for TC2 is much better than that for TC3. This is because index differences for TC3 are smaller than

those for TC2. Larger errors in the approximate dispersion of TC3 are attributed to larger values for the derivatives of index differences in this fiber. It is evident from Fig. 51 that Δ'_1 for TC3 is about three to four times larger than that for TC2.

It is thus concluded that smaller index differences do not necessarily imply smaller derivatives and hence better accuracy for approximate methods. Another example with small index differences and yet with a poor accuracy in the approximate dispersion was reported before [72]. Finally, the numerical analysis presented here includes primarily GeO_2-doped fibers, because the Sellmeier coefficients for these fibers are more readily available. For fluorine-doped fibers approximate methods *a* and *b* become the same.

As last examples, we consider one 7-layer fiber with data given in Table 2 (fiber no. 6). Fiber no. 6 has a chromatic dispersion less than 1 ps/km-nm in the 1.31 $\mu m < \lambda <$ 1.66 μm range. The approximate characteristics *b* and *c* are in very good agreement with the actual one. The accuracy of the characteristic *a*, however, is not satisfactory as shown in Fig. 53. With 7-layer fiber again we have proved that the accuracy of approximate methods is largely governed by the index differences and their derivatives with respect to wavelength. In order to have small errors in the chromatic dispersion calculated by an approximate method, it is necessary for both the index differences and their derivatives to be small. For most doped silica-based glass materials, however, it suffices to have small derivatives for the index differences. But small index differences alone do not guarantee small errors. The influence of the derivatives of index differences thus appears to be more significant. For fibers with index differences less than 0.8 % and with pure fused silica as the lowest index material, the approximate methods based on the weighted average material dispersion and the dispersion of the core material are adequate.

It is shown in Fig. 54 for fiber no. 6 that there is not too much difference for the dispersion spectra with approximate method *a* by using core material index at different wavelengths. This is also true for any number layer fibers.

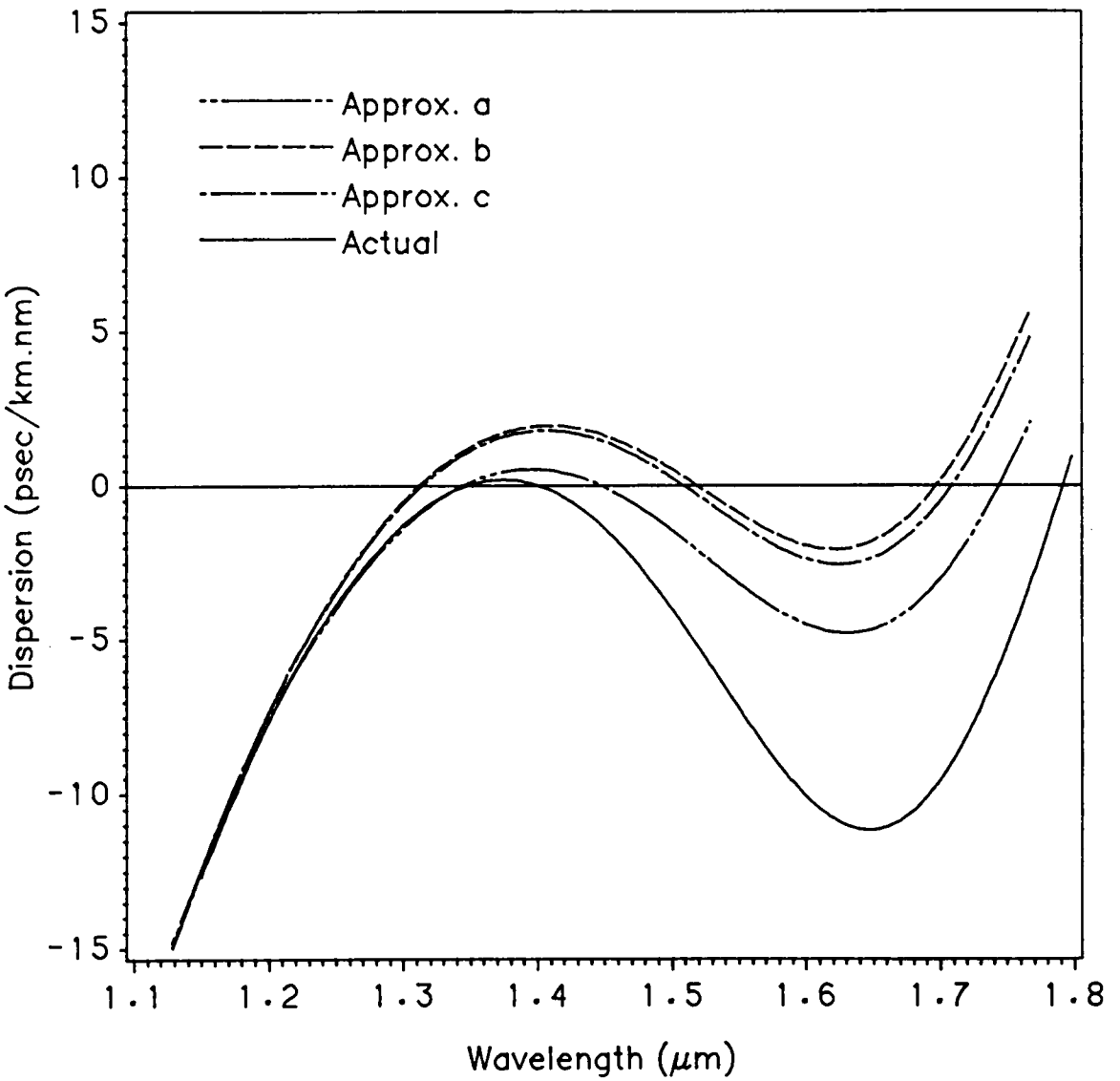

Figure 49. Comparison of actual and approximate dispersion characteristics for quadruple-clad fiber QC1.

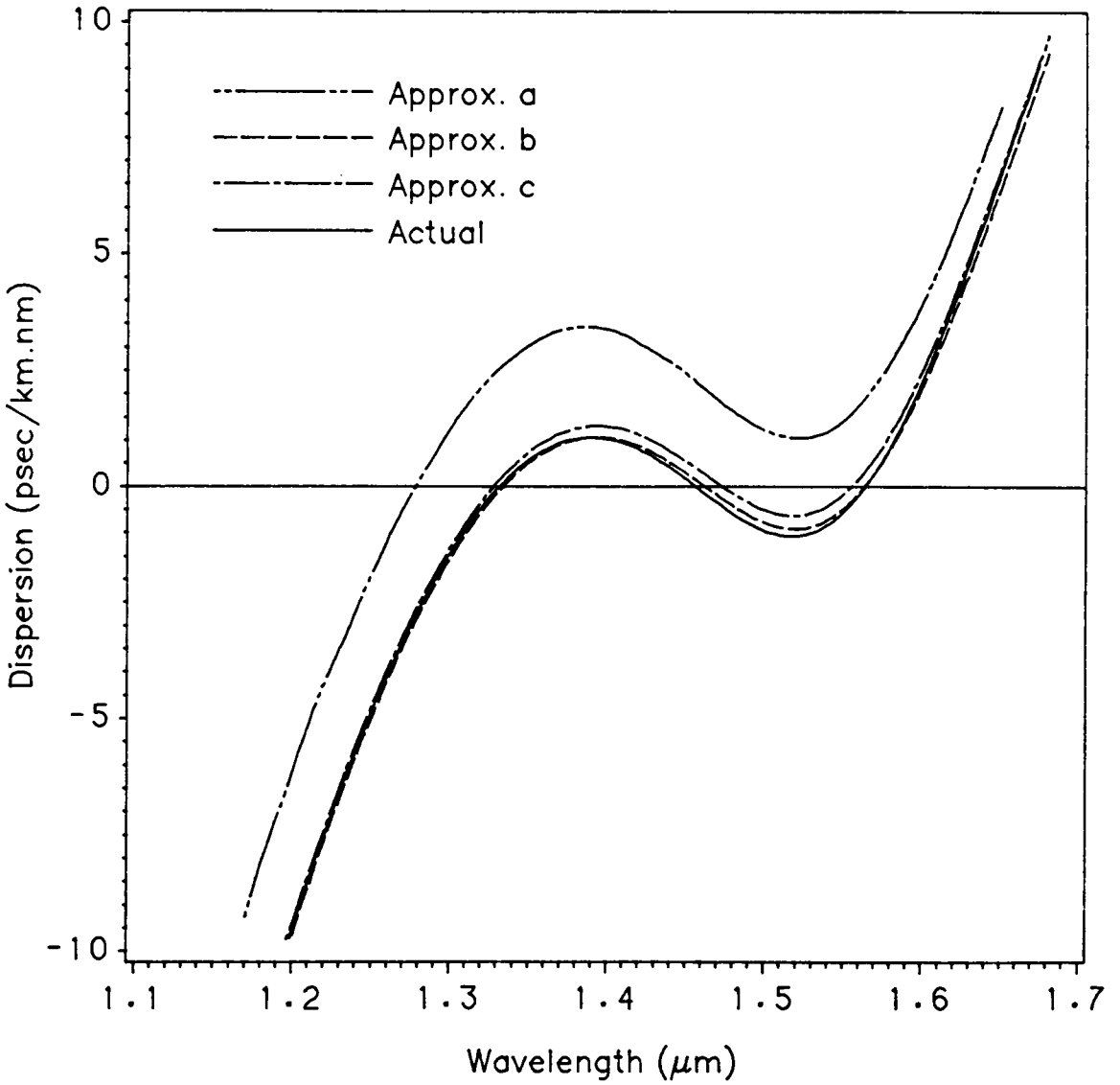

Figure 50. Comparison of actual and approximate dispersion characteristics for quadruple-clad fiber QC2.

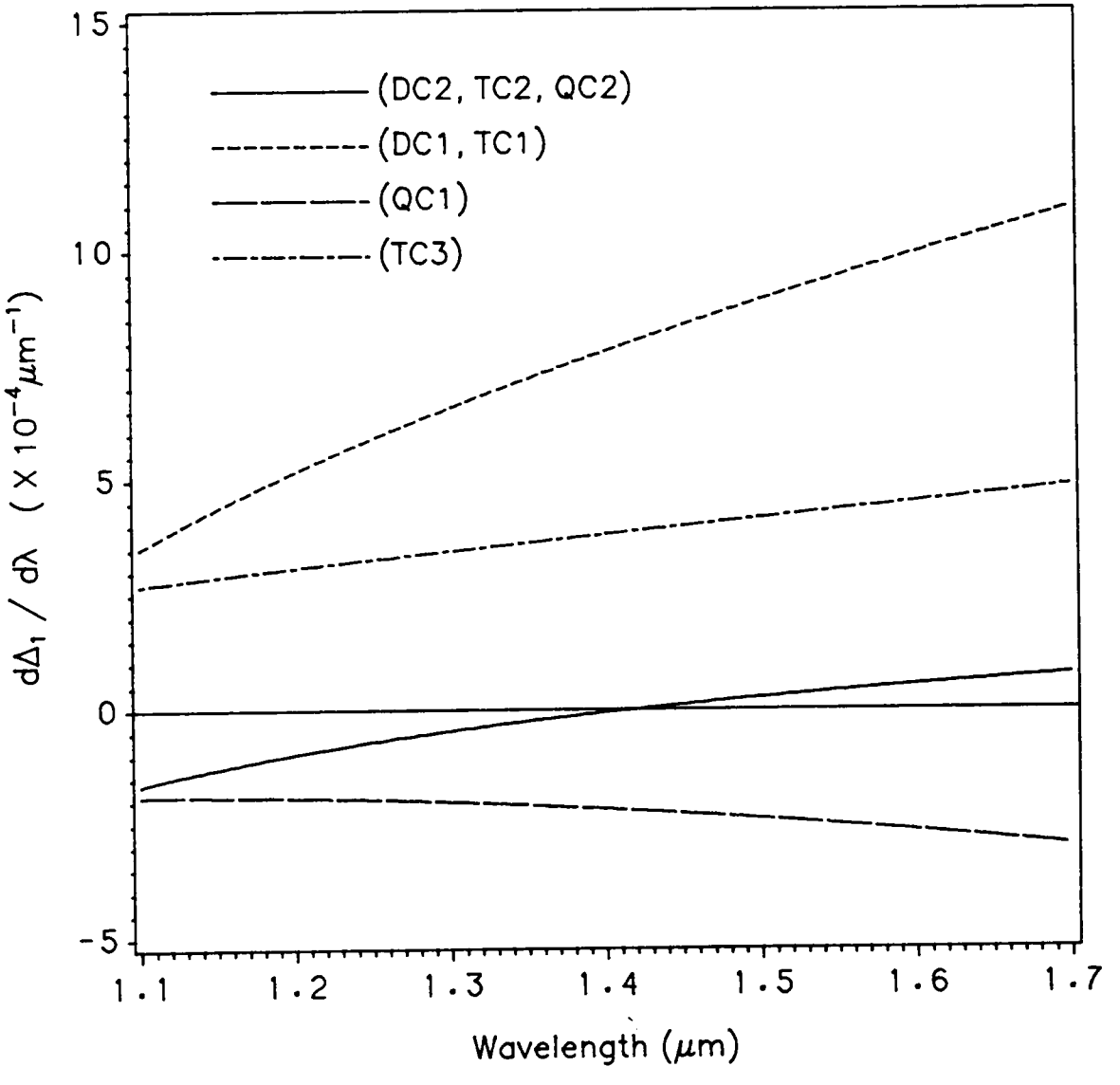

Figure 51. Variations of $d\Delta_1/d\lambda$ versus wavelength.

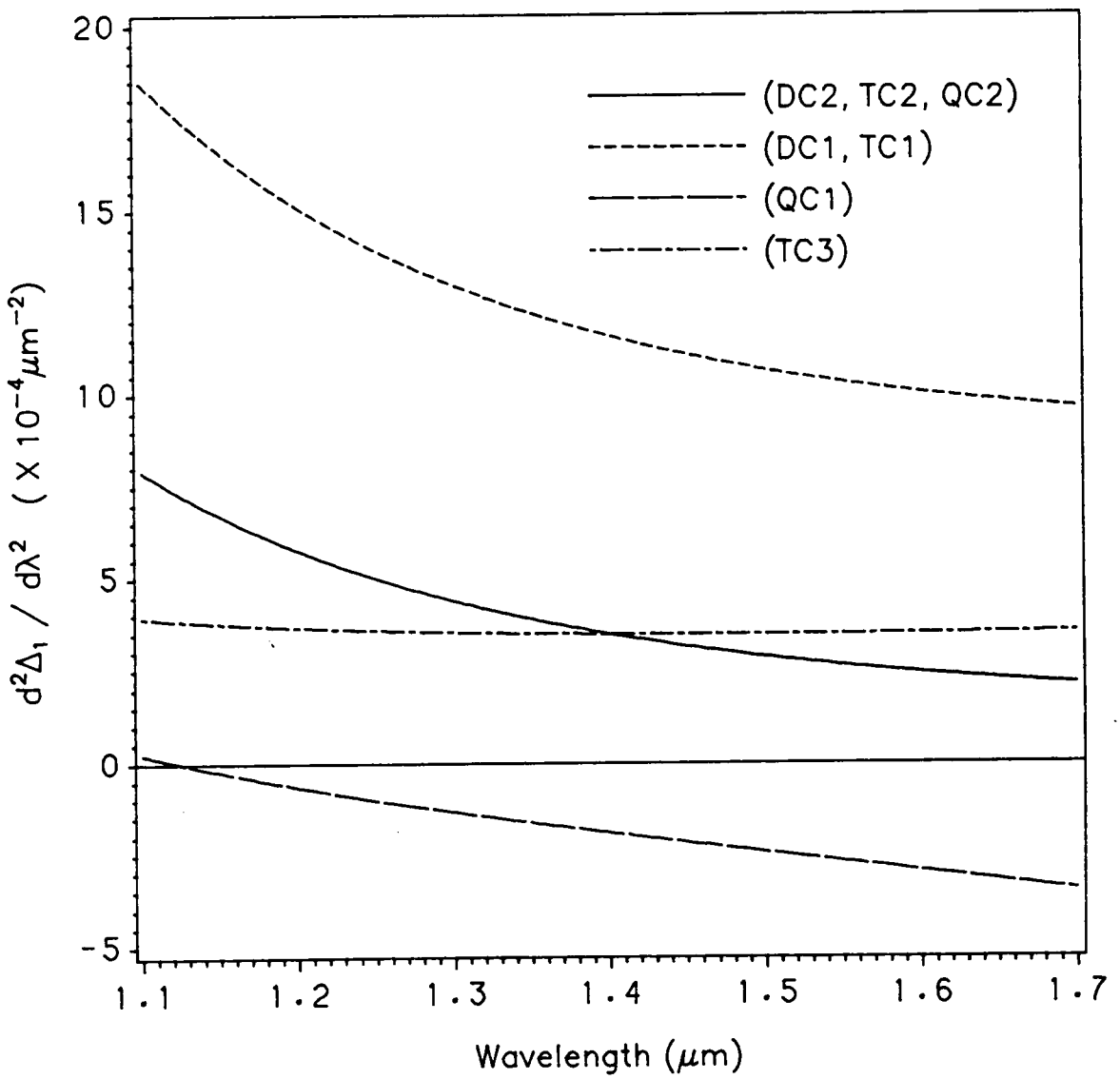

Figure 52. Variations of $d^2\Delta_1/d\lambda^2$ versus wavelength.

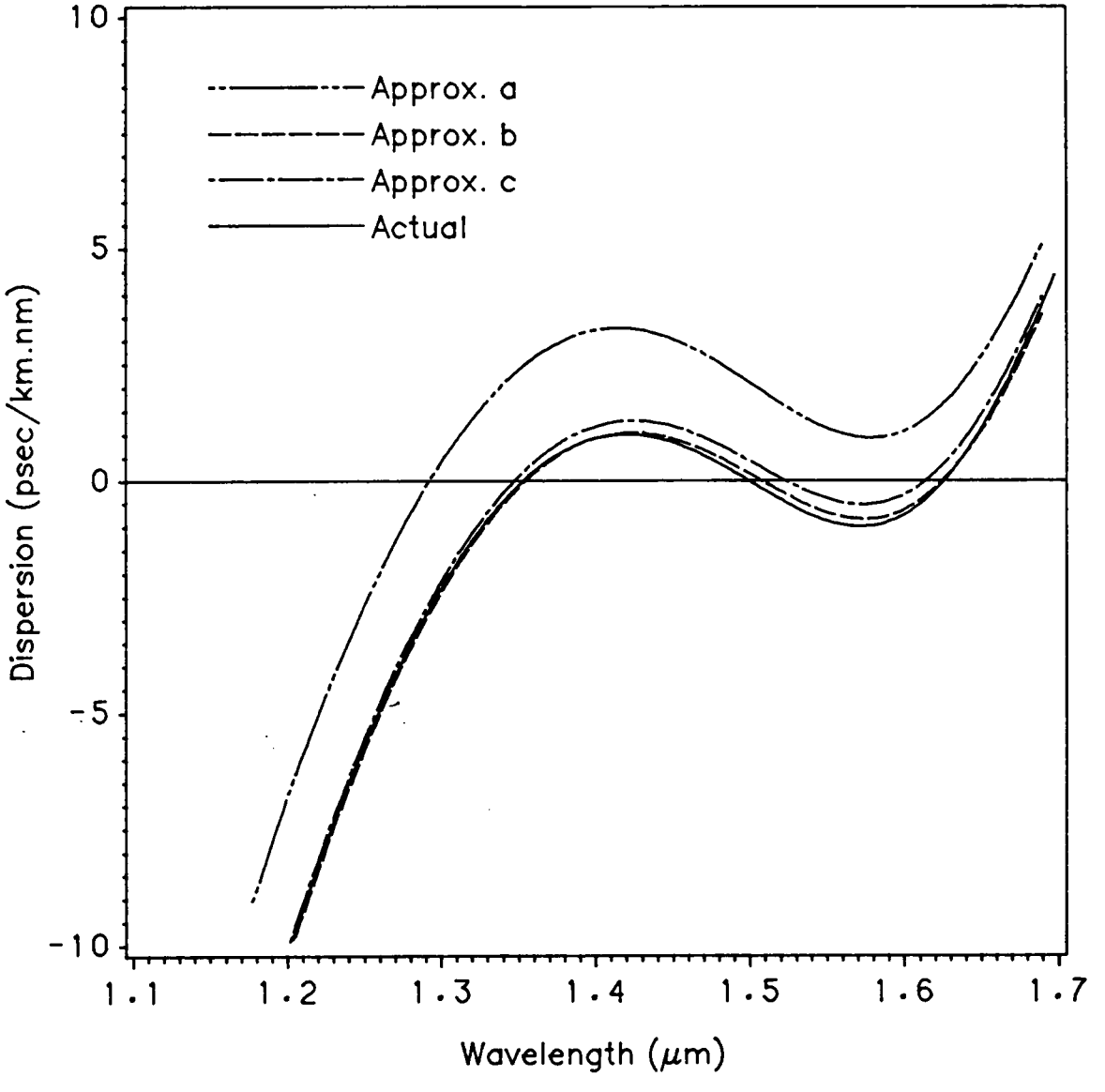

Figure 53. Comparison of actual and approximate dispersion characteristics for 7-layer fiber.

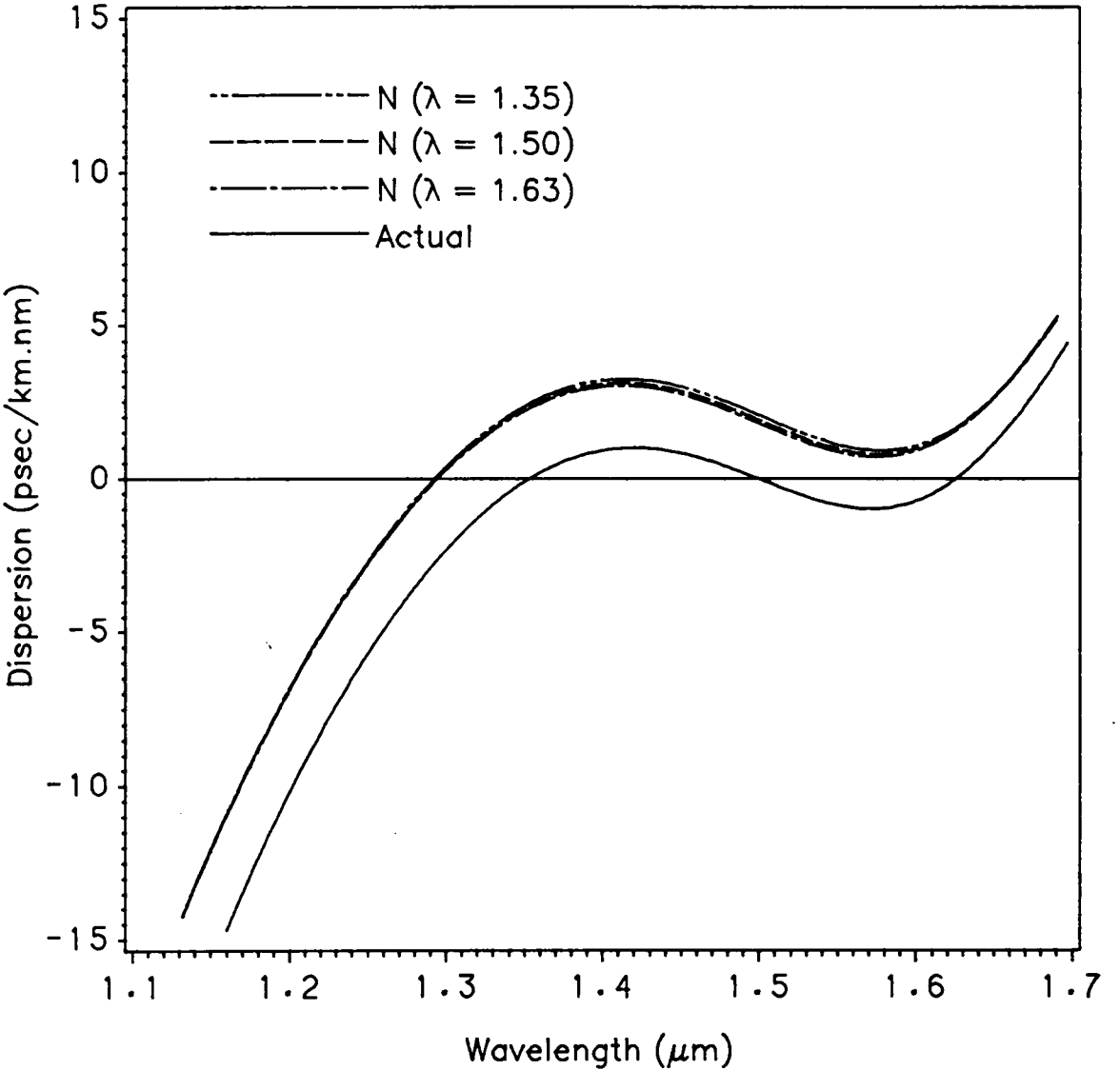

Figure 54. Comparison of actual and approximate dispersion characteristics by core material at different wavelengths for 7-layer fiber.

Chapter 9. Conclusions and Recommendations

We have proposed a series of new single-mode dispersion-flattened fibers with three zero-dispersion wavelengths. These fibers have potential application in long distance optical fiber communications and also for wavelength division multiplexing throughout the spectral range of 1.3 μm to 1.7 μm. The zero chromatic dispersion wavelengths of these fibers are less dependent on cladding index and dimensional variations than those of DC, TC, and QC fibers. Optimized in the 1.31 μm to 1.68 μm wavelength range, they exhibit lower dispersion (< 1 ps/km-nm), wider dispersion-flattened windows, and larger mode-field radii than those of DC, TC, and QC fibers. These new fibers have small splice and bend losses as compared with DC, TC, and QC fibers with the same value of dispersion. An optimization program is used to determine the optimum fiber profile data. The proposed multi-clad fibers are strictly single-mode and have the lowest dispersion over the widest range of wavelengths reported to date.

Ultralow dispersion fibers whose dispersion is < 0.01 ps/km-nm throughout a 1 μm spectral range centered at 1.55 μm and whose first-order and second-order of dispersion are zero at 1.55 μm have been designed and analyzed. All dispersion-

shifted fibers in the open literature have dispersion values of 8 - 20 ps/km-nm in the neighborhood of the zero-dispersion point 1.55 μm. To our knowledge, this is the first report on DFSM fibers with ultralow disperion and large bandwidth. The drawback of this type of fiber is the very critical production tolerance requirements. But as manufacturing technology advances tight tolerances will become less of a problem.

The accuracy of three approximate methods for evaluating chromatic dispersion in multi-clad low dispersion single-mode fibers has been examined. These methods are different only in estimating the material dispersion of the fiber. Method *a*, which approximates the material dispersion of fibers by that of pure fused silica, is generally the least accurate for GeO_2 -doped fibers. Methods *b* and *c*, which approximate the material dispersion of fibers by that of the core material and by the weighted average of material dispersion of various layers, respectively, have nearly the same accuracy. It has been shown that the accuracy of approximate methods is influenced not only by the layer index differences, but also by their derivatives with respect to wavelength. The smaller the layer index differences and their first and second-order derivatives, the better the accuracy of approximate methods *b* and *c*. For fibers with layer index differences less than 0.6% - 0.8 % and with pure fused silica as the lowest index material, the approximate methods *b* (method *a* for *F*-doped fibers) and *c* are adequate.

In search of an optimum solution, various types of fibers, with step-index as well as graded-index profiles, have been attempted for optimization using different objective functions which have four, five, and six zero-dispersion wavelengths. Multi-clad fibers with as many as fifty-one layers and with different profile shapes have been tested. The numerical results show that maximum of three zero-dispersion wavelengths can be obtained in the wavelength range of 1.3 μm to 1.7 μm with dispersion less than 1 ps/km-nm. It seems impossible to have a sinusoidal dispersion spectrum

with a negative dispersion slope around its first and third zero-dispersion wavelengths, or, quadratic dispersion spectrum with a negative dispersion slope at the first zero-dispersion wavelength and with a positive dispersion slope at the second zero-dispersion wavelength. The purpose of construction of mirror dispersion spectra is that positive dispersion cancels negative dispersion. If two fibers in series have mirror-image dispersion curves, the negative dispersion of the one will cancel the positive dispersion of the other, so that network repeaters will be required due to attenuation alone. From Fig. 16, we notice that if a QC fiber is connected with the 7-layer fiber and operating at 1.53 μm the positive dispersion of the QC fiber will be compensated by the negative dispersion of the 7-layer fiber. Is it possible to find a fiber profile structure which produces a negative dispersion slope at the first zero-dispersion point? In order to do so, material dispersion, which is the dominant factor in low wavelength dispersion, must be overcome.

After extensive computer simulation it has been found that TC, QC, and 7-layer fibers can be single-mode fibers as long as the difference of the cutoff wavelength of λ_{c11} and λ_{c01} for TC fiber is larger than 0.5 μm, that for QC fiber is larger than 0.7 μm, and that for 7-layer fiber is larger than 0.9 μm. 7-layer fiber can be multimode fiber also if the cutoff wavelengths of λ_{c11} and λ_{c01} are close. The major advantage of 7-layer fiber is that its parameter change is not as sensitive to mode nature change and dispersion spectrum change as that of DC, TC, and QC fibers.

Numerical results show that a profile with any number of layers can be used to modify fiber structures to produce dispersion-flattened spectra. For the same maximum dispersion, the dispersion-flattened window of 7-layer fibers is larger than that of DC, TC, and QC fibers, and the dispersion-flattened window of 9-layer fibers is larger than that of 7-layer fibers. Increasing the number of layers and simultaneously increasing total core radius would increase the span of the dispersion-flattened win-

dow. But considering production cost and overall fiber transmission performance, such as low core and cladding index differences, proper layer thickness, larger mode-field radius, lower bend loss, and a larger dispersion-flattened window, a 7-layer fiber with step-index structure, shown in Fig. 1, appears to be the best structure to date.

DC, TC, QC, and 7-layer fibers having equal dispersion magnitude of 0.97 ps/km-nm have been compared. With DC, TC, and QC structures, if dispersion is kept lower than 1 ps/km-nm, only quadratic dispersion spectra can be constructed. It has been found that for $D'(\lambda_0) \geq 0$ lower production tolerances can be achieved. For better design tolerances, a sinusoidal dispersion curve is preferred, since the dispersion slope at the third zero-dispersion point is always > 0. This would take full advantage of the low D'_{max} at longer wavelengths and reduce the dispersion sensitivity coefficients, resulting in relatively relaxed production tolerances under certain dispersion requirements. Therefore, in the design of dispersion-flattened fibers dispersion spectra with sinusoidal curves are preferred.

Developing a DFSM fiber optimization design program which can trace multiple objective functions simultaneously is an important possible objective. The multiple objective function would involve the integration of (1) minimum dispersion, (2) a flexible choice of the wavelengths of the zero-dispersion, (3) the maximum width of the dispersion-flattened window, (4) reasonable splice and bend losses, (5) small index differences between the layers, and (6) reasonable layer thickness and production tolerances. Designing fiber profile from fiber specifications is an inverse design process worth pursuing. Since multi-clad DFSM fiber design involves multi-dimensional parameter optimization problems with multi-objective functions, it is important to find a straightforward two dimensional design chart which defines the relationships between the mode-field radius, LP_{11} mode cutoff wavelength, dispersion,

refractive index difference of each layer, layer thickness ratio, splice loss, and bend loss. It is also important to define the upper and lower limits of these design specifications.

With the optimization method described in Chapter 6 the user can have a simple step-index profile with many desirable characteristics. There is no starting value problem, and as long as the objective function is reasonable, the computer will give an optimum solution in any case. Since solving wave equations involves computation of a transcendental equation, and obtaining the propagation constant β requires a very high accuracy, and both these procedures require a great deal of CPU time, a new computational method described in [73] is worth examining. This method calculates the propagation constant and the modal field of fibers with arbitrary profiles by transforming arbitrarily cylindrically symmetric refractive index profiles into equivalent planar profiles, and uses straightforward multiplication of 2×2 matrices developed to solve planar optical waveguides, and it does not require the solution of any transcendental or differential equations. Finally, the CAD DFSM fiber design program would link to IBM CADAM or other graphic packages to give the designer a comprehensive specification data set and graphic outputs for fiber index profile, dispersion characteristic, splice loss, bend loss, and field distribution.

References

1. F. P. Kapron, D. B. Keck, and R. D. Maurer, *Radiation losses in glass optical waveguides*, Appl. Phys. Lett., Vol. 17, pp. 423-425, 1970.

2. T. Suzaki, S. Fujita, Y. Inomoto, T. Terakado, K. Kasahara, K. Asano, T. Torikai, T. Itoh, M. Shikada, and A. Suzuki, *1.2 Gbit/s, 52.5 km optical fiber transmission experiment using OEICs on GaAs-ON-InP heterostructure*, Electro. Lett., Vol. 24, pp. 1283-1284, 1988.

3. T. Matsuoka, H. Nagai, Y. Itaya, Y. Noguchi, Y. Suzuki, and T. Ikegami, *CW operation of DFB-BH GaInAsP/InP lasers in 1.5 μm wavelength region*, Electron. Lett., Vol. 18, pp. 27-28, 1982.

4. Y. Abe, K. Kishino, T. Tanbun-Ek, S. Arai, F. Koyama, K. Matsumoto, T. Watanabe, and Y. Suematsu, *Room-temperature CW operation of 1.60 μm GaInAsP/InP buried-heterostructure integrated laser with butt-jointed built-in distributed-bragg-reflection waveguide*, Electro. Lett., Vol. 18, pp. 410-411, 1982.

5. J. Yamada, S. Kobayashi, H. Nagai, and T. Kimura, *Modulated single-longitudinal mode semiconductor laser and fiber transmission characteristics*, IEEE J. Quantum Electron., Vol. QE-17, pp. 1006-1009, 1981.

6. N. A. Olsson, C. H. Henry, R. F. Kazarinov, H. J. Lee, K. J. Orlowsky, B. H. Johnson, R. E. Scotti, D. A. Ackerman, and P. J. Anthony, *Performance characteristics of a 1.5 μm single-frequency semiconductor laser with an external waveguide bragg reflector*, IEEE J. Quantum Electron., Vol. 24, pp. 143-147, 1988.

7. B. L. Kasper, R. A. Linke, K. L. Walker, L. G. Cohen, T. L. Koch, T. J. Bridges, E. G. Burkhardt, R. A. Logan, R. W. Dawson, and J. C. Campbell, *A 130 km transmission experiment at 2 Gb/s using silica-core fiber and a vapor phase transported DFB laser*, Proceedings of the Tenth European Conference on Optical Communication, Stuttgart, FRG, pp. 342-343, 1984.

8. T. Miya, Y. Terunuma, T. Hosaka, and T. Miyashita, *Ultimate low-loss single-mode fiber at 1.55 μm* Electron. Lett., Vol. 15, pp. 106-108, 1979.

9. K. Okamoto, T. Edahiro, K. Kawana, and T. Miya, *Dispersion minimization in single-mode fibers over a wide spectral range*, Electron. Lett. Vol. 15, pp. 729-731, 1979.

10. K. I. White and B. P. Nelson, *Zero total dispersion in step-index monomode fibers at 1.30 and 1.55 μm*, Electro. Lett., Vol. 15, pp. 396-397, 1979.

11. K. I. White and B. P. Nelson, *Minimum dispersion at 1.55 μm for single-mode step-index fibers* Electron. Lett., Vol. 15, pp. 765-767, 1979.

12. C. R. South, *Total dispersion in step-index monomode fibers* , Electro. Lett., Vol. 15, pp. 394-395, 1979.

13. H. Tsuchiya and N. Imoto, *Dispersion-free single mode fiber in 1.5 μm wavelength range*, Electron. Lett., Vol. 15, pp. 476-478, 1979.

14. L. Jeunhomme, *Dispersion minimisation in single-mode fibers between 1.3 μm and 1.7 μm* , Electron. Lett., Vol. 15, pp. 478-479, 1979.

15. W. A. Gambling, H. Matsumura, and C. M. Ragdale, *Mode dispersion, material dispersion and profile dispersion in graded-index single-mode fibers*, Microwaves, Opt., Acoust., Vol. 3, pp. 239-246, 1979.

16. U. C. Paek, G. E. Peterson, and A. Carnevale, *Dispersionless single-mode lightguides with α index profile*, Bell Syst. Tech. J., Vol. 60, pp. 583-598, 1981.

17. A. Kawana, T. Miya, N. Imoto, and H. Tsuchiya, *Pulse broadening in long-span dispersion-free single-mode fibers at 1.5 μm* , Electron. Lett., Vol. 16, pp. 188-189, 1980.

18. L. G. Cohen and W. L. Mammel, *Tailoring the shapes of dispersion spectra to control bandwidths in single-mode fibers*, Proceedings of the 7th European Conference on Optical Communication, Copenhagen, pp. 3.3.1-3.3.4, 1981.

19. P. D. Lazay and A. D. Pearson, *Developments in single-mode fiber design, materials, and performance at Bell Laboratories*, IEEE J. Quantum Electron., Vol. QE-18, pp. 504-510, 1982.

20. T. Miya, M. Nakahara, and N. Inagaki, *Fabrication of dispersion-free VAD single-mode fiber in the 1.5-μm wavelength region*, J. Lightwave Technol., Vol. LT-1, pp. 14-19, 1983.

21. L. G. Cohen, C. L. Lin, and W. G. French, *Tailoring zero chromatic dispersion into the 1.5-1.6 μm low-loss spectral region of single-mode fibers*, Electron. Lett., Vol. 15. pp. 334-335, 1979.

22. N. Imoto, A. Kawana, S. Machida, and H. Tsuchiya, *Characteristics of dispersion-free single-mode fiber in the 1.55 μm wavelength region*, IEEE J. Quantum Electron., Vol. QE-16, pp. 1052-1058, 1980.

23. K. I. White, *Design parameter for dispersion-shifted triangular-profile single-mode fibers*, Electron. Lett., Vol. 18, pp. 725-727, 1982.

24. U. C. Paek, *Dispersionless single-mode fibers with trapezoidal-index profiles in the wavelength region near 1.5 μm* , Appl. Opt., Vol. 22, pp. 2363-2369, 1983.

25. M. A. Saifi, S. J. Jang, L. G. Cohen, and J. Stone, *Triangular-profile single-mode fiber*, Opt. Lett., Vol. 7, pp. 43-45, 1982.

26. H. T. Shang, T. A. Ienahan, P. F. Glodis, and D. Kalish, *Design and fabrication of dispersion-shifted depressed-clad triangular-profile (DDT) single-mode fiber*, Electron. Lett., Vol. 21, pp. 201-203, 1985.

27. S. Kawakami and S. Nishida, *Characteristics of a doubly clad optical fiber with a low-index inner cladding*, IEEE J. Quantum Electron., QE-10, pp. 879-887, 1974.

28. T. Miya, K. Okamoto, Y. Ohmori, and Y. Sasaki, *Fabrication of low dispersion single-mode fibers over a wide spectral range*, IEEE J. Quantum Electron., Vol. QE-17, pp. 858-861, 1981.

29. S. J. Jang, L. G. Cohen, W. L. Mammel, and M. S. Saifi, *Experimental verification of ultra-wide bandwidth spectra in double-clad single-mode fiber*, Bell Syst. Tech. J., Vol. 61, pp. 385-390, 1982.

30. H. Etzkorn and W. E. Heinlein, *Low-dispersion single-mode silica fiber with undoped core and three F-doped claddings*, Electron. Lett., Vol. 20, pp. 423-424, 1984.

31. H. Etzkorn, W. Lieber, M. Loch, W. E. Heinlein, H.-U. Bonewitz, K.-F. Klein, and A. Mühlich, *Dispersion characteristics of broadband only-F-doped single-mode silica fibers*, Proceedings of the Tenth European Conference on Optical Communication, Stuttgart, FRG, pp. 278-279, 1984.

32. W. Lieber, M. Loch, H. Etzkron, W. E. Heinlein, K.-F. Klein, H. U. Bonewitz, and Mühlich , *Three-step index strictly single-mode, only F-doped silica fibers for broad-band low dispersion* , J. Lightwave Technol., Vol. LT-4, pp. 715-718, 1986.

33. L. G. Cohen, W. L. Mammel, and S. J. Jang, *Low-loss quadruple-clad single-mode lightguides with dispersion below 2 ps/km-nm over 1.28 μm - 1.65 μm wavelength range*, Electron. Lett., Vol. 18, pp. 1023-1024, 1982.

34. V. A. Bhagavatula, M. S. Spotz, W. F. Love, and D. B. Keck, *Segmented-core single-mode fibers with low loss and low dispersion* , Electro. Lett., Vol. 19, pp. 317-718, 1983.

35. V. A. Bhagavatula, M. S. Spotz, and W. F. Love, *Dispersion-shifted segmented-core single-mode fibers*, Opt. Lett., Vol. 9, pp. 186-188, 1984.

36. P. K. Bachmann, D. Leers, H. Wehr, D. U. Wiechert, J. A. Van Steenwijk, D. L. A. Tjaden, and E. R. Wehrhahn, *Dispersion-flattened single-mode fibers prepared with PVCD: performance, limitations, design optimization*, J. Lightwave Technol., Vol. LT-4, pp. 858-863, 1986.

37. S. J. Jang, J. Sanchez, K. D. Pohl, and D. L. L'Esperance, *Graded-index single-mode fibers with multiple claddings*, Proceedings of the Fourth International Conference on Integrated Optics and Optical Fiber Communication, Tokyo, Japan, pp. 396-397, 1983.

38. D. M. Cooper, B. J. Ainslie, K. J. Beales, S. P. Craig, C. R. Day, and J. V. Wright, *Multiple index monomode fibers for dispersion modification*, Proceedings of the

Tenth European Conference on Optical Communication, Stuttgart, FRG, pp. 280-281, 1984.

39. P. K. Mishra and I. C. Goyal, *Single mode graded-core W-type fibers with low dispersion over a wide spectral range*, Opt. Commun., Vol. 49, pp. 413-417, 1984.

40. K. D. Pohl, L. D. L'Esperance, S. J. Jang, and J. Sanchez, *Transmission properties of graded-index triple-clad single-mode fiber for 1.55-μm system operation*, J. Lightwave Technol., Vol. LT-3, pp. 586-589, 1985.

41. K.-B. Chung and S. S. Choi, *Propagation characteristics of triangular-index doubly clad monomode fiber*, Electron. Lett., Vol. 21, pp. 271-272, 1985.

42. U. K. Das and I. C. Goyal, *Mode field radius of dispersion flattened single mode fibers*, Opt. Commun., Vol. 61, pp. 16-21, 1987.

43. A. Safaai-Jazi and G. L. Yip, *Cutoff conditions in three-layer cylindrical dielectric waveguides*, IEEE Trans. on Microwave Theory and Techniques, Vol. MTT-26, pp. 898-903, 1978

44. P. L. Francois, *Propagation mechanisms in quadruple-clad fibers: mode coupling, dispersion and pure band losses* , Electron. Lett., Vol. 19, pp. 885-886, 1983.

45. P. L. Francois, F. Alard, J. F. Bayor, and B. Rose, *Multimode nature of quadruple-clad fibers* Electron. Lett., Vol. 20, pp. 37-38, 1983.

46. P. L. Francois, J. F. Bayon, and F. Alard, *Design of monomode quadruple-clad fibers*, Electron. Lett., Vol. 20, pp. 688-689, 1984.

47. B. J. Ainslie and C. R. Day, *A review of single-mode fibers with modified dispersion characteristics*, J. Lightwave Technol., Vol. LT-4, pp. 967-979, 1986.

48. J. Gowar, *Optical communication systems*, Prentice-Hall International, Inc., 1984.

49. M. J. Adams, *An introduction to optical waveguide*, John Wiley & Sons, Chichester, 1981.

50. Y. Kokubun and K. Iga, *Mode analysis of graded-index optical fibers using a scalar wave equation including gradient-index terms and direct numerical integration*, J. Opt. Soc. Am., Vol. 70, pp. 388-394, 1980.

51. R. J. Black, A. Henault, and V. Pupo, *Comparison of numerical methods for lightguide mode analysis*, Numerical Simulation and Analysis in Guided-Wave Optics and Optoelectronics, 1989 Technical Digest Series, Houston, Texas, Vol. 3, pp. 65-70, 1989.

52. A. Safaai-Jazi and G. L. Yip, *Classification of hybrid modes in cylindrical dielectric optical waveguides*, Radio Science, Vol. 12, pp. 603-609, 1977.

53. *IMSL user's manual* Vol. 3, Version 1.0, IMSL, Inc., pp. 633-639, 1987.

54. R. H. Stolen, *Modes in fiber optical waveguides with ring index profiles*, Appl. Opt., Vol. 14, pp. 1533-1537, 1975

55. J. J. Bernard, C. Brehm, J. Y. Boniort, Ph. Dupont, J. M. Gabriagues, C. Le Sergent, M. Liegois, P. L. Francois, M. Monerie, and P. Sansonetti, *Investigation*

of the properties of depressed inner cladding single mode fibers, Proceedings of the 8th European Conference on Optical Communication, Cannes AV 1, pp. 133-138, 1982.

56. M. Monerie, *Propagation in doubly clad single-mode fibers*, IEEE J. Quantum Electron., Vol. QE-535, pp. 535-541, 1982.

57. W. Lieber and S. Rabov, *Interferometric measurement of dispersion characteristics of broadband low-dispersion single-mode silica fibers: bending sensitivity*, Proceedings of the Tenth European Conference on Optical Communication, Stuttgart, FRG, pp. 82-83, 1984.

58. K. Petermann, *Constraints for fundamental-mode spot size for broadband dispersion-compensated single-mode fibers* , Electron. Lett., Vol. 19, pp. 712-714, 1983.

59. G. Trommer, *Tolerance requirements for the drawing ratio of single-mode fibers with arbitrary refractive-index profile*, Electron. Lett., Vol. 23, pp. 79-80, 1987.

60. S. B. Andreasen, *Dispersion-determined limits on production tolerances of single-mode fibers*, Electron. Lett., Vol. 22, pp. 1051-1052, 1986.

61. *IMSL user's manual* Vol. 3, Version 1.0, IMSL, Inc., pp. 625-628, 1987.

62. P. Francois, *Tolerance requirements for dispersion free single-mode fiber design: influence of geometrical parameters, dopant diffusion, and axial dip*, IEEE J. Quantum Electron., Vol. QE-18, no. 10, pp. 1490-1499, 1982.

63. J. H. Povlsen, *Design tolerances for dispersion-flattened SiO_2 -cladded single mode fibers*, Electron. Lett., Vol. 20, pp. 1035-1036, 1984.

64. G. Trommer, *A universal method for the synthesis of monomode fibers*, ntzArchiv Bd. 7, H. 11, pp. 285-289, 1985.

65. Y. Namihira, Y. Horiuchi, M. Kuwazuru, M. Nunokawa, and Y. Iwamoto, *Optimum fiber parameters of low-loss single-mode optical fibers for use in 1.55 μm-wavelength region*, Electron. Lett., Vol. 23, pp. 963-964, 1987.

66. B. J. Ainslie, K. J. Beales, C. R. Day, and J. D. Rush, *The design and fabrication of monomode optical fiber*, IEEE J. Quantum Electron., Vol. QE-18, pp. 514-523, 1982.

67. *IMSL user's manual* Vol. 3, Version 1.0, IMSL, Inc., pp. 847-852, 1987.

68. A. Sugimura, K. Daikoku, N. Imoto, and T. Miya, *Wavelength dispersion characteristics of single-mode fibers in low-loss region* IEEE J. Quantum Electron., Vol. QE-16, no. 2, pp. 215-225, 1980.

69. J. Augé, C. Brehm, P. Dupont, L. Fersing, C. Le Sergent, J. Ramos, F. Alard, J. F. Bayon, Y. Durteste, P. L. Francois, D. Grot, J-Y. Guilloux, P. Lamouler, M. Monerie, and L. Rivoallan, *Cables and links with long lengths of low loss dispersion flattened multiple-clad single mode fibers*, Proceedings of the Fifth International Conference on Integrated Optics and Optical Fiber Communication, Venice, Italy, pp. 205-208, 1985.

70. C. T. Chang, *Minimum dispersion in a single-mode step-index optical fiber*, Appl. Opt., Vol. 18, pp. 2516-2522, 1979.

71. F. P. Kapron, *Maximum information capacity of fiber-optic waveguides*, Electron. Lett., Vol. 13, pp. 96-97, 1977.

72. A. Safaai-Jazi and L. J. Lu, *On the evaluation of chromatic dispersion in W-type fibers*, Opt. Lett. Vol. 14, pp. 760-762, 1989.

73. M. R. Shenoy, K. Thyagarajan, and A. K. Ghatak, *Numerical analysis of optical fibers using matrix approach*, J. Lightwave Technol., Vol. 6, pp. 1285-1291, 1988.

74. C. N. Kurtz and W. Streiffer, *Guided waves in inhomogeneous focussing media, Part I: formulation, solution for quadratic inhomogeneity*, IEEE Trans., MTT-17, pp. 11-15, 1969.

75. D. Gloge, *Weakly Guiding Fibers*, Appl. Opt., Vol. 10, pp. 2252-2258, 1971.

76. C. M. Miller, S. C. Mettler, and I. A. White, *Optical fiber splices and connectors theory and methods*, Marcel Dekker Inc. 1986.

Appendix A. Weakly Guiding Approximation

Even with the simplifying assumption that the cladding is infinitely thick, Maxwell's equations, although they have exact solutions for the dielectric cylinder, are too involved to be evaluated without a computer. Kurtz and Streiffer [74] used the existence of scalar optical fields for the modes of circular cylindrical fibers, and later Gloge [75] demonstrated the simplifying expression of these fields as linearly polarized (LP) electromagnetic fields. Under the weakly guiding approximation, most results apply for all frequencies and propagation conditions, even at cutoff, with an accuracy of the order of the index difference between core and cladding [75].

If the dielectric difference Δ between core and cladding is small, as is the case for most optical fibers, the weakly guiding approximation can be applied, thus greatly simplifying the form of the electromagnetic fields in dielectric waveguides. The basic results and the physical explanation for the validity of this approximation can be seen by considering plane waves reflected from planar interfaces [76]. For the practically important case of small index differences with $n_{co}/n_{cl} \simeq 1$, the acceptance angle at the interface, θ_a, is

$$\theta_a \simeq \sqrt{1 - n_{cl}^2/n_{co}^2} = \sqrt{2\Delta} \ll 1. \tag{1}$$

A Taylor series expansion in Δ demonstrates that, to first order, different polarizations behave identically in the presence of the interface, so that if higher-order terms in Δ, are ignored, descriptions of the electromagnetic field are simplified and both polarizations behave identically. This approximation yields the same results as ignoring terms of order Δ in the boundary conditions and $\nabla\varepsilon$ terms in the wave equations for the field components. The total field can be defined by one scalar field shape, corresponding to the variation of the field in the transverse plane, from these simplified wave equations. By using the approximate form of equations which ignores the $\nabla\varepsilon$ terms, the longitudinal field components can be evaluated directly

$$E_z = \frac{1}{i\beta} \nabla_t \cdot (\bar{E}_T), \tag{2a}$$

$$H_z = \frac{1}{i\beta} \nabla_t \cdot (\bar{H}_T), \tag{2b}$$

where subscript T stands for the transverse field components, and all transverse field components satisfy simplified Helmholtz equations of the form

$$(\nabla_t^2 + K_0^2 n^2 - \beta^2)\bar{E}_T = 0, \tag{3a}$$

$$(\nabla_t^2 + K_0^2 n^2 - \beta^2)\bar{H}_T = 0. \tag{3b}$$

For small Δ, the longitudinal components E_z and H_z of the fields are much smaller than the transverse field components

$$|E_z/E_T| \simeq |H_z/H_T| \ll 1. \tag{4}$$

Equation (4) demonstrates that, to first-order, the effects of the longitudinal field components can be ignored and the total electromagnetic field can be approximated by the transverse field components, (r, ϕ), alone, since these plane waves which undergo total internal reflection are the bound modes that carry energy along an optical fiber. The solution for the radially dependent scalar field, $\Psi(r)$, in the various regions should satisfy the weakly guiding fiber approximations to the boundary conditions. For fibers with profile discontinuities, one simply applies the continuity conditions of the transverse field shapes and their radial derivative across the boundaries. Applying the approximation $\Delta \ll 1$ leads to much simpler field solutions, the total number of field components is reduced to one, (r), and the necessity of considering polarization sensitivity is eliminated. In general, we choose linearly polarized (LP) field notation [75,76] because both polarization components behave identically within this approximation. Since the interface between slightly different indices completely reflects internally only a very small range of possible plane wave directions incident upon it, this approximation for small Δ has been called the weakly guiding approximation. Since the total electromagnetic field can be defined by one scalar field, this approximation has also been referred to as the scalar wave approximation.

The weakly guiding approximation produces an exact solution at cutoff, exhibiting a maximum relative error of up to 2% for very high frequencies [75]. But fields derived from this method are not adequate to describe polarization effects in fibers. More details can be found in the references [75,76].

Appendix B. Material Composition

Table 15. Material composition [49]

No.	Composition
M1	SiO_2
M2	4.1 m/o GeO_2, 95.9 m/o SiO_2
M3	4.03 m/o GeO_2, 9.7 m/o B_2O_3, 86.27 m/o SiO_2
M4	0.1 m/o GeO_2, 5.4 m/o B_2O_3, 94.5 m/o SiO_2
M5	13.5 m/o B_2O_3, 86.5 m/o SiO_2 (chilled)
M6	3.1 m/o GeO_2, 96.9 m/o SiO_2
M7	3.5 m/o GeO_2, 96.5 m/o SiO_2
M8	5.8 m/o GeO_2, 94.2 m/o SiO_2
M9	3.5 m/o B_2O_3 96.5 m/o SiO_2
M10	2.2 m/o GeO_2, 3.3 m/o B_2O_3, 94.5 m/o SiO_2
M11	13.3 m/o B_2O_3 86.7 m/o SiO_2
M12	1.0 m/o F 99.0 m/o SiO_2
M13	3.3 m/o GeO_2, 9.2 m/o B_2O_3, 87.5 m/o SiO_2
M14	9.1 m/o P_2O_5, 90.9 m/o SiO_2
M15	9.1 m/o GeO_2, 7.7 m/o B_2O_3, 83.2 m/o SiO_2
M16	7.9 m/o GeO_2, 92.1 m/o SiO_2
M17	13.5m/o GeO_2, 86.5 m/o SiO_2

The vita has been removed from the scanned document